

**Laminins and fluid shear stress control  
hepatic stellate cell maintenance and function  
as components of their stem cell niche**

Inaugural-Dissertation

zur Erlangung des Doktorgrades  
der Mathematisch-Naturwissenschaftlichen Fakultät  
der Heinrich-Heine-Universität Düsseldorf

vorgelegt von

**Friederike Rohn**  
aus Aachen

Düsseldorf, Juni 2020

aus der Klinik für Gastroenterologie, Hepatologie und Infektiologie  
des Universitätsklinikums der Heinrich-Heine-Universität Düsseldorf

Gedruckt mit der Genehmigung der  
Mathematisch-Naturwissenschaftlichen Fakultät der  
Heinrich-Heine-Universität Düsseldorf

Berichterstatter:

1. Professor Dr. Dieter Häussinger

2. Professor Dr. Eckhard Lammert

Tag der mündlichen Prüfung: 5. Juni 2020

**Excerpts of this doctoral thesis are included in the following original research articles:**

**Rohn F**, Kordes C, Castoldi M, Götze S, Poschmann G, Stühler K, Herebian D, Benk AS, Geiger F, Zhang T, Spatz, JP, Häussinger D. Laminin-521 promotes quiescence in isolated stellate cells from rat liver. *Biomaterials*, 2018;180:36-51.

Contributions of Friederike Rohn: Prepared samples, performed experiments, analyzed data, embedded results into the scientific context, and contributed to manuscript writing.

**Rohn F**, Kordes C, Buschmann T, Wammers M, Reichert D, Poschmann G, Stühler K, Benk AS, Geiger F, Zhang T, Spatz JP, Häussinger D. Impaired integrin  $\alpha_5/\beta_1$ -mediated hepatocyte growth factor release by stellate cells of the aged liver. *Aging Cell*, 2020;19:e13131.

Contributions of Friederike Rohn: Prepared samples, performed experiments, analyzed data, embedded results into the scientific context, and contributed to manuscript writing.

## Contents

<b>Zusammenfassung</b> .....	<b>III</b>
<b>Abstract</b> .....	<b>IV</b>
<b>1. Introduction</b> .....	<b>1</b>
1.1. The stem cell niche.....	1
1.2. Hepatic stellate cells and their niche.....	2
1.3. Laminin as an element of the extracellular matrix in stem cell niches.....	3
1.4. Liver regeneration.....	5
1.5. Mesenchymal stem cells in liver regeneration and fibrosis.....	9
1.6. Senescence and liver aging.....	10
1.7. Influence of shear stress on stem cells.....	11
1.8. Aims of the thesis.....	14
<b>2. Materials and Methods</b> .....	<b>16</b>
2.1. Liver and serum sample preparation, HSC isolation, and cell culture.....	16
2.1.1. Isolation of HSC and culture on ECM protein-coated surfaces.....	16
2.1.2. Sample preparation from young and old rat livers.....	18
2.1.3. Culture of HSC under pulsatile laminar fluid flow.....	18
2.2. CRISPR/Cas9-mediated <i>Itga5</i> and <i>Itgb1</i> knockouts in HSC.....	20
2.3. Liver injury models.....	21
2.4. Gene expression analyses by microarray and qPCR.....	22
2.5. Immunofluorescence analyses of isolated HSC and liver sections.....	24
2.6. Western blot analyses of isolated HSC and liver tissue.....	25
2.7. Quantitative mass spectrometric analysis of rat liver matrix.....	27
2.8. Liquid chromatography-tandem mass spectrometry (LC-MS/MS).....	29
2.9. Generation of nanostructured glass surfaces.....	30
2.10. Scanning electron microscopy.....	31
2.11. Analysis of SASP factors in serum and HSC culture medium.....	31
2.12. Statistics.....	32
<b>3. Results</b> .....	<b>33</b>
3.1. Influence of LN-521 on HSC maintenance.....	33

3.1.1.	Laminin $\alpha 5$ expression patterns in normal and regenerating rat liver.....	33
3.1.2.	Improved HSC adhesion and maintenance on LN-521 .....	36
3.1.3.	Reduced HSC activation on LN-521.....	38
3.1.4.	LN-521-coated nanostructured surfaces provide a biomimetic stem cell microenvironment.....	46
3.1.5.	Reversal of HSC activation on LN-521 .....	50
3.2.	Aging alters HSC and their niche.....	53
3.2.1.	Quality control of gene expression microarray raw data.....	54
3.2.2.	Altered ECM composition in aged rat liver .....	55
3.2.3.	Impaired HSC characteristics in aged rat liver .....	60
3.2.4.	Differentiation of HSC in aged rat liver .....	65
3.2.5.	SASP factors in HSC and serum from aged rats.....	66
3.2.6.	Oxidative stress in liver tissue from aged rats .....	70
3.2.7.	Influence of fluid shear stress and ECM composition on HSC function.....	72
3.2.8.	<i>Itga5</i> and <i>Itgb1</i> knockouts in HSC impair mechanosensing .....	77
<b>4.</b>	<b>Discussion.....</b>	<b>82</b>
4.1.	LN-521 promotes quiescence in HSC.....	82
4.1.	Mechanosensing of stellate cells from aged liver is impaired .....	87
<b>5.</b>	<b>Conclusion and Future Research.....</b>	<b>94</b>
<b>6.</b>	<b>References.....</b>	<b>95</b>
<b>7.</b>	<b>List of Abbreviations .....</b>	<b>113</b>
<b>8.</b>	<b>List of Figures .....</b>	<b>117</b>
<b>9.</b>	<b>List of Tables.....</b>	<b>119</b>
	<b>List of Publications, Scientific Presentations, and Awards.....</b>	<b>V</b>
	<b>Danksagung.....</b>	<b>VII</b>
	<b>Eidesstattliche Erklärung .....</b>	<b>VIII</b>

## Zusammenfassung

Hepatische Sternzellen (HSC) sind mesenchymale Stammzellen der Leber, welche auf einer Basalmembran-ähnlichen Struktur im Disse'schen Raum – ihrer Stammzellnische – einen ruhenden Zustand sowie ihre Stammzeleigenschaften erhalten. Die Laminin  $\alpha 5$  (LAMA5) Kette kommt in Basalmembranen vor und unterstützt die Erhaltung von Stammzellen. Zusammen mit Laminin  $\beta 2$  (LAMB2) und  $\gamma 1$  (LAMC1) bildet LAMA5 das Laminin-521 (LN-521). In der vorliegenden Doktorarbeit wurde nun erstmalig gezeigt, dass LAMA5 im Disse'schen Raum der normalen Rattenleber vorhanden ist. Weiterhin wurde festgestellt, dass die Kultur von isolierten HSC auf LN-521 beschichteten Oberflächen ihren ruhenden Zustand sowie ihre Stammzeleigenschaften unterstützt und die Expression des HGF (*hepatocyte growth factor*) erhöht. In Lebern alter Ratten zeigte sich, dass die LAMB2- und LAMC1-Ketten deutlich reduziert waren. Außerdem wiesen HSC im Alter eine signifikant verringerte Expression von HGF und einen Seneszenz-assoziierten Phänotyp auf. In früheren Arbeiten wurde ein Rückgang des hepatischen Blutflusses im Alter von bis zu 50% beschrieben, so dass von einer deutlich verringerten Fluidmechanik in den Lebersinusoiden auszugehen ist. HSC, die einem Flüssigkeitsstrom ausgesetzt wurden, zeigten eine signifikant erhöhte Expression von LAMB2 und LAMC1 sowie eine verstärkte Freisetzung von HGF. Weiterhin wurde festgestellt, dass auch die Expression von Integrin  $\alpha 5$  (ITGA5) in HSC durch Scherkräfte deutlich erhöht wird und ITGA5 in diesen Zellen sowie der gesamten Leber alter Ratten signifikant reduziert ist. Der CRISPR/Cas9-vermittelte *knockout* von ITGA5 in HSC konnte die Scherkraft-induzierte Expression von LAMB2 und LAMC1 aufheben. Weiterhin verringerte der *knockout* von ITGA5 und Integrin  $\beta 1$  (ITGB1) die Ausschüttung von HGF deutlich. ITGA5 und ITGB1 sind somit für die Wahrnehmung und Transduktion mechanischer Stimuli in HSC wichtig. Zusammenfassend zeigen die Ergebnisse, dass das LN-521 als ein wichtiges Element der Stammzellnische von HSC betrachtet werden kann und dass eine Reduktion des Mechanosensors ITGA5 im Alter durch eine verringerte Fluidmechanik die Abnahme einzelner Proteinketten des LN-521 in der Leber erklären könnte. Die Beeinträchtigung ihrer Nische ist vermutlich für die Induktion der Seneszenz in HSC verantwortlich. In der Folge können HSC andere Leberzelltypen nicht mehr mit Wachstumsfaktoren wie dem HGF versorgen und im Falle einer Verletzung des Lebergewebes die bereits bekannte verminderte Regeneration der Leber im Alter hervorgerufen.

**Abstract**

Hepatic stellate cells (HSC) are liver-resident mesenchymal stem cells, which reside in a quiescent state on a basement membrane-like structure in the space of Disse, their stem cell niche. The laminin  $\alpha 5$  (LAMA5) protein chain is an element of basement membranes and important to maintain stem cells. In this thesis, the LAMA5 chain was detected in the space of Disse of normal rat liver. Together with laminin  $\beta 2$  (LAMB2) and  $\gamma 1$  (LAMC1), LAMA5 composes the laminin-521 (LN-521) trimer, which is known to support stem cell characteristics. Culture of isolated HSC on surfaces coated with LN-521 improved the quiescence- and stem cell-associated phenotype of HSC. Furthermore, LN-521 significantly elevated the expression and release of hepatocyte growth factor (HGF), an essential inductor of liver regeneration. Interestingly, the LAMB2 and LAMC1 chains decreased markedly in the liver matrix of old rats. In addition, HSC from aged livers acquired a senescence-associated secretory phenotype (SASP) and significantly reduced the expression of HGF. An age-related reduction of the hepatic blood flow by up to 50% was reported previously. Consequently, a markedly reduction of fluid mechanical forces in liver sinusoids is associated with aging. Exposure of isolated HSC to fluid shear stress significantly upregulated the expression of LAMB2 and LAMC1 and triggered the release of HGF. Interestingly, also integrin  $\alpha 5$  (ITGA5) was observed to be markedly reduced in HSC from old rats and its expression could be significantly increased when HSC were exposed to shear stress. A Clustered Regularly Interspaced Short Palindromic Repeats (CRISPR)/Cas9-mediated knockout of ITGA5 abolished the shear stress-induced expression of LAMB2 and LAMC1. In addition, ITGA5 and Integrin  $\beta 1$  (ITGB1) knockouts significantly reduced HGF release by HSC. Thus, ITGA5 and ITGB1 seem to be important for mechanosensing in HSC. In conclusion, this thesis provides evidence that LN-521 can be regarded as an important niche element in the space of Disse and that the reduction of ITGA5 in HSC due to a decreased hepatic blood flow leads to impaired mechanosensing during aging. Impaired mechanosensing, in turn, could have been contributed to the reduced LN-521 protein deposition in the aged rat liver. The reduction of important ECM proteins normally present in their stem cell niche seems to be responsible for the loss of proper HSC function such as HGF synthesis and for the induction of senescence. The results obtained in this study suggest that age-related alterations in HSC and their niche can contribute to the declined regenerative capacity of the aged liver.

## 1. Introduction

The stem cell fate is controlled by environmental cues such as the composition of the extracellular matrix (ECM) or mechanical forces (Lane *et al.*, 2014). Stem cells require a protective microenvironment, which is defined by the term “stem cell niche” (Schofield, 1978). Aging markedly alters the niche components resulting in senescence and impaired function of stem cells (O'Hagan-Wong *et al.*, 2016). Since stem cells are critically involved in tissue repair, the regeneration capacity during aging diminishes (Rogers *et al.*, 2018). Also the liver as the central metabolic organ is affected by aging processes, which is reflected by the impaired regenerative potential of the aged liver. (Biondo-Simões Mde *et al.*, 2006; Zhu *et al.*, 2014; Enkhbold *et al.*, 2015; Saito *et al.*, 2017). Hepatic stellate cells (HSC) are liver-resident mesenchymal stem cells (MSC), which reside in the space of Disse representing their stem cell niche (Sawitza *et al.*, 2009; Kordes and Häussinger, 2013). This study elucidates important components of the HSC niche and how age-related alterations might affect the stem cell niche integrity as well as the HSC maintenance and function.

### 1.1. The stem cell niche

In 1906, Alexander Maximow already observed a supportive influence of the bone marrow microenvironment on blood progenitor cells and, thus, he laid the foundation for the concept of a stem cell-supporting niche (Maximow, 1906). Half a century later, Till and McCulloch (1961) discovered hematopoietic stem cells in the bone marrow. In the last decades several tissues had been described as sources for stem cells, such as skin (Fuchs, 2009), intestine (Tan and Barker, 2014), nerve system (Conover and Notti, 2008) or liver (Kordes and Häussinger, 2013). It took more than seventy years since Maximow's discovery until the stem cell microenvironment was defined as the “stem cell niche” (Schofield, 1978). Since then, stem cell research mainly focused on hematopoietic stem cells, but fibroblasts with stem cell characteristics were also identified in the bone marrow (Friedenstein *et al.*, 1970). Caplan (1991) coined the term “mesenchymal stem cells” (MSC) for these fibroblasts, which possess the capacity to self-renew and to differentiate in order to maintain or regenerate tissue (Watt and Hogan, 2000). MSC from different organs share a perivascular origin and can differentiate along multiple lineages, for

instance, the osteo-, adipo-, and chondrogenic lineages (Crisan *et al.*, 2008). This multipotent differentiation potential distinguishes MSC from pluripotent stem cells, which can differentiate along ecto-, meso- or endodermal lineages (Itskovitz-Eldor *et al.*, 2000) and can either be obtained from the inner cell mass of the blastocyst (embryonic stem cells) (Guo *et al.*, 2016) or artificially induced from any somatic cell of the adult body (Takahashi and Yamanaka, 2006; Yu *et al.*, 2007).

The niche crucially controls the stem cell fate (Schofield, 1978). Alterations of niche components either support stem cell self-renewal and proliferation to maintain tissue homeostasis or can trigger differentiation processes to regenerate injured tissue (Lane *et al.*, 2014). For example, the onset of differentiation is prevented by cellular adhesion to their surrounding ECM (Jones and Watt, 1993; Jones *et al.*, 1995; Quesenberry and Becker, 1998; Zhu *et al.*, 1999). Cell-ECM interactions are driven by numerous classes of receptors such as integrins, which not only anchor stem cells in their niche but also serve as signal transducers (Moro *et al.*, 1998; Katsumi *et al.*, 2004). Furthermore, proliferative and developmental processes in stem cells can be influenced by soluble factors such as transforming growth factor  $\beta$  (TGF $\beta$ ) and Wnt (Watt and Hogan, 2000). Another mechanism influencing stem cell fate is direct cell-cell contact. Here, especially the evolutionary conserved Notch signaling plays a dominant role due to its involvement in diverse processes such as proliferation, differentiation, and apoptosis (Artavanis-Tsakonas *et al.*, 1999).

## **1.2. Hepatic stellate cells and their niche**

HSC reside as liver-resident MSC in the space of Disse between sinusoidal endothelial cells (SEC) and hepatocytes (Figure 1). Here, HSC are surrounded by a basement membrane-like structure, which contains several ECM proteins, such as collagens and laminins, that contribute to the stem cell niche of stellate cells (Sawitza *et al.*, 2009; Kordes and Häussinger, 2013; Kordes *et al.*, 2013).

In normal liver, HSC maintain a quiescent state and express a set of typical markers, for instance, glial fibrillary acidic protein (*Gfap*), Notch1, reelin, secreted protein acidic and rich in cysteines-like 1 (*Sparcl1*), lecithin retinol acyltransferase (*Lrat*), and peroxisome proliferator activated receptor  $\gamma$  (*Ppar $\gamma$* ) (Miyahara *et al.*, 2000; Kobold *et al.*, 2002; Sawitza *et al.*, 2009; Coll *et al.*, 2015). Furthermore, quiescent HSC contain retinoid-storing lipid droplets (Blaner *et al.*, 2009).

After liver injury, HSC undergo an activation process by which they lose their retinoids (Mabuchi *et al.*, 2004) and develop a myofibroblast-like phenotype that is characterized by the increased expression of  $\alpha$ -smooth muscle actin ( $\alpha$ -Sma), different collagens, fibronectin, nestin (Rockey *et al.*, 1992; Michalopoulos and DeFrances, 1997; Niki *et al.*, 1999; Hui and Friedman, 2005), and reduced Notch1 expression (Sawitza *et al.*, 2009). Persistent activation of HSC is a driving force for the development of liver fibrosis that is indicated by an increased extracellular matrix stiffness due to the deposition of the fibrillar collagen types I and III (Hahn *et al.*, 1980).

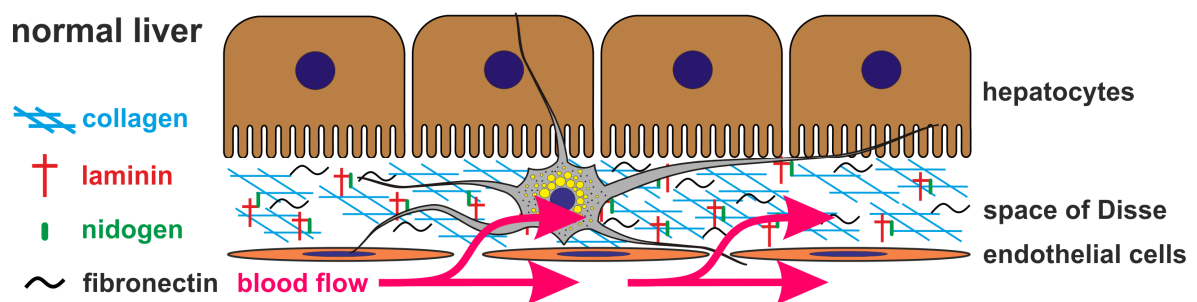


**Figure 1: The hepatic stellate cell niche in the space of Disse.** Here, hepatic stellate cells (HSC) are located between hepatocytes and endothelial cells and are embedded into a network of extracellular matrix proteins such as collagen, laminin, and fibronectin – a basement membrane-like structure. Furthermore, quiescent stellate cells store retinoid-containing lipid droplets (yellow) and are exposed to shear stress due to blood flow (pink arrows) through endothelial fenestrations.

HSC also activate after isolation from the liver and incubation under standard culture conditions on polystyrene (PS). During this activation process, HSC downregulate the expression of Notch1 and *Sparcl1* and upregulate the expression of Notch3,  $\alpha$ -Sma, nestin, and fibrillar collagens (Niki *et al.*, 1999; Sawitza *et al.*, 2009; Reister *et al.*, 2011; Coll *et al.*, 2015; Schumacher *et al.*, 2017).

### 1.3. Laminin as an element of the extracellular matrix in stem cell niches

In normal liver, the ECM proteins compose the perisinusoidal matrix related to basement membranes (Hui and Friedman, 2005) that contains collagen, proteoglycans, and fibronectin as well as laminin. The latter one has been firstly described as a large non-collagenous glycoprotein by Timpl *et al.* (1979), who isolated laminin from a mouse tumor. A functional laminin molecule is composed of one  $\alpha$ , one  $\beta$ , and one  $\gamma$  protein chain and exhibits a coiled-coil structure with four arms as schematically illustrated in Figure 2 (Timpl *et al.*, 1979; Ekblom *et al.*, 2003;

Aumailley *et al.*, 2005). Binding of laminin to collagen IV (COL4) is mediated by nidogen (NID) (Fox *et al.*, 1991) via the  $\gamma$  chain (Pöschl *et al.*, 1994; Gersdorff *et al.*, 2005).

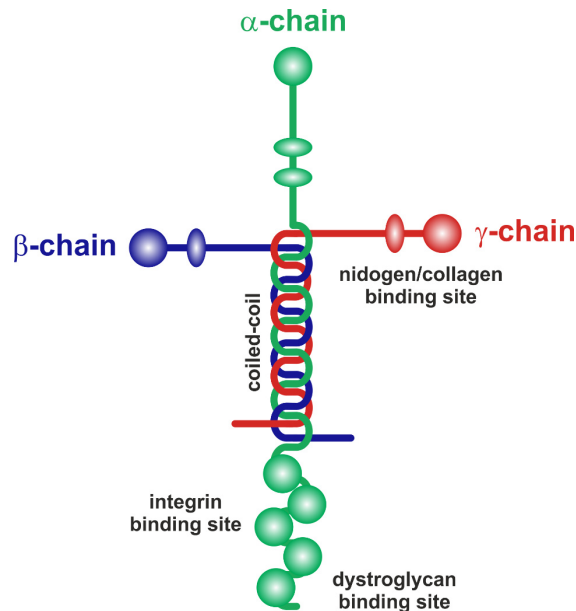


**Figure 2: Schematic overview of the laminin protein structure.** Laminin is an element of stem cell niches and plays an important role during embryogenesis. A functional laminin molecule is composed of three different protein chains:  $\alpha$  (green),  $\beta$  (blue), and  $\gamma$  (red) chain. These three chains together form a coiled-coil structure. Most of the binding sites for laminin receptors, such as integrins or dystroglycan, are located on the  $\alpha$  chain. Thus, cell adhesion and laminin-mediated behavior is mainly dependent on the five different  $\alpha$  chains. To compose a basement membrane-like structure laminins and collagens build a network. Here, binding of laminin to collagen is mediated by nidogen via the  $\gamma$  chain.

Five  $\alpha$ , three  $\beta$ , and three  $\gamma$  chains as well as at least 16 different trimeric combinations of laminin chains have been described in mouse and human tissue thus far (Aumailley *et al.*, 2005). Cellular binding is mediated by several laminin-specific receptors, which are located on the  $\alpha$  chain, for instance, diverse integrins, dystroglycan, syndecans, and Lutheran blood group protein/basal cell adhesion molecule (LU/BCAM) (Durbeej, 2010). Hence, laminin-mediated cellular behavior mainly depends on the presence of the five  $\alpha$  chains. Moreover, laminins are crucially involved in embryo- and organogenesis. For example, laminins containing the  $\alpha 2$  (LAMA2) chain are important for the development of the peripheral nervous system (Wallquist *et al.*, 2005). Furthermore, the laminin chains  $\alpha 1$  (LAMA1) and  $\alpha 5$  (LAMA5) play an important role during embryogenesis. Thereby, LAMA1 is more prominent in the trophectoderm, whereas LAMA5 is expressed in the inner cell mass of the blastocyst where it supports self-renewal and maintenance of embryonic stem cells (Klaffky *et al.*, 2001). Absence of LAMA5 in mouse and zebrafish knockout models leads to severe developmental defects and mouse embryos lacking LAMA5 are not viable after E17 (Miner *et al.*, 1998; Webb *et al.*, 2007). Furthermore, LAMA5 also promotes self-renewal and hepatic specification of human pluripotent stem cells

*in vitro* as demonstrated in several studies (Cameron *et al.*, 2015; Laperle *et al.*, 2015; Kanninen *et al.*, 2016).

First hints that indicated a supportive effect of laminin on HSC quiescence were observed by Stone *et al.* (2015), who described elevated cytoglobin expression and a rounded cell morphology in the stellate cell line HSC-T6 cultured on laminin-coated surfaces. However, the trimeric composition of the laminin used in that study was not further characterized and, hence, it is not known which laminin chains maintain the quiescent state in HSC thus far. As described in section 1.2 HSC are liver-resident MSC (Kordes *et al.*, 2013). Therefore, this work addressed the question whether LAMA5 maintains characteristics of quiescent HSC as suggested by its presence in their stem cell niche, the space of Disse. In addition to LAMA5, the laminin chains  $\beta 2$  (LAMB2) and  $\gamma 1$  (LAMC1) are mainly retained in the normal rat liver matrix after decellularization and, thus, seem to be abundant in hepatic ECM (Li *et al.*, 2016). For this reason, laminin-521 (LN-521) was used for the present study. *Lama2*, *Lamb1*, and *Lamc1* mRNA are also detectable in human and rodent liver (Liétard *et al.*, 1998; Zhao *et al.*, 1999) and, therefore, the laminin trimer LN-211 was employed for comparison. Since LAMA2 and LAMA5 had been described as components of adult stem cell niches (Shen *et al.*, 2008; Kazanis *et al.*, 2010), the expression of different laminin chains was analyzed in normal, injured, and aged rat liver and their relevance for the maintenance of HSC was investigated in this study.

#### **1.4. Liver regeneration**

Liver injury can be caused by surgically removing two thirds of the liver mass, a procedure called partial hepatectomy (PHx) (Higgins and Anderson, 1931). The subsequent complex process of liver regeneration involves several hepatic cell types as well as growth factors, cytokines, and remodeling of the hepatic ECM (Figure 3). A complete restoration of the ratio between the liver mass and body weight is reached four weeks after liver injury (Higgins and Anderson, 1931; Michalopoulos, 2007). Since hepatocytes are the most frequent cells in liver, tissue regeneration is mainly driven by their proliferation (Gilgenkrantz and Collin de l'Hortet, 2018). One growth factor is crucial for initiation of hepatocyte proliferation shortly after liver injury, that is hepatocyte growth factor (HGF) (Nakamura *et al.*, 1984). HGF is synthesized by HSC (Schirmacher *et al.*, 1993) and sinusoidal

endothelial cells (SEC) (LeCouter *et al.*, 2003) and binds to hepatocytes via its receptor c-Met (Naldini *et al.*, 1991). Shortly after PHx, HGF is activated due to its cleavage from the matrix where it is normally bound as pro-HGF (Masumoto and Yamamoto, 1991; Kim *et al.*, 1997). This mechanism is dependent on increased blood pressure shortly after PHx (Michalopoulos, 2007). Since only one third of the original liver tissue remains left after surgical intervention during PHx, the entire hepatic blood flow has to pass a respective small vessel diameter and dilates the liver sinusoids (Michalopoulos, 2007; Lorenz *et al.*, 2018). Through the fenestration of the endothelium of the liver sinusoid the increased blood flow also reaches HSC as well as hepatocytes (Figure 1).

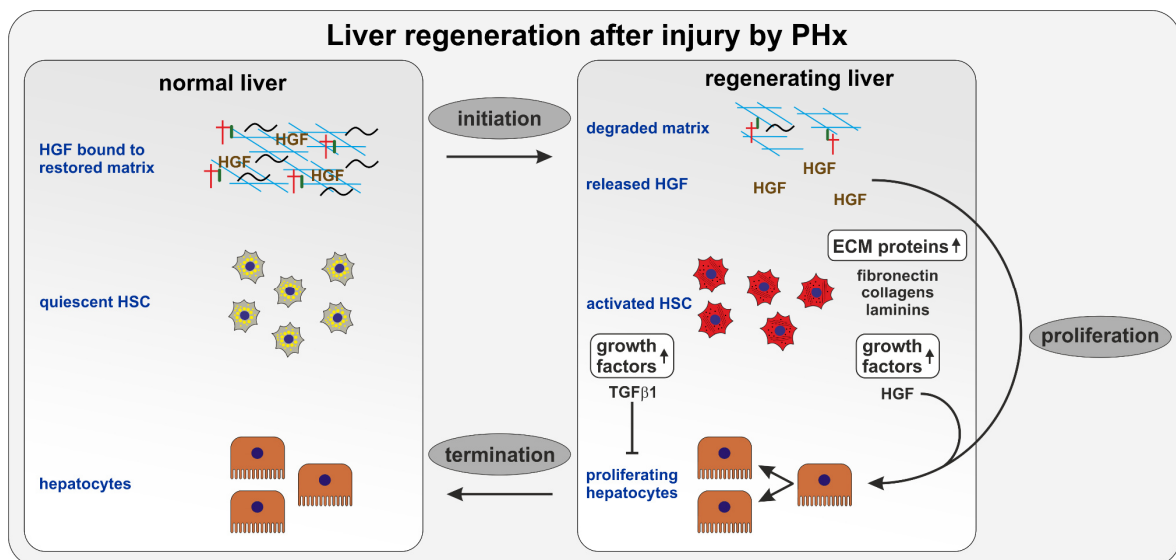


**Figure 3: Scheme of processes after PHx involved in liver regeneration.** Shortly after liver injury, regenerative stimuli initiate tissue regeneration. For example, HGF is released from the matrix by enzymatic cleavage of its larger matrix-bound precursor protein pro-HGF. Furthermore, HSC activate and increase the expression of ECM proteins as well as of growth factors such as TGFβ1 and HGF. Consequently, hepatocyte proliferation is initiated by HGF. As soon as the liver has restored its original size, regenerative stimuli are terminated. Termination of liver regeneration involves elevated TGFβ1 release by HSC. In addition, the restoration of hepatic ECM is sensed by hepatocytes via integrin signaling leading to their proliferation stop. Other hepatic cell types involved in the process of liver regeneration such as SEC, cholangiocytes or Kupffer cells are not shown.

Marubashi *et al.* (2004) showed that by keeping the portal blood pressure constant after PHx, activation of HGF was decreased. In addition to HGF, also the serine protease urokinase plasminogen activator (uPA) is increased in different cell types in response to elevated fluid flow (Sokabe *et al.*, 2004), which in turn triggers matrix remodeling after PHx (Michalopoulos, 2007). The latter process involves matrix metalloproteinases (MMP) and their inhibitors (tissue inhibitors of

metalloproteinases; TIMP) (Mohammed and Khokha, 2005). Since HGF is claimed to be bound to the hepatic ECM as pro-HGF (Masumoto and Yamamoto, 1991), remodeling and degradation of matrix components after liver injury leads to the release and activation of HGF. Kim *et al.* (1997) observed rapid ECM degradation by a marked reduction of laminin and fibronectin during the first minutes to hours after PHx. In addition to hepatocytes, HSC, and SEC also cholangiocytes and Kupffer cells are involved in the process of liver regeneration (Michalopoulos, 2007). As soon as hepatocyte number and the hepatic sinusoidal network are restored similar to its original, several events could terminate hepatic cell proliferation. For instance, reassembly of hepatic ECM proteins might lead to the termination of hepatocyte proliferation mediated by integrin signaling due to direct cell-ECM interaction (Michalopoulos, 2010; Gilgenkrantz and Collin de l'Hortet, 2018). Furthermore, HGF concentration recovers to its baseline since TGF $\beta$ 1 inhibits synthesis of new HGF by HSC and soluble HGF binds to the restored ECM (Michalopoulos, 2007; Michalopoulos, 2010). Another possible terminator of the regeneration process could be the reduction of portal blood flow after restoration of liver vascularization resulting in decreased regenerative stimuli (Michalopoulos, 2007; Lorenz *et al.*, 2018).

For a liver regeneration model associated with the appearance of liver progenitor cells, rats can be treated with 2-acetylaminofluorene (2AAF) seven days before PHx (Tatematsu *et al.*, 1984; Kordes *et al.*, 2014). Consequently, 2AAF is enzymatically converted selectively in hepatocytes into toxic compounds such as N-sulfoxy-AAF, which interact with nucleic acids and proteins resulting in impaired hepatocyte proliferation (Scarabelli *et al.*, 1992; Hanaoka, 2001). Afterwards, putative progenitor cells expressing the cholangiocyte marker cytokeratin 19 (CK19) form duct-like structures (ductular reaction) that proceed from the area around the portal field. The origin of these duct-forming cells has been controversially discussed over decades. Until today, several concepts had been presented. It was suggested that hepatic progenitor cells derive from stem/progenitor cells in the canals of Hering and from HSC that reside in the space of Disse (Kordes and Häussinger, 2013; Kordes *et al.*, 2014). An alternative mechanism involves migrating MSC from other tissues such as the bone marrow via the recruitment by the chemokine (C-X-C motif) ligand 12 (CXCL12) (Petersen *et al.*, 1999; Kordes and Häussinger, 2013). Further proposals suggest that the facultative liver stem cells arise from proliferating bile

ducts or even from hepatocytes which are reprogrammed to fetal-like cells by YAP1 signaling (Raven *et al.*, 2017; Hyun *et al.*, 2019). The relevance of MSC in liver regeneration will be further discussed in section 1.5.

The two different liver injury models described above were used to analyze alterations in the expression levels of different laminin  $\alpha$  chains in rat liver tissue since the  $\alpha$  chain plays a key role in cell binding to laminin (see section 1.3). PHx of rat livers was performed since it has been shown previously that matrix remodeling appears shortly after liver injury (Kim *et al.*, 1997). Subsequently, the *Lama1*, *Lama2*, and *Lama5* mRNA amounts were analyzed by qPCR in whole liver tissue at different time points after PHx and compared to normal rat liver (0d; Figure 4). Expression of *Lama5* was upregulated in the PHx model during the first week after surgery (1d-7d), but reached its normal level represented by normal livers without PHx (0d) within two weeks (Figure 4A).

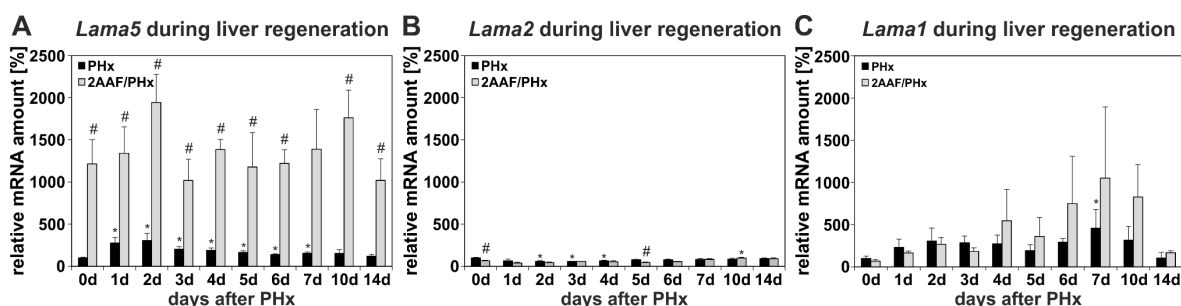


**Figure 4: Expression of different laminin  $\alpha$  chains during liver regeneration<sup>1</sup>.** (A) During liver regeneration associated with the appearance of putative liver progenitor cells (2AAF/PHx), *Lama5* mRNA expression was markedly increased compared to the PHx model as analyzed by qPCR. (B) In contrast, *Lama2* mRNA expression exhibited only minor changes when both injury models were compared. (C) *Lama1* mRNA levels were markedly lower compared to *Lama5* and its expression was only slightly increased in both injury models compared to control (0d). The mean expression of *Lama5* / *Lama2* / *Lama1* in the PHx model at day 0 (0d) was set to 100% and data are indicated as means  $\pm$  SEM. Significant differences between day 0 (normal liver) and different time points after PHx are indicated by an asterisk (\*), whereas a hash (#) indicates significant differences between both injury models at the same time point (n = 3-5 per indicated time point; p < 0.05). Modified from Rohn *et al.* (2018).

To induce the appearance of facultative liver progenitor cells, the hepatocyte proliferation after PHx was inhibited by 2AAF treatment of rats for one week before surgery was performed. During the following regeneration process, *Lama5* mRNA

<sup>1</sup> The qPCR analyses were performed by Dr. Silke Götze (Clinic of Gastroenterology, Hepatology and Infectious Diseases, Heinrich Heine University Düsseldorf) and further processing of the data was carried out by Friederike Rohn.

levels were markedly upregulated in the liver tissue of the 2AAF/PHx model compared to the PHx model without 2AAF pre-treatment (Figure 4A). The pre-treatment with 2AAF before PHx (0d) already led to an increased *Lama5* expression which remained high until the end of observation phase (i.e. 14 days after PHx). In contrast, *Lama2* mRNA levels were not substantially altered in both injury models (Figure 4B). Although *Lama1* mRNA amounts were slightly elevated in both liver injury models (Figure 4C), the *Lama1* gene expression remained well below *Lama2* and *Lama5* in qPCR analysis. These previous observations suggest that the LAMA5 chain plays an exclusive role for liver homeostasis and regeneration associated with facultative liver progenitor cells and, thus, might also influence HSC function.

### 1.5. Mesenchymal stem cells in liver regeneration and fibrosis

In the last decade, numerous studies had been published in which the positive effects of MSC on liver regeneration are described and clinical trials were performed with MSC to treat chronic liver disease (Alfaifi *et al.*, 2018). Thereby, various mechanisms had been discussed by which MSC can contribute to liver regeneration. For example, injured cells might be supported by MSC through the release of paracrine growth factors or by direct cell-cell-interaction (Christ *et al.*, 2015). Another approach could be that MSC directly differentiate along the hepatic lineage since it was demonstrated that MSC from different tissues including HSC as liver-resident MSC can develop into hepatocyte-like cells (Theise *et al.*, 2000; Shu *et al.*, 2004; Banas *et al.*, 2007; Chamberlain *et al.*, 2007; Kordes *et al.*, 2014; Saito *et al.*, 2017).

Besides supportive effects of MSC during the regenerative processes, it was also observed that MSC can exhibit a myofibroblast-like phenotype and, thus, contribute to the development of fibrosis. Kramann *et al.* (2015) performed lineage tracing experiments of PDGF $\beta$ -/GLI1-positive cells, which have MSC characteristics and are detectable at the perivascular site. Shortly after injury, these cells proliferate rapidly and develop to myofibroblasts independent of the affected organ. Interestingly, ablation of GLI1-positive cells lowered signs of fibrosis and the authors claimed that tissue-resident perivascular MSC are a major source for myofibroblasts. In contrast to the positive influence of MSC on repair processes of acutely injured tissue as described above, these results of Kramann *et al.* (2015) indicate that in chronically injured tissue MSC even promote fibrosis. This concept

was confirmed by additional studies involving multiple organs (Marriott *et al.*, 2014; Liu *et al.*, 2015; Ieronimakis *et al.*, 2016; Trial *et al.*, 2016).

Recent insights into the involvement of MSC in fibrotic processes are important since in chronic liver diseases HSC-derived myofibroblasts are a major source of fibrotic ECM rich in collagen I. Therefore, in the literature HSC are predominantly associated with liver fibrosis and great effort is put on the inhibition of HSC activation after liver injury (Bataller and Brenner, 2001; Reeves and Friedman, 2002; Higashi *et al.*, 2017). In contrast, the regeneration-supporting potential of HSC due to their MSC phenotype is often neglected in case of drug development for the treatment of fibrosis.

### **1.6. Senescence and liver aging**

The ECM composition of several tissues is affected by aging processes. For example, in aged skin the matrix composition changes due to a gradual breakdown by MMP and alterations in ECM protein synthesis that can lead to a lost or weakened connection of cells to their surrounding matrix (Cole *et al.*, 2018). Furthermore, in aged cardiac ECM the collagen mRNA is downregulated (Meschiari *et al.*, 2017). Moreover, it has been shown that there are changes in biomechanical properties of collagen type II fibers in articular ECM leading to a decrease in fiber elasticity during aging (Buckwalter *et al.*, 1993).

While hepatic matrix remodeling during liver regeneration has been studied extensively (Kim *et al.*, 1997; Kim *et al.*, 2000), little is known about alterations of hepatic ECM during aging. Although liver function is only slightly affected by aging (Kitani, 1991), some age-related changes in liver physiology have been described such as a decreased hepatic blood flow and declined sinusoidal endothelial fenestration (Le Couteur and McLean, 1998; McLean *et al.*, 2003). In addition to the altered physiology of the hepatic endothelium, aging also affects hepatocytes. For example, the hepatocyte organelle structure is significantly altered during senescence, they accumulate dense bodies and lipofuscin inclusions and show an increased activity of hydrolases as well as a decreased activity of glucose-6-phosphatase (Schmucker, 1990; Schmucker and Sachs, 2002). Moreover, HSC from old livers rise in cell number and show increased retinoid storage (Warren *et al.*, 2011). Nevertheless, data on age-related alterations in the stem cell niche of

HSC and the influence of these changes on HSC function had not yet been published. All these age-related changes of hepatic cells result in impaired liver regeneration as demonstrated by several groups in human and rodent liver after PHx (Biondo-Simões Mde *et al.*, 2006; Zhu *et al.*, 2014; Enkhbold *et al.*, 2015; Saito *et al.*, 2017). One potential explanation for the impaired regenerative capacity of the aged liver after injury could be the significantly reduced HGF expression compared to young individuals (Zhu *et al.*, 2014; Enkhbold *et al.*, 2015).

The process of aging is accompanied by cellular senescence. Senescent cells secrete a collective batch of proteins known as the senescence-associated secretory phenotype (SASP) (Coppé *et al.*, 2008) which mainly includes various cytokines and chemokines associated with inflammation (Coppé *et al.*, 2010; Freund *et al.*, 2010). These proteins induce senescence and secretion of SASP factors in neighboring cells in a paracrine manner (Acosta *et al.*, 2013).

It has been shown previously that MSC require a stem cell niche to maintain their properties and that their niche is affected by aging which results in impaired MSC function (Li *et al.*, 2015; O'Hagan-Wong *et al.*, 2016; Sui *et al.*, 2016; Maryanovich *et al.*, 2018). For instance, aged human bone marrow-derived MSC markedly increase the secretion of SASP factors such as IL6 which leads to a diminished support of hematopoietic stem cells (O'Hagan-Wong *et al.*, 2016; Maryanovich *et al.*, 2018).

### 1.7. Influence of shear stress on stem cells

Fluid shear stress  $\tau$  is defined as the force  $F$  per unit area  $A$ . The unit of shear stress is given by dyn/cm<sup>2</sup> which is equal to  $\mu\text{N}/\text{cm}^2$ . Laminar flow of a Newtonian fluid in a tube is given by the following formula (Espinosa *et al.*, 2018):

$$\tau = \frac{F}{A} = \eta \frac{\partial v}{\partial r}$$

The velocity  $v$  of the fluid flow and its dynamic viscosity  $\eta$ , which is dependent on temperature and pressure, are proportional, while the radial distance from the centerline  $r$  is inversely proportional to the shear stress (Espinosa *et al.*, 2018). Since blood is a non-Newtonian fluid, its viscosity is not only dependent on

temperature and pressure but also on the forces acting on the blood (Haynes and Burton, 1959).

In the vascular system, shear stress is the frictional force of flowing blood upon the inner cell layer of the vessel wall (Davies, 1995). Thus, endothelial cells are mainly exposed to shear stress (Noh *et al.*, 2012). About 25% of the cardiac output are received by the liver, which serves as a blood volume reservoir (Lautt, 2009). The fenestration of SEC in the liver allows the fluid to pass through the vessel wall and to reach the hepatocytes (Wisse *et al.*, 1985). Interestingly, fenestrae are dynamic structures that regulate the influx to the space of Disse (Arias *et al.*, 1986). The relevance of the fluid flow pattern in the liver sinusoids has been modeled by Rani *et al.* (2006). The calculations presented in their study demonstrate that the blood fluid enters the space of Disse (Rani *et al.*, 2006), which thereby constitutes a para-vascular part of the plasma volume (Poisson *et al.*, 2017). HSC are pericytes that are in close contact to blood vessels (Häussinger and Kordes, 2019) and, therefore, also exposed to shear stress (Sera *et al.*, 2018). The influence of shear stress on HSC has been studied previously but only with regard to their migration behavior (Sera *et al.*, 2018).

As described in section 1.4, increase in blood pressure after PHx and, therefore, enhanced shear stress is a critical parameter during the initiation phase of liver regeneration (Michalopoulos, 2007; Poisson *et al.*, 2017). Since two thirds of the liver are surgically removed during PHx, the entire blood needs to pass through the remaining vessel diameter. According to the formula above shear stress and radius are inversely proportional meaning that a reduced vessel diameter leads to increased shear stress. As a consequence of the increased blood pressure after PHx, the sinusoids are dilated (Morsiani *et al.*, 1998). Vasodilation leads to stretching of SEC, which then release angiocrine signals important for liver growth and regeneration (Lorenz *et al.*, 2018). Since HSC are located close to SEC, mechanical forces exerted by vasodilation will also lead to HSC stretching. Furthermore, Morsiani *et al.* (1995) observed enlarged endothelial fenestration six hours after PHx resulting in increased permeability of the sinusoidal wall in rat liver. Thus, the elevated amount of plasma flowing from the sinusoid into the space of Disse also reaches HSC. These previous observations indicate that HSC can be directly exposed to mechanical stimuli such as stretching and shear stress after liver injury.

In contrast to PHx, the hepatic blood flow was observed to be decreased by about 20-55% in humans and rodents during aging (Le Couteur and McLean, 1998) suggesting reduced shear stress in the aged liver. Rashidi *et al.* (2016) demonstrated that fluid mechanical forces support the cell function of human pluripotent stem cell-derived hepatocyte-like cells indicating that shear stress seems to be important for liver homeostasis. Furthermore, lowered shear stress is reported to reduce ECM protein deposition in embryonic dorsal aorta (Espinosa *et al.*, 2018) and integrin  $\alpha_5$  (*Itga5*) expression in endothelial cells (Urbich *et al.*, 2000). On the contrary, increased shear stress downregulates *Il6* expression in endothelial cells or vice versa reduced fluid mechanical forces increase the expression of the SASP factor *Il6* (Lund *et al.*, 2010).

Manifold studies demonstrated the influence of mechanical forces such as shear stress, cell stretch, compression, and strain on stem cell maintenance and differentiation (Stolberg and McCloskey, 2009; Nava *et al.*, 2012). Especially fluid shear stress can promote the development along the endothelial, osteogenic, and cardiomyogenic lineages (Wang *et al.*, 2005; Yamamoto *et al.*, 2005; Ahsan and Nerem, 2010; Huang *et al.*, 2010; Liu *et al.*, 2010; Yourek *et al.*, 2010). Thus, mechanical forces seem to be important players in developmental and regenerative processes involving stem cells, but seem to be crucial for tissue homeostasis as well.

Various mechanisms responsible for sensing of mechanical stimuli were discussed in the past. One approach could be that mechanosensing and -transduction is mediated by the primary cilium that bends due to direct exposure to fluid flow (Janmey and McCulloch, 2007). The deflection of the cilium subsequently activates signaling cascades in which ion channels, integrins, and G proteins might be involved (Janmey and McCulloch, 2007; Stolberg and McCloskey, 2009). One further potential sensor could be the glycocalyx, which directly transmits mechanical forces exerted by fluid flow to the cytoskeleton (Tarbell and Pahakis, 2006; Stolberg and McCloskey, 2009). Another possible mechanism that had been reported is shear stress-induced vascular endothelial growth factor (VEGF) signaling (Yamamoto *et al.*, 2003). Upon shear stress exposure, endothelial progenitor cells increase the expression of VEGF receptor (VEGFR) whose activation is critically involved in endothelial differentiation (Yamamoto *et al.*, 2005). Liver growth and maintenance correlate with organ perfusion during embryogenesis and depend on

mechanotransduction via activated VEGFR3 and integrin  $\beta_1$  (ITGB1), which induce angiocrine signals and the release of HGF by SEC (Lorenz *et al.*, 2018). Thus, integrins not only mediate focal adhesions but also act as mechanosensors- and transducers (Häussinger *et al.*, 2003; vom Dahl *et al.*, 2003; Katsumi *et al.*, 2004; Schliess *et al.*, 2004; Häussinger *et al.*, 2006; Reinehr *et al.*, 2010; Ross *et al.*, 2013). Further integrins reviewed to be involved in mechanotransduction are the  $\alpha_v$ ,  $\alpha_6$ ,  $\beta_3$ , and  $\beta_6$  subunits (Tschumperlin *et al.*, 2018). Interestingly, the signaling cascades activated by integrins in response to mechanical forces are dependent on the underlying ECM to which the cells are adhered (Katsumi *et al.*, 2004). For example, fibroblasts cultured on fibronectin activate extracellular-signal-related kinase 2 (ERK2) signaling, while the incubation on laminin, vitronectin, and fibronectin activates c-Jun N-terminal kinase 1 (JNK1) signaling (MacKenna *et al.*, 1998). In contrast, culture on collagens does not activate any mitogen-activated protein kinase (MAPK) (MacKenna *et al.*, 1998). HSC from humans were reported to express several integrins such as  $\alpha_1\beta_1$ ,  $\alpha_2\beta_1$ ,  $\alpha_5\beta_1$ ,  $\alpha_6\beta_4$ ,  $\alpha_8\beta_1$ ,  $\alpha_v\beta_1$ , and  $\alpha_v\beta_3$  (Carloni *et al.*, 1996).

### 1.8. Aims of the thesis

Several factors might impair the stem cell niche integrity, for instance, injury, acute and chronic liver diseases, and aging. This thesis aimed to elucidate key factors from the microenvironment in the space of Disse that govern the maintenance and function of HSC. As described in section 1.4 the previous observations by the group of Professor Dr. Dieter Häussinger suggest that LAMA5 plays an exclusive role during liver regeneration associated with facultative liver progenitor cells. Thus, the focus was put on the composition of the hepatic ECM with regard to laminin and its influence on the maintenance of HSC characteristics such as the expression of quiescence and stem cell-associated markers as well as of growth factors. Since the process of liver regeneration, in which MSC are involved (see section 1.5), is impaired during aging (Biondo-Simões Mde *et al.*, 2006; Zhu *et al.*, 2014; Enkhbold *et al.*, 2015; Saito *et al.*, 2017), this study elucidated age-related alterations in HSC and their microenvironment and how these changes might contribute to the impaired regenerative potential of the aged liver. Therefore, identified niche components were investigated in normal, injured, and aged liver tissue of rats to clarify their possible dysregulation. In the aged rat liver, the central issues were alterations in the hepatic

ECM composition as well as the presence of SASP factors in HSC from old compared to young rats, which indicate cellular senescence and might contribute to the impaired regenerative capacity of the aged liver. The fluid flow of the blood stream reaches stellate cells through endothelial fenestration (Figure 1). Since fluid mechanical forces are increased after liver injury and reduced in the aged liver (see sections 1.4 and 1.7), it was analyzed how stellate cells respond to shear stress and how they might sense this fluid mechanical force. Overall, this thesis should provide new insights into the composition and function of the stellate cell niche.

## 2. Materials and Methods

In the following sections the materials and methods used for the experiments presented in this thesis are listed and explained.

### 2.1. Liver and serum sample preparation, HSC isolation, and cell culture

Preparation of rat liver and serum samples as well as isolation and culture of HSC are described in the following sections. The liver and HSC sample preparation protocols were authorized by the *Landesamt für Natur, Umwelt und Verbraucherschutz* (Recklinghausen, Germany; 82-02.04.2015.A287). Animals were kept according to the German animal welfare act.

#### 2.1.1. Isolation of HSC and culture on ECM protein-coated surfaces

HSC were isolated by Claudia Rupprecht (Clinic of Gastroenterology, Hepatology and Infectious Diseases, Heinrich Heine University Düsseldorf) from mid-aged Wistar rats (> 500 g, > 6 months of age), which were obtained from the animal facility of the Heinrich Heine University Düsseldorf (Germany). To analyze age-related changes, HSC were isolated from 2-months and 22-months-old rats delivered by Janvier Labs (France; see section 2.1.2).

Liver tissue was digested by liver perfusion with collagenase and pronase E solutions as described previously (Hendriks *et al.*, 1985). The lipid-storing HSC were obtained from the non-parenchymal cell fraction by density-gradient centrifugation using 28% Nycodenz (Nycomed Pharma, Oslo, Norway). After cell isolation, HSC were seeded either on uncoated polystyrene (PS) culture dishes or on dishes coated with fibronectin (FN; F0895-1MG; Sigma-Aldrich, Munich, Germany), collagen IV (COL4; C6745-1ML; Sigma-Aldrich), laminin-211 (LN-211-03; BioLamina, Stockholm, Sweden) or laminin-521 (LN-521-03; BioLamina). For the coating of plastic culture dishes a protein concentration of 1.0 µg/cm<sup>2</sup> was used. After two hours at 37°C, the coating solutions were aspirated and the HSC suspensions were added after adjustment of the cell-density (50,000 cells/cm<sup>2</sup>) with the exception of FN, which was aspirated and air dried before cell seeding. HSC were plated out in Dulbecco's Modified Eagle Medium (DMEM; Gibco, Thermo Fisher Scientific, Waltham, MA, USA) supplemented with 10% fetal calf serum (FCS; Merck/Millipore, Darmstadt, Germany) and 1% antibiotic-antimycotic solution (Gibco, Thermo Fisher

Scientific). After four hours of incubation at 37°C and 5% CO<sub>2</sub>, HSC were washed with phosphate buffered saline (PBS; Sigma-Aldrich) and the number of adherent cells per area was determined by counting the cells using the cellSens Dimension 1.16 software (Olympus, Shinjuku, Tokyo, Japan) from at least three different positions of the culture dishes. Subsequently, HSC were cultured for 24 hours in Iscove's Modified Dulbecco's Medium (IMDM; Gibco) with 10% FCS and 1% antibiotic-antimycotic solution. The next day, cells were washed with PBS to remove FCS and the culture medium was changed to a serum-free medium composed of IMDM with 1% insulin-selenite-transferrin/ITS (I3146; Sigma-Aldrich) containing albumin and linoleic acid (L9530-5ML; Sigma-Aldrich) supplemented with 1% antibiotic-antimycotic solution. The purity of cultured HSC was determined by ultra-violet light (UV light) excitation, resulting in characteristic emission of retinoid fluorescence, and by their typical cell morphology showing lipid-containing droplets encircling the cell nucleus. In case of cell culture experiments with bio-functionalized surfaces (see section 2.9), similar culture conditions were used. After seven days of culture, cells were either harvested for mRNA and protein analyses or fixed for immunostaining. Furthermore, conditioned culture media were harvested for analysis of HGF release with the Mouse/Rat HGF Quantikine ELISA Kit (MHG00; R&D Systems, Minneapolis, MN, USA).

In a different approach, HSC were cultured under serum-free conditions on uncoated PS surfaces to enable the development of myofibroblast-like cells. After one week, cells were washed with PBS without Mg<sup>2+</sup>/Ca<sup>2+</sup>, detached by trypsin/EDTA solution (59417C; Sigma-Aldrich), and centrifuged for 5 min at 500xg. Afterwards, cells were re-seeded on either uncoated or laminin-coated (LN-211, LN-521) PS surfaces and cultured for 24 hours in IMDM with 10% FCS and 1% antibiotic-antimycotic solution to enable cell attachment. Subsequently, remaining FCS was removed by washing with PBS and the HSC-derived myofibroblast-like cells were cultured for another week under serum-free conditions as described above before they were harvested for analysis.

To analyze the presence of ITGA5 in quiescent and culture-activated HSC, cells were isolated as described above and cultured on uncoated PS dishes either for one, three or seven days in DMEM containing 10% FCS and 1% antibiotic-antimycotic solution. Subsequently, HSC were collected for protein extraction from whole cell lysates at indicated time points and ITGA5 protein amount was analyzed

by Western blot (see section 2.6). Cell culture media were exchanged every second to third day in all *in vitro* experiments.

### **2.1.2. Sample preparation from young and old rat livers**

Livers for tissue preparation and HSC isolation were derived from 2 months (average body mass  $335 \pm 6$  g) and 22 months (average body mass  $655 \pm 18$  g) old male Wistar rats from Janvier Labs (France). Prior to sample preparation, the blood was harvested from the portal vein for analysis of SASP factors (see section 2.11). Therefore, blood was collected in Plus Blood Collection Tubes (366566; BD Biosciences, Heidelberg, Germany) and kept for 30 min at room temperature. Subsequently, blood samples were centrifuged for 11 min at 5000xg and the upper aqueous phase was collected and frozen at  $-80^{\circ}\text{C}$ . Remaining blood was removed from liver tissue by perfusion with PBS and samples from three different lobes (median lobe, left lateral lobe, right lateral lobe) of each liver were collected and pooled for tissue analysis by gene expression arrays, qPCR, and Western blot. Liver samples were snap frozen in liquid nitrogen and stored at  $-80^{\circ}\text{C}$  for further analysis.

HSC isolation from young and old rat livers was performed as described in section 2.1.1 by Claudia Rupprecht and Dr. Kordes (Clinic of Gastroenterology, Hepatology and Infectious Diseases, Heinrich Heine University Düsseldorf). Isolated HSC were suspended in PBS containing 2% FCS and purified by fluorescence-activated cell sorting (FACS) using their typical retinoid fluorescence emitted after UV light excitation (370 nm; FACS Aria III, BD Biosciences). Sorted HSC were collected in IMDM supplemented with 10% FCS and 1% antibiotic-antimycotic solution. The purity of HSC obtained by FACS was determined at day one by UV light excitation and their typical cell morphology showing lipid-containing droplets encircling the cell nucleus. Afterwards, HSC were washed with PBS and either harvested for RNA isolation or medium was changed to serum-free conditions. After two days of culture, conditioned serum-free culture medium of HSC from young and old rats was analyzed with regard to SASP factors (see section 2.11).

### **2.1.3. Culture of HSC under pulsatile laminar fluid flow**

HSC were isolated as described in section 2.1.1 and 3,000,000 cells were seeded on 10 cm petri dishes in DMEM with 10% FCS and 1% antibiotic-antimycotic

solution. At the following day, the HSC were washed with PBS without  $Mg^{2+}/Ca^{2+}$ , then detached by trypsin/EDTA and centrifuged for 5 min at 500xg. Afterwards, 250,000 cells in 100  $\mu$ l medium (DMEM with 10% FCS and 1% antibiotic-antimycotic solution) were seeded into so called ibidi  $\mu$ -Slides I<sup>0.4</sup> pre-coated with COL4 (80172; ibidi, Martinsried, Germany). When HSC adhered, each of the two reservoirs were filled with 60  $\mu$ l medium. In total eight  $\mu$ -Slides were prepared per experiment. After 24 hours, HSC were washed with PBS and medium was changed to serum-free (IMDM, 1% ITS containing albumin and linoleic acid, 1% antibiotic-antimycotic solution). On day three after isolation, the perfusion sets “yellow/green” (10964; ibidi) were mounted to the Fluidic Unit (10903; ibidi) and filled with 13.6 ml IMDM supplemented with 1% ITS/albumin/linoleic acid and 1% antibiotic-antimycotic solution. Furthermore, two  $\mu$ -Slides were connected by a serial connector (10830; ibidi) and connected  $\mu$ -Slides were integrated into the perfusion system. Subsequently, the tubes from the first Fluidic Unit (P1) were routed through the front pinch valves of the second Fluidic Unit (P2) as shown in Figure 5.



**Figure 5: Setup for HSC exposed to laminar pulsatile fluid flow with the ibidi perfusion system.** The perfusion system was mounted to a Fluidic Unit and filled with 13.6 ml of pre-warmed serum-free medium. Subsequently, two  $\mu$ -Slides with HSC were connected by a serial connector and integrated into the perfusion system. The tubing was then routed through the front pinch valves of a second Fluidic Unit in order to generate a pulsatile flow. Before the perfusion experiment was started, culture supernatant and cells were collected from one separate  $\mu$ -Slide as a starting point (0  $\text{dyn}/\text{cm}^2$ ). Subsequently, the channels with HSC were perfused for one hour with a low (2.9  $\text{dyn}/\text{cm}^2$ ), medium (15  $\text{dyn}/\text{cm}^2$ ) or high (29  $\text{dyn}/\text{cm}^2$ ) shear stress. Furthermore, the pulsatile flow was generated with a pulse of 150 bpm (2.5 Hz). Directly after the perfusion has been stopped, the culture supernatant was collected and analyzed using an HGF ELISA. HSC were collected for mRNA expression analyses by qPCR.

Next, pump, Fluidic Units, and computer were connected and settings for different shear stress experiments (Table 1) were applied in the PumpControl software (ibidi).

Before experiments were started, the medium from two separate  $\mu$ -Slides was collected as a starting point (0 dyn/cm<sup>2</sup>) and frozen at -20°C. Moreover, cells were collected for further analysis. Then, pulsatile flow experiments were performed for one hour. After each run, the cell culture supernatant was directly collected, frozen at -20°C, and stored until further analysis with the Mouse/Rat HGF Quantikine ELISA Kit (MHG00; R&D Systems). Finally, HSC were lysed for RNA extraction.

**Table 1: Settings for low, medium, and high shear stress during culture of HSC under laminar pulsatile flow.**

Parameter	Low shear stress	Medium shear stress	High shear stress
$\tau$ [dyn/cm <sup>2</sup> ]	2.9	15	29
p [mbar]	5.8	32.8	73.8
Q [ml/min]	3.06	15.82	30.6
Switching time P1 unidirectional [s]	120	20	12
Switching time P2 oscillating [s]	0.2	0.2	0.2
cycle duration [h]	1	1	1

P1: Fluidic Unit 1, P2: Fluidic Unit 2

## 2.2. CRISPR/Cas9-mediated *Itga5* and *Itgb1* knockouts in HSC

For the *Itga5* and *Itgb1* knockouts in freshly isolated HSC the guide RNA (gRNA) were designed with the program ChopChop V2 (Labun *et al.*, 2016) and synthesized with the GeneArt Precision gRNA Synthesis Kit (A29377; Invitrogen, Carlsbad, CA, USA) according to manufacturer's instructions. The target sequences for the gRNA as well as the forward and reverse primers are listed in Table 2.

**Table 2: Target sequences and primer pairs for *Itga5* and *Itgb1* gRNA.**

Gene	gRNA	Sequence	
<i>Itga5</i>	gRNA 1	target sequence	GGGCTTCAACCTAGACGCGGAGG
		forward primer	TAATACGACTCACTATAGGGGCTTCAACCTAGAC
		reverse primer	TTCTAGCTCTAAAACCCGCGTCTAGGTTGAAGCC
	gRNA 2	target sequence	CTCCGTGGAGTTTTACCGGCCGG
		forward primer	TAATACGACTCACTATAGCTCCGTGGAGTTTTAC
		reverse primer	TTCTAGCTCTAAAACGCCGGTAAAACCTCCACGGA
<i>Itgb1</i>	gRNA3	target sequence	GTTGGTCAGCAGCGCATATCTGG
		forward primer	TAATACGACTCACTATAGGTTGGTCAGCAGCGCA
		reverse primer	TTCTAGCTCTAAAACGATATGCGCTGCTGACCAA

HSC from mid-aged rats were isolated as described in section 2.1.1 and transfection was performed with the TrueCut Cas9 Protein v2 (A36499; Invitrogen) and the gRNA using the P3 Primary Cell 4D-Nucleofector X Kit L (V4XP-3024; Lonza, Basel, Switzerland) and the 4D-Nucleofector (Lonza) according to manufacturer's

recommendations. Therefore, 2,000,000 cells in 1 ml culture medium (DMEM, 10% FCS, 1% antibiotic-antimycotic solution) were centrifuged at 300xg for 5 min and re-suspended in 100  $\mu$ l of the transfection master mix composed of 82  $\mu$ l Nucleofactor solution (Lonza), 18  $\mu$ l supplement (Lonza), 1  $\mu$ l Cas9 protein (5  $\mu$ g), and 1  $\mu$ l gRNA (2  $\mu$ g). As control (mock), cells were transfected in presence of Cas9 protein but without gRNA. Subsequently, HSC were seeded in two wells of a 6-well plate in DMEM containing 10% FCS and 1% antibiotic-antimycotic solution. Furthermore, untransfected cells were seeded as a control. The next day, HSC were washed with PBS and fresh medium was added. After two additional days, HSC were collected for protein extraction in order to determine the knockout efficiency by Western blot as described below (see section 2.6) using the anti-integrin  $\alpha_5$  (ab150361; Abcam) and anti-integrin  $\beta_1$  (ab52971; Abcam) antibodies. For shear stress experiments, HSC were transferred to 10 ml of DMEM with 10% FCS and 1% antibiotic-antimycotic solution directly after transfection and then centrifuged at 300xg for 5 min. Afterwards, the cell pellet was re-suspended in 300  $\mu$ l medium and 100  $\mu$ l cell suspension of HSC with and without CRISPR/Cas9-mediated *Itga5* or *Itgb1* knockout were seeded in  $\mu$ -Slides I<sup>0.4</sup> pre-coated with COL4 (ibidi). Overall three  $\mu$ -Slides per condition were prepared. After cell attachment (~30 min) the two reservoirs of the  $\mu$ -Slide were each filled with 60  $\mu$ l medium. After 24 hours, cells were washed with PBS and serum-free medium was added (IMDM, 1% ITS/albumin/linoleic acid, 1% antibiotic-antimycotic solution). The next day, experiments were performed as described in section 2.1.3 under serum-free condition and a medium shear stress of 15 dyn/cm<sup>2</sup> (for settings see Table 1) was applied for one hour. Culture supernatants and cells from static (0 dyn/cm<sup>2</sup>) and shear conditions were collected before and after each experiment for further analyses by qPCR and the HGF Quantikine ELISA (MHG00; R&D Systems).

### 2.3. Liver injury models

After anesthesia of male Wistar rats (~250 g body weight, 8-10 weeks), the two largest liver lobes (70% of the liver mass) were surgically removed as described (Higgins and Anderson, 1931; Kordes *et al.*, 2014). For a liver regeneration model associated with the appearance of duct-forming liver progenitor cells, pellets containing 2-acetylaminofluorene (2AAF; 70 mg 2AAF release for 14 days; Innovative Research of America, Sarasota, FL, USA) were implanted under the skin

of the neck of Wistar rats seven days before PHx was performed as described (Tatematsu *et al.*, 1984; Kordes *et al.*, 2014). Tissue samples were taken after liver perfusion with physiologic buffer during the first two weeks of regeneration at indicated time points and included in qPCR (n = 3-5 per indicated time point) and immunofluorescence (n = 3) analyses. For quantification of HGF fluorescence intensity in tissue sections from normal and regenerating (PHx) rat liver, images from six different positions were analyzed with the cellSens Dimension 1.16 software (Olympus). The animal experiments were approved by the *Landesamt für Natur, Umwelt und Verbraucherschutz* (Recklinghausen, Germany; 9.93.2.10.34.07.163) and carried out by Dr. Claus Kordes and Dr. Iris Sawitza (Clinic of Gastroenterology, Hepatology and Infectious Diseases, Heinrich Heine University Düsseldorf).

#### **2.4. Gene expression analyses by microarray and qPCR**

The RNA was extracted from isolated HSC or whole liver tissue using the RNeasy Mini Kit (74106; Qiagen, Hilden, Germany) or the innuPREP RNA Mini Kit 2.0 (845-KS-2040250; Analytik Jena AG, Jena, Germany) according to the manufacturer's instructions. Afterwards, RNA amount and quality were measured in a DropSense spectrometer (Trinean, Gentbrugge, Belgium). The Revert Aid H Minus First Strand cDNA Synthesis Kit (K1632; Thermo Fisher Scientific, Waltham, MA, USA) was used for cDNA synthesis from 2 µg total RNA in a volume of 40 µl reaction buffer according to manufacturer's recommendations.

Quantitative PCR (qPCR) was performed with the qTower3 cycler (Analytik Jena AG, Jena, Germany). Therefore, 20 ng cDNA as well as 0.6 µM of the appropriate primer pair (Table 3) were applied for each reaction in the Maxima SYBR Green qPCR Mastermix (K0253; Thermo Fisher Scientific, Waltham, MA USA). The protocol started with an initial heating phase at 95°C for 5 min. Overall 45 cycles were performed with a denaturation phase at 95°C for 15 seconds, annealing at 60°C for 15 seconds, and elongation at 72°C for 20 seconds. Finally, a melting curve was assessed from 60°C to 95°C with a temperature increase of 1°C per 15 seconds.

RNA samples obtained from cultured HSC and whole liver tissues from young (2 months) and old (22 months) rats were sent to IMG M Laboratories (Martinsried,

Germany) for gene expression analyses by gene expression microarrays (Affymetrix, GeneChip Rat Gene 2.0 ST Array, Thermo Fisher Scientific) in triplicates for each age group. The array data were processed by the Transcriptome Analysis Console 3.0 (Thermo Fisher Scientific) and are available online at ArrayExpress database (<http://www.ebi.ac.uk/arrayexpress>; accession number: E-MTAB-7423).

**Table 3: Primer pairs for qPCR analyses.**

Gene	Accession no.	Forward primer	Reverse primer
CD133	NM_021751	TGCTCATGAGTCTTGGCATC	TGTGTTGTATTGCCCCAGAA
Col1a2	NM_053356	ACCTCAGGGTGTTC AAGGTG	GGGATTCCAATAGGACCAGA
Col4a1	NM_001135009	GTCCTCACTGTGGATTGGCTA	AGTAATTGCACGTTCTCTGC
Dag1	NM_053697	CGAGTGAGCATTCCAACAGAT	TGCAGCACTCACTGAGATGTAA
desmin	NM_02253	ACCTTCCGATCCAGACCTTCT	TTCATGTTGTTGCTGTGTGGC
e-cadherin	NM_031334	ACTTTGGTGTGGGTCTGGAG	GTTGACGGTCCCTTCACAGT
Eln	NM_012722	GTGGCTATGGACTGCCCTATAC	CCTCCAGCAGCTCCATACTTAG
Fn	NM_019143	ATGTTGGAGTGTGGTGTCTGG	GTGTCCTGATCATTGCATCTGT
Gfap	NM_017009	ACATCGAGATCGCCACCTAC	TCCACCGTCTTTACCACGAT
Hgf	NM_017017	CGAGCTATCGCGGTAAGAC	TGTAGCTTTCACCGTTGCAG
Hprt1	NM_012583	AAGTGTGGATACAGGCCAGA	GGCTTTGTA CTGGCTTTTCC
Il6	NM_012589	TACCCCAACTTCCAATGCTC	GGTTTGCCGAGTAGACCTCA
Itga3	XM_006247215	CCCTCAAGAACGATTGTGAAC	AGACCACAGCACCTTGGTGTA
Itga5	NM_001108118	CCCAAAGGAAACCTCACCTAT	TCATCTAGCCCATCTCCATTG
Itga6	NM_053725	GGCTCTTGTGACGCAAGGAGTA	CAACTTCATAGGGCCCATCTT
Itgb1	NM_017022	TTGGACACTGTTCCATGCGTA	TTGAAGGCTCTGCACTGAACA
Itgb3	NM_153720	GGCCTCAAGATTGGAGACAC	GCAGTCACAGTCACAGTCGAA
Itgb4	NM_013180	CTGCTCATCTTCTCCTGTTG	TCCCGCAGCATATAGTGATCT
Lama1	NM_001108237	TTTAAGGGCTGCATGGGAGAG	TTATCTGTGTCACGGTGGGAC
Lama2	XM_017590488	GGGACACGAACGATGAGGAAA	TTTTCACTTCGATGGGCTGCT
Lama4	NM_001309447	ACTATGTCAGTGAGGCCAACG	CTGGCTTGATTGAGAAGGTTG
Lama5	NM_001191609	CAAATGAGCATCGCCTTCCTG	CCAGCACCATCATGAGTTCCT
Lamb1	XM_003750137	CGTGGACTCTGTGGAGAAGAA	CTCCGTGAAGCTGTGTCAGAT
Lamb2	NM_012974	CAGAGCTGGAATTGGTGGTG	TGTAGGAGAGACCAGGCTCAA
Lamc1	NM_053966	GCCTTTTCAACTCTGGAAGGA	ACTTGAGGACTTTGGGGTTCAT
Lrat	NM_022280	GACCTACTGCAGATACGGCTC	TATGATGCCAGGCCTGTGTAG
Lu/Bcam	NM_031752	GAGGATTACGATGCTGACGAG	ATCTGCAACGGTCACAGAATC
nestin	NM_001308239	GATCGCTCAGATCCTGGAAG	AGGTGTCTGCAACCGAGAGT
Nid1	XM_213954	TGTGCCAACAATAGACACCAG	AAGATCCTTCCCTTCACCTTG
Nid2	NM_001012005	ATTCACCATGGAGGCAGTTC	CCGGGGTATTGTAACAGATG
Notch1	NM_001105721	ACAGTGGGGTATGCAAGGAG	ATTGGTGTCTGGCAAGAGG
Notch3	NM_020087	CTACCTTGGCTCTGCTGAAAA	AGCCTGTCCAAGTGATCTGTG
Pparγ	NM_013124	GAGCCTTCAAACCTCCCTCAT	CTTCAATCGGATGGTTCTTC
reelin	NM_080394	CTGCAATACAGCGTCAACAAC	CCACTGATCATGACCTGTTCC
Sdc1	NM_013026	CCTTTTGGACAGGAAGGAAGT	GGCTCCTCCAAGGAGTAACTG
Sparcl1	NM_012946	CCTCAAATACGGAGAGGAGAC	GTCCCTTTTACTACTGGAAGT
α-Sma	NM_031004	GCACTACCATGTACCCAGGCA	TGCGTTCTGGAGGAGCAATA

Gene ontology (GO) term analysis of significantly altered genes (fold change > 2,  $p < 0.05$ ) with regard to biological processes was performed with the Gene ontology enrichment analysis and visualization software GOrilla (October 2018; <http://cbl-gorilla.cs.technion.ac.il/>) published by Eden *et al.* (2009).

Additionally, RNA from liver tissue of six additional animals per age group was isolated for qPCR analyses as described above. The sequences of all expression primers are listed in Table 3. The oligonucleotides were obtained from Eurofins MWG Synthesis GmbH (Ebersberg, Germany) or Eurogentec Deutschland GmbH (Cologne, Germany). The qPCR raw data were normalized to the Ct values of the housekeeping gene hypoxanthine-guanine phosphoribosyl transferase 1 (*Hprt1*) and the  $\Delta\Delta\text{Ct}$ -method was used for the calculation of relative expression changes (Livak and Schmittgen, 2001).

## 2.5. Immunofluorescence analyses of isolated HSC and liver sections

Cultured HSC were either fixed with ice-cold methanol for 5 min or 4% formalin for 15 min according to the antibody manufacturer's recommendations. In case of formalin fixation, the cells were permeabilized with 0.1% Triton X-100 (T8787; Sigma-Aldrich) for 5 min and washed with PBS. Cryosections (10  $\mu\text{m}$ ) of normal and regenerating rat liver tissue sections were fixed in ice-cold methanol for 5 min and then air dried, while liver sections from young and old rats were either fixed in ice-cold methanol or 4% formalin (Roti-Histofix; P087; Carl Roth, Karlsruhe, Germany) for 15 min depending on the binding properties of the primary antibody. After blocking of unspecific binding sites with 10% FCS in PBS for one hour at room temperature, cells or tissue sections were incubated with primary antibodies in PBS containing 2% FCS at 4°C overnight in a humid atmosphere. The primary antibodies used for staining of isolated HSC and tissue sections from normal, regenerating, and aged rat liver are listed in Table 4. At the following day, samples were washed with PBS and incubated with anti-mouse or anti-rabbit secondary antibodies (dilution 1:200) labelled with cyanine dye 3 (Cy3; AP192C; Merck/Millipore) or fluorescein isothiocyanate (FITC; AP192F; Merck/Millipore) for two hours at room temperature. Subsequently, cells or tissue sections were washed and mounted with Fluoromount G containing 4',6-diamidino-2-phenylindole (DAPI; 0100-20; Southern Biotech, Birmingham, AL, USA) and a cover slip. For each staining, images of isolated HSC and of different liver tissue sections were acquired with the same exposure times

using an Olympus IX50 inverted microscope equipped with a DP71 camera (Olympus). All immunofluorescence analyses were repeated with HSC and tissue sections from normal, regenerating, and aged rat liver that derived from at least three different animals. For quantification of fluorescence intensities in rat liver tissue, images from at least three different positions per section were taken and analyzed with the cellSens Dimension 1.16 software (Olympus).

**Table 4: Primary antibodies for immunofluorescence analyses.**

Antibody	Catalog no.	Manufacturer	Fixation	Dilution
<b>CD133</b>	ab19898	abcam, Cambridge, UK	methanol	1:100
<b>CK18</b>	BM2275P	Acris, Herford, Germany	methanol	1:100
<b>CK19</b>	NB100-687	Novus Biologicals, Littleton, CO, USA	methanol	1:100
<b>COL1</b>	C2456	Sigma-Aldrich, Munich, Germany	methanol	1:100
<b>COL4</b>	ab6586	abcam, Cambridge, UK	methanol	1:100
<b>desmin</b>	ab8592	abcam, Cambridge, UK	methanol	1:100
<b>FN</b>	610078	Becton Dickinson, Franklin Lakes, NJ, USA	formalin	1:100
<b>GFAP</b>	12389	Cell Signaling, Danvers, MA, USA	methanol	1:100
	MAB3402	Merck/Millipore, Darmstadt, Germany	methanol	1:100
<b>HGF</b>	80429-R052	Sino Biological, Beijing, China	methanol	1:100
<b>ITGA5</b>	ab150361	abcam, Cambridge, UK	methanol	1:100
<b>ITGB1</b>	ab52971	abcam, Cambridge, UK	formalin	1:100
<b>ITGB4</b>	ab29042	abcam, Cambridge, UK	formalin	1:100
<b>LAMA2</b>	AMAb91166	Atlas Antibodies, Bromma, Sweden	methanol	1:100
<b>LAMA5</b>	NBP2-42391	Novus Biologicals, Littleton, CO, USA	methanol	1:100
<b>LU/BCAM</b>	MAB1481	R&D Systems, Minneapolis, MN, USA	methanol	1:50
<b>nestin</b>	sc-33677	Santa Cruz, Dallas, TX, USA	methanol	1:50
<b>Notch1</b>	sc-6014-R	Santa Cruz, Dallas, TX, USA	methanol	1:100
<b>p-47phox</b>	SAB4504721	Sigma-Aldrich, Munich, Germany	methanol	1:200
<b>reelin</b>	ab78540	abcam, Cambridge, UK	methanol	1:50
<b>SPARCL1</b>	sc-514275	Santa Cruz, Dallas, TX, USA	formalin	1:50
<b><math>\alpha</math>-SMA</b>	M0851	Dako/Agilent, Santa Clara, CA, USA	methanol	1:100
<b>8-OHG</b>	12501	QED Bioscience, San Diego, CA, USA	formalin	1:200

## 2.6. Western blot analyses of isolated HSC and liver tissue

Protein samples were obtained from HSC cultured for three days on uncoated PS, from HSC cultured for seven days on laminin-coated and uncoated PS or from HSC three days after CRISPR/Cas9 transfection. Protein analyses of whole cell lysates or membrane fraction (Membrane Protein Extraction Kit, K3014005; BioChain, Newark, CA, USA) were performed using the semidry Western blot technique according to standard protocols. For this purpose, 40  $\mu$ g of protein lysates were separated by 10% sodium dodecyl sulfate (SDS) polyacrylamide gels and blotted

on nitrocellulose membranes (10600002; GE Healthcare, Chicago, IL, USA). In case of  $\alpha$ -SMA protein analysis only 5  $\mu$ g protein was loaded. To verify the specificity of different laminin  $\alpha$  chain antibodies for immunofluorescence analysis of normal, regenerating and aged liver cryosections, 5  $\mu$ g of commercially available recombinant LN-111, LN-211, and LN-521 (BioLamina, Sweden) were separated by 10% SDS polyacrylamide gels, blotted on nitrocellulose membranes, and incubated with the primary antibodies against laminin  $\alpha$  chains (Table 5).

**Table 5: Primary antibodies for Western blot analyses.**

Antibody	Catalog no.	Sample	Manufacturer	Dilution
<b>Annexin II</b>	610068	membrane fraction	Becton Dickinson, Franklin Lakes, NJ, USA	1:5,000
<b>CD133</b>	ab19898	membrane fraction	abcam, Cambridge, UK	1:5,000
<b>COL4</b>	ab6586	cell lysate	abcam, Cambridge, UK	1:5,000
<b>desmin</b>	ab8592	liver tissue	abcam, Cambridge, UK	1:5,000
<b>e-cadherin</b>	610182	cell lysate	Becton Dickinson, Franklin Lakes, NJ, USA	1:5,000
<b>FN</b>	610078	cell lysate liver tissue	Becton Dickinson, Franklin Lakes, NJ, USA	1:5,000
<b>GFAP</b>	MAB360	cell lysate liver tissue	Merck/Millipore, Darmstadt, Germany	1:5,000
<b>HGF</b>	LS-C486534	liver tissue	Lifespan Biosciences, Seattle, WA, USA	1:2,500
<b>ITGA5</b>	ab150361	cell lysate liver tissue	abcam, Cambridge, UK	1:5,000
<b>ITGB1</b>	ab52971	cell lysate liver tissue	abcam, Cambridge, UK	1:5,000
<b>LAMA1</b>	TA322579 L9393	recombinant LN-111	OriGene, Rockville, MD, USA Sigma-Aldrich, Munich, Germany	1:2,500 1:5,000
<b>LAMA2</b>	AMAb91166	recombinant LN-211	Atlas Antibodies, Bromma, Sweden	1:5,000
<b>LAMA5</b>	NBP2-42391 sc-20145	recombinant LN-521	Novus Biologicals, Littleton, CO, USA Santa Cruz, Dallas, TX, USA	1:5,000 1:1,000
<b>Notch1</b>	sc-6014-R	cell lysate	Santa Cruz, Dallas, TX, USA	1:1,000
<b>Notch3</b>	55114-1-AP	cell lysate	Proteintech, Manchester, UK	1:1,000
<b><math>\alpha</math>-SMA</b>	M0851	cell lysate liver tissue	Dako/Agilent, Santa Clara, CA, USA	1:10,000
<b><math>\gamma</math>-tubulin</b>	T5326	cell lysate liver tissue	Sigma-Aldrich, Munich, Germany	1:10,000

For the protein analyses of liver tissue from young (2 months) and old (22 months) rats, 150  $\mu$ g of whole protein lysates were separated by 10% SDS polyacrylamide gels and blotted on nitrocellulose membranes.

All primary antibodies were diluted either in 5% fat-free milk powder (T145.3; Carl Roth) or 5% bovine serum albumin (BSA; 8076.3, Carl Roth) according to manufacturer's recommendations and are listed in Table 5. Incubation of nitrocellulose membranes with the primary antibodies was conducted on a rocking

platform overnight at 4°C. The Precision Plus Protein All Blue Standards (161-0373; BioRad, München, Germany) was used as a marker for protein molecular weights. The detection was carried out by incubating the nitrocellulose membranes with horseradish peroxidase (HRP)-coupled goat-anti-mouse (AP192P; Merck/Millipore) or goat-anti-rabbit (AP182P; Merck/Millipore) antibodies (dilution 1:20,000), respectively, on a rocking platform for two hours at room temperature and Western Bright Quantum (K-12042-D20) or Sirius (K-12043-D20) HRP substrates (Advansta, Menlo Park, CA, USA). Finally, visualization and documentation was performed with the ChemiDoc Imaging System (BioRad). The intensities of Western blot protein bands were analyzed using the multiplex band analysis tool of the AlphaView 3.4.0.0 software (Proteinsimple, San Jose, USA). The intensity of  $\gamma$ -tubulin bands was used for normalization of the data obtained by the analyses of whole cell or liver tissue lysates, while the intensity of Annexin II bands was used for normalization of membrane fractions. Stripping was performed by incubating the nitrocellulose membranes with Roti-Free Stripping Puffer 2.0 (3319.2; Carl Roth) on a rocking platform for 15 min at room temperature.

## 2.7. Quantitative mass spectrometric analysis of rat liver matrix

To investigate the laminin composition in hepatic ECM, three normal rat livers were perfused once with PBS (without  $\text{Ca}^{2+}/\text{Mg}^{2+}$ ) and three times with 500 ml PBS (with  $\text{Ca}^{2+}/\text{Mg}^{2+}$ ) containing increasing concentrations of Triton X-100 (1%, 2%, and 3%; T8787; Sigma-Aldrich). Afterwards, three perfusion steps were performed with 1,000 ml PBS (with  $\text{Ca}^{2+}/\text{Mg}^{2+}$ ) supplemented with increasing amounts of SDS (0.1%, 0.5%, and 1%; 1057.1; Carl Roth) each containing 20 mg DNase (DN25-1G; Sigma-Aldrich). Finally, decellularized liver tissue was flushed with 1,000 ml of deionized water and frozen in liquid nitrogen. All perfusion steps were performed at a flow rate of 10-15 ml/min at room temperature. For the comparison of the protein composition in young and old rat hepatic ECM, three livers from 2-months-old and three livers from 22-months-old rats were decellularized as described above. Samples from the remaining ECM were collected from three different liver lobes per animal, pooled, and finally lyophilized for bottom-up mass spectrometric analysis essentially as described for muscle cell cultures (Grube *et al.*, 2018).

The following steps were performed by the Molecular Proteomics Laboratory (*Biologisch-Medizinisches Forschungszentrum*, Heinrich Heine University

Düsseldorf, Germany) as described in Rohn *et al.* (2018). Protein samples of ECM proteins were analyzed as previously described (Grube *et al.*, 2018). Briefly, decellularized liver tissue from three rat livers were prepared in cell lysis buffer (30 mM Tris-HCl; 2 M thiourea; 7 M urea; 4% CHAPS (w/v) pH 8.0 in water) and 5 µg of protein shortly separated in a polyacrylamide gel (about 5 mm running distance). The gel was subjected to silver staining and protein bands were cut out from the gel and further processed for mass spectrometric analysis. Therefore, proteins were reduced and alkylated followed by tryptic digestion. Resulting peptides were extracted from the gel and finally resuspended in 0.1% trifluoroacetic acid. Subsequently, 500 ng of peptides plus 20 fmol Peptide Retention Time Calibration Mixture (Pierce/Thermo Fisher Scientific, Darmstadt, Germany) were first separated over two hours using an UltiMate 3000 rapid separation liquid chromatography system. The chromatography system was online coupled to a QExactive high resolution mass spectrometer operated in positive mode via a nano-electrospray interface. First, survey scans were carried out at a resolution of 70,000 (at 400 m/z) over a scan range from 350-2000 m/z. The target value for the automatic gain control was 3,000,000 and the maximum fill time 80 ms. The 10 most intense doubly and triply charged peptide ions were isolated within a 2 m/z window by the build in quadrupole and fragmented by higher energy collisional dissociation (HCD). Peptide fragments were analyzed over a maximal scan range from 200-2000 m/z with a maximal fill time of 60 ms and automatic gain control target value of 100,000 at a resolution of 17,500 (at 400 m/z). Already fragmented ions were excluded from fragmentation for 100 seconds. Protein and peptide identification and quantification were carried out within the MaxQuant environment (version 1.6.1.0, MPI for Biochemistry, Planegg, Germany) with standard parameters if not otherwise stated. Searches were carried out using the peptide sequences from the spiked in peptides as well as the 29966 UP000002494 rat proteome sequences downloaded from the UniProt KB on 10<sup>th</sup> April 2018. Label-free quantification and iBAQ was enabled as well as the match between the runs option. In a first search, carbamidomethyl on cysteines was considered as fixed and methionine oxidation, N-terminal acetylation, and Arginine +10 and Lysine +8 as variable modifications. The latter two modifications were omitted in a second search. Proteins and peptides were accepted with a false discovery rate of 1% and only proteins accepted showing at least two different peptides and valid values in at least two replicates. For further

calculations, iBAQ intensities were used: absolute protein amounts were calculated on the results of the second search after normalization on iBAQ intensities of the spiked in peptides (20 fmol/sample, results of the first search).

Processed raw data were provided by the Molecular Proteomics Laboratory (*Biologisch-Medizinisches Forschungszentrum*, Heinrich Heine University Düsseldorf, Germany) and data was further used for calculating mean values of relative laminin amounts in the hepatic ECM by Friederike Rohn. In case of young and old rat liver matrix, mean values of different laminins, nidogens (NID), collagens (COL), elastin (ELN), and fibronectin (FN) were calculated.

## **2.8. Liquid chromatography-tandem mass spectrometry (LC-MS/MS)**

Isolated HSC were cultured on either uncoated PS or PS coated with LN-211 or LN-521 as described in section 2.1.1. After one week, cells were washed twice with PBS, collected in 500 µl PBS, and stored at -20°C until quantification of retinoids was performed.

Analyses of retinol and retinyl palmitate contents in cell extracts were conducted by Dr. Diran Herebian (Department of General Pediatrics, Neonatology and Pediatric Cardiology, Medical Faculty, Heinrich Heine University Düsseldorf, Germany) with LC-MS/MS as described (van Breemen *et al.*, 1998) and are published in Rohn *et al.* (2018). The system consisted of an ExionLC AD UHPLC (ultra-performance high pressure liquid chromatography; SCIEX, Framingham, MA, USA) coupled to a QTRAP 5500 mass spectrometer (SCIEX), which was equipped with an electrospray ionization (ESI) source. A Kinetex EVO C18 column (Phenomenex, Torrance, CA, USA) was used for separation of the analytes (100 mm x 2.1 mm x 2.6 µm). Mobile phase A consisted of water containing 10 mM ammonium formate with 0.1% formic acid. Mobile phase B consisted of acetonitrile/2-propanol (v/v; 5/2) including 10 mM ammonium formate and 0.1% formic acid. Gradient mode of 6 minutes was used with a flow rate of 0.4 ml/min. The detection was performed in a positive ion mode. The data were collected in the multiple reaction monitoring (MRM) mode. Retinol (R7632; Sigma-Aldrich) and retinyl palmitate (46959; Sigma-Aldrich) were used as external standards and retinyl acetate (46958; Sigma-Aldrich) was used as internal standard. The data were acquired by Analyst 1.6 software, quantified by MultiQuant 3.0.2 software (SCIEX) and submitted to Friederike Rohn

for further processing. The data were normalized to total cell number, which was assessed by counting the cells with the cellSens Dimension 1.16 software (Olympus) on microscopic images at five different positions prior to sample collection.

## 2.9. Generation of nanostructured glass surfaces

Generation, passivation, and bio-functionalization of nanostructured glass surfaces was carried out by the group of Professor Dr. Joachim P. Spatz (Max-Planck-Institute for Medical Research, Heidelberg, Germany) as described in Rohn *et al.* (2018). Nanostructured glass surfaces were produced by diblock-copolymer micelle nanolithography as previously described (Spatz *et al.*, 2000; Glass *et al.*, 2003; Lohmüller *et al.*, 2011) with an average particle spacing of  $71 \pm 12$  nm,  $102 \pm 12$  nm or  $151 \pm 35$  nm as determined by scanning electron microscopy. Briefly, 2 mg/ml of polystyrene(1200)-b-poly-2-vinylpyridine(556) (Polymer Source, Dorval, QC, Canada), 1.5 mg/ml of polystyrene(1680)-b-poly-2-vinylpyridine(666) or 1 mg/ml of polystyrene(1680)-b-poly-2-vinylpyridine(666) (Polymer Source), respectively, were dissolved in toluene p.a. Subsequently, tetrachloroauric acid to vinylpyridine monomer ratio of 0.5 were added to the solutions and stirred for 24 hours. The solutions were spin-coated on 20 x 20 mm N°1 glass coverslips (Carl Roth). Afterwards, the substrates were subjected to a plasma procedure (10% H<sub>2</sub> / 90% Ar, 350 W, 0.4 mbar, 45 min), followed by a thermal treatment in an oven at 500°C for 24 h. To prevent non-specific adhesion of any proteins to the glass substrate in-between the gold nanostructures, the glass surfaces were passivated as described (Blümmel *et al.*, 2007). Therefore, the nano-patterned surfaces were activated in an oxygen plasma (150 W, 0.4 mbar, 10 min) and incubated at 80°C overnight in dry toluene p.a. (Acros Organics, USA) containing 0.25 mM  $\alpha$ -methoxy- $\omega$ -trimethoxysilyl poly(ethylene glycol) (PEG; molecular weight 2000 g/mol) (Iris Biotech, Marktredwitz, Germany), 5.5  $\mu$ M water and 20 mM dried trimethylamine (Acros Organics) under nitrogen atmosphere. Finally, the substrates were washed thrice with ethyl acetate (Acros Organics, USA), once with methanol (VWR, Radnor, PA, USA) and dried under N<sub>2</sub> flow. The gold-nanoparticles glass surfaces with PEG passivation layers were bio-functionalized by incubating with 50 nM of LN-211 or LN-521 (BioLamina) in Dulbecco's PBS supplemented with 0.5 mM MgCl<sub>2</sub> and 1 mM CaCl<sub>2</sub> for one hour at room temperature. The bio-functionalized surfaces were

subsequently washed thrice with PBS for 5 min and sent to Friederike Rohn for performing the cell culture experiments described in section 2.1.1.

### **2.10. Scanning electron microscopy**

Acquisition of scanning electron microscopy images was performed by the group of Professor Dr. Joachim P. Spatz as described in Rohn *et al.* (2018). Therefore, bio-functionalized glass surfaces were dehydrated by washing with increasing concentrations of ethanolic solutions (10% (v/v) steps in PBS). Subsequently, samples were critical-point-dried in a CPD 030 critical-point-dryer, (Bal-Tec, Pfäffikon, Switzerland) and coated with an 8 nm carbon layer (MED020 coating system; Bal-Tec). Images were acquired using a Zeiss Ultra 55 scanning electron microscopy system (Carl Zeiss AG, Oberkochen, Germany) equipped with an in-lens detector operated at 5 kV.

### **2.11. Analysis of SASP factors in serum and HSC culture medium**

For the detection of SASP factors in the rat blood serum or in the serum-free conditioned culture medium of isolated HSC from young and old rats, the Proteome Profiler Rat Cytokine Array Kit (ARY008; R&D Systems) was used according to the manufacturer's instructions. For this purpose, 750 µl of the serum samples from each rat (n = 4 for both age groups) were used and 10 out of 29 factors showed a reaction on the membrane and could be analyzed. In case of culture supernatants, in which HSC from young and old rats had been cultured for two days under serum-free conditions, 1 ml of the medium was used for analysis (n = 3 for both age groups). Here, only two factors could be detected on the membrane. Visualization and documentation were performed with ChemiDoc Imaging System (BioRad) and protein dot intensities were analyzed with the AlphaView 3.4.0.0 software (Proteinsimple, San Jose, CA, USA).

Furthermore, the concentrations of CXCL3 and IL6 in culture supernatants of HSC from young (n = 5) and old (n = 3) rats were quantified with the Rat CXCL3/CINC-2 alpha/beta Quantikine ELISA Kit (RCN200, R&D Systems) and the Rat IL6 Quantikine ELISA Kit (R6000B, R&D Systems) according to manufacturer's recommendations. Data from the cytokine array and ELISA analyses were normalized to cell number per area which was assessed by counting the cells with

the cellSens Dimension 1.16 software at three different positions of each culture dish (Olympus).

## **2.12. Statistics**

Values from at least 3 independent experiments or from at least 3 different rats are presented as means and their variation is indicated as standard error of the mean ( $\pm$  SEM). For multiple testing the significance of differences was determined by the Kruskal-Wallis test and a significance level smaller than 0.05 was applied. For comparisons between two groups the Mann-Whitney U test was used and p-values smaller than 0.05 were considered significant. Significantly different groups are indicated by different symbols (\*, #) or letters (a, b, c, d). Groups sharing the same letters did not differ significantly. Statistical analysis was carried out by the winSTAT software version 2012.1.0.96 (R. Fitch Software, Bad Krozingen, Germany). The boxplot in Figure 30 shows the median, the box represents 50% of the data and the upper and lower whiskers represent the maximum and minimum, respectively.

Microarray gene expression analyses of HSC and liver tissue from 2-months and 22-months-old rats performed by IMG Laboratory (section 2.4) were conducted in triplicates for each group and significant differences were determined by analysis of variance (ANOVA) with p-values smaller than 0.05. Principal component analysis (PCA) on microarray raw data was conducted with the software Transcriptome Analysis Console 4.0.0.25 (AppliedBiosystems, Thermo Fisher Scientific).

### 3. Results

The presence of different laminin chains in normal rat liver was investigated as well as their expression during liver regeneration and aging. Furthermore, experiments are presented in which the influence of laminins on HSC maintenance and function was analyzed.

In addition, analyses of alterations in HSC and their niche due to aging processes are described. In this regard, the influence of fluid mechanical forces – known to be decreased in the aged liver – on HSC function was investigated. Finally, a possible receptor involved in sensing and transduction of shear stress in HSC was identified.

#### 3.1. Influence of LN-521 on HSC maintenance

The LAMA5 chain is an important element of stem cell niches and supports stem cell maintenance (Laperle *et al.*, 2015). Since HSC are liver-resident MSC (Kordes *et al.*, 2013), the presence of the LAMA5 chain in normal and injured rat liver was investigated (section 3.1.1) and its effect on the maintenance of HSC quiescence and their stem cell characteristics was analyzed *in vitro* (sections 3.1.2 to 3.1.5).

##### 3.1.1. Laminin $\alpha$ 5 expression patterns in normal and regenerating rat liver

The specificity of several anti-laminin  $\alpha$  chain antibodies was evaluated by Western blot analysis of commercially available laminin trimers (LN-111, LN-211, LN-521; Figure 6) before they have been used for immunofluorescence analysis of liver tissue sections. Monoclonal antibodies against LAMA1 (OriGene), LAMA2 (Atlas Antibodies), and LAMA5 (Novus Biologicals) specifically labeled protein bands of commercially available recombinant LN-111, LN-211, and LN-521 proteins, respectively (Figure 6). These antibodies were used for immunofluorescence staining of normal and regenerating rat liver sections.

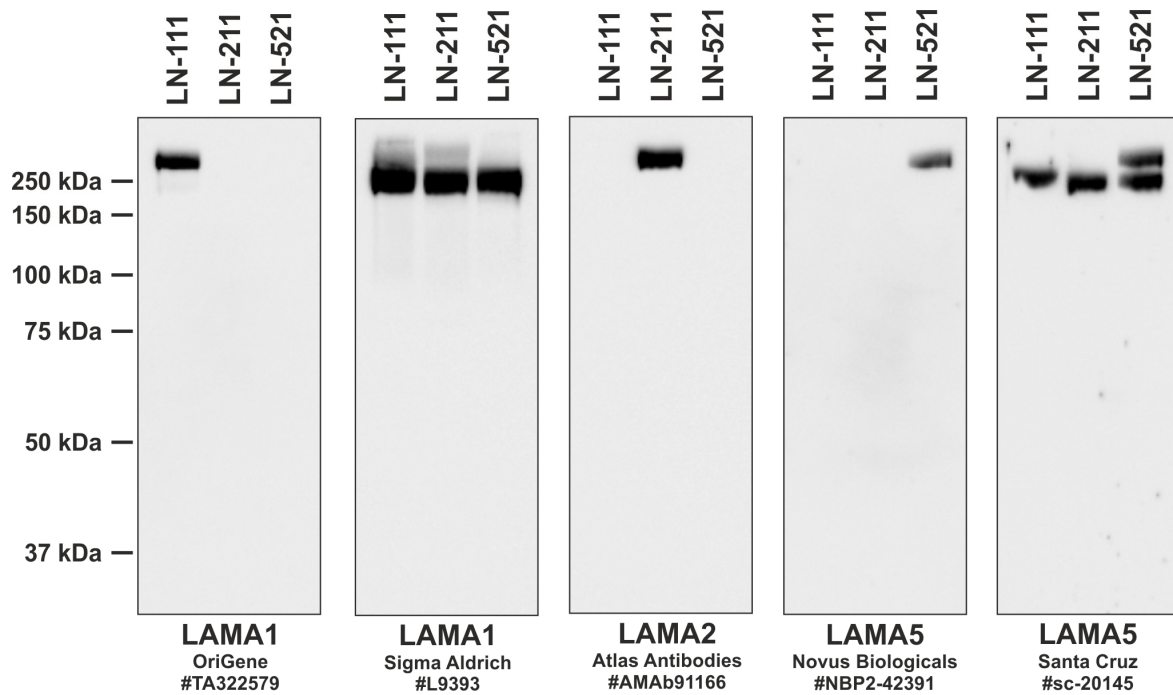


**Figure 6: Verification of the specificity of anti-laminin  $\alpha$  chain antibodies.** Different anti-laminin  $\alpha$  chain (LAMA1, LAMA2, LAMA5) antibodies were tested regarding their specificity by Western blot analyses with commercially available recombinant laminins LN-111, LN-211, and LN-521 (BioLamina, Sweden). Only three of five tested antibodies labeled the correct  $\alpha$  chains. Specific monoclonal antibodies against LAMA1 (OriGene), LAMA2 (Atlas Antibodies), and LAMA5 (Novus Biologicals) were considered suitable for further analyses. Modified from Rohn *et al.* (2018).

LAMA5 was present in liver sinusoids of normal rat liver (Figure 7A) where it co-localized with GFAP-positive quiescent HSC (Figure 7B).

Furthermore, normal rat liver tissue was decellularized by detergents in order to investigate the presence of different laminin chains in the hepatic ECM. Quantitative mass spectrometric analysis revealed that LAMA5 was the most abundant  $\alpha$  chain, laminin  $\beta$ 2 (LAMB2) the dominant  $\beta$  chain and LAMC1 the only detectable  $\gamma$  chain in the rat liver matrix (Figure 7C). These three laminin chains are subunits of a functional LN-521 trimer. Since also the LAMB1 chain was detectable in the rat liver matrix another possible trimer composition could be LN-511.

Furthermore, the matrisome analysis revealed presence of the laminin  $\alpha$ 4 chain (LAMA4) in the hepatic ECM (Figure 7C). In accordance with the low *Lama1* mRNA levels (see section 1.4) and the weak LAMA1 immunofluorescence in rat liver tissue, the LAMA1 protein chain was not detectable by proteome analysis of normal rat liver matrix (Figure 7C).

It was previously observed that the *Lama5* mRNA expression was significantly upregulated during liver regeneration associated with facultative liver progenitor cells (see section 1.4; Figure 4A).

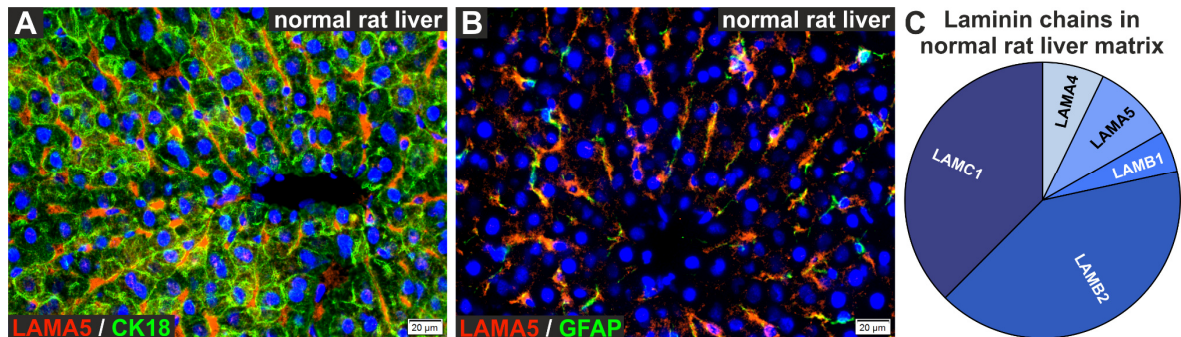


**Figure 7: Laminin protein chains in normal rat liver.** (A) LAMA5 (red) was detected in liver sinusoids between CK18-positive hepatocytes (green) as determined by immunofluorescence of normal rat liver sections. (B) GFAP-positive HSC (green) co-localized with LAMA5 (red) in liver sinusoids. Cell nuclei were stained by DAPI (blue). Representative images are shown. (n = 3; scale bars A, B: 20  $\mu$ m). (C) Quantitative mass spectrometric analysis (iBAQ method) of hepatic ECM revealed that LAMA5 was the most abundant  $\alpha$  chain, LAMB2 the dominant  $\beta$  chain, and LAMC1 the only detectable  $\gamma$  chain in normal rat liver matrix (n = 3). Modified from Rohn *et al.* (2018).

Inhibition of hepatocyte proliferation after liver injury by the treatment of rats with 2AAF one week before PHx caused duct-like structures (ductular reaction), which were generated by cytokeratin 19-positive (CK19) putative liver progenitor cells (Figure 8B2, D2). In the 2AAF/PHx liver injury model, LAMA5 co-localized with COL4 that surrounded the CK19-positive duct forming cells (Figure 8A, B). Additionally, LAMA5 was still detectable in the liver sinusoids.

On the contrary, LAMA2 chain was not found in areas of ductular reaction, suggesting differential functions of LAMA5 and LAMA2 chains during liver regeneration (Figure 8C, D). The overall weak fluorescence signal of LAMA2 was in line with the proteome analysis of rat liver matrix, which did not detect LAMA2 in the hepatic ECM (Figure 8C1, D1; Figure 7C).

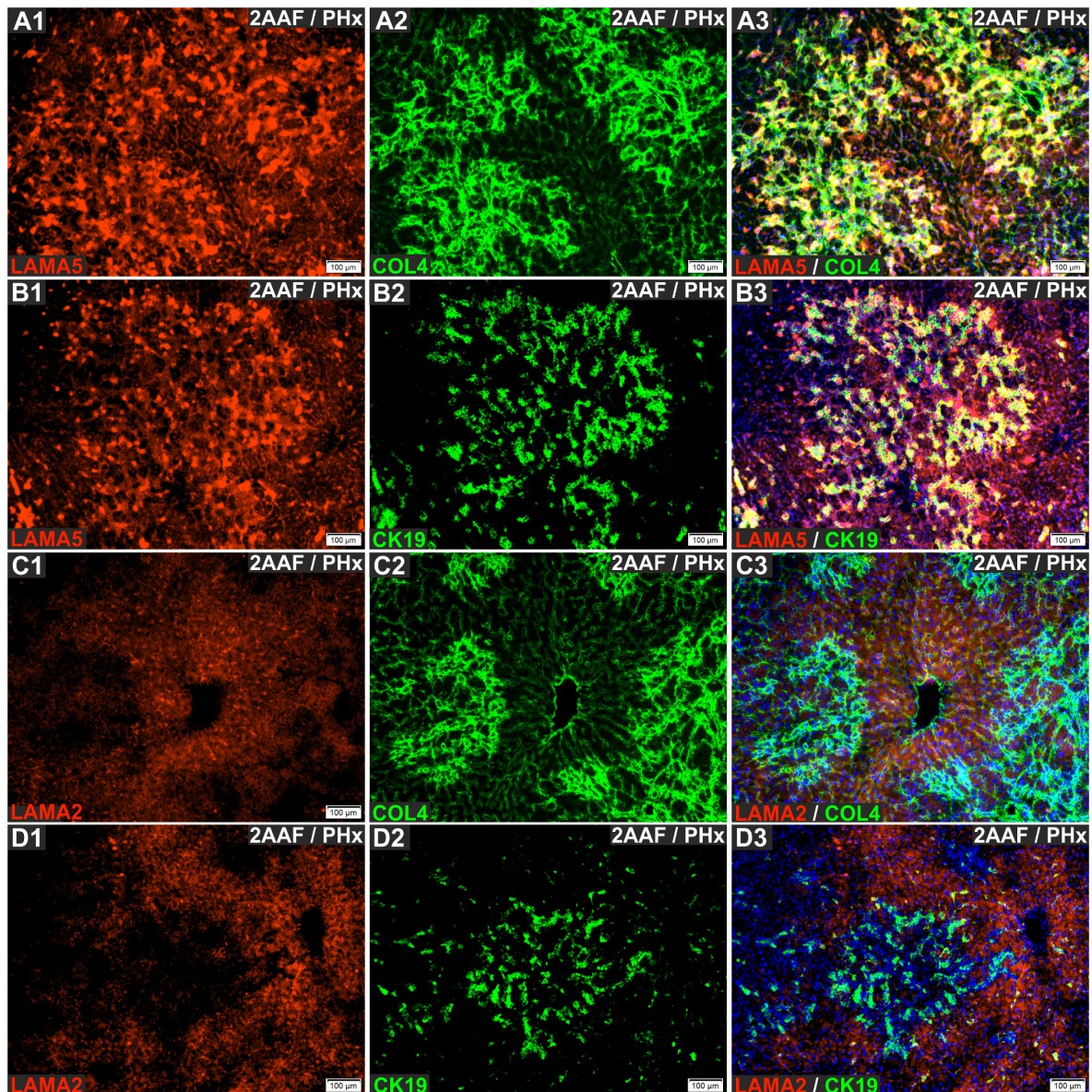


**Figure 8: Laminin  $\alpha$  protein chains in regenerating rat liver.** (A1-3) During liver regeneration associated with the appearance of liver progenitor cells seven days after PHx, LAMA5 (red) was mainly detected in liver sinusoids and areas of ductular reaction that were also indicated by pronounced COL4 (green) deposition. (B1-3) CK19-positive duct-forming cells (green) co-localized with LAMA5 (red). LAMA2 (red; C1, D1) fluorescence signal intensity was overall weaker and nearly undetectable in areas of ductular reaction. Hence, it did not co-localize with (C1-3) COL4 or (D1-3) CK19-positive cells (green). Cell nuclei were stained by DAPI (blue). Representative images are shown (n = 3; scale bars: 100  $\mu$ m). Modified from Rohn *et al.* (2018).

### 3.1.2. Improved HSC adhesion and maintenance on LN-521

Freshly isolated rat HSC were cultured on uncoated PS or surfaces coated with LN-521 (PS/LN-521) or LN-211 (PS/LN-211) for 7 days under serum-free conditions and finally characterized. HSC seeded on PS/LN-521 adhered significantly better than on PS and PS/LN-211 as analyzed four hours after cell seeding (Figure 9A, E).

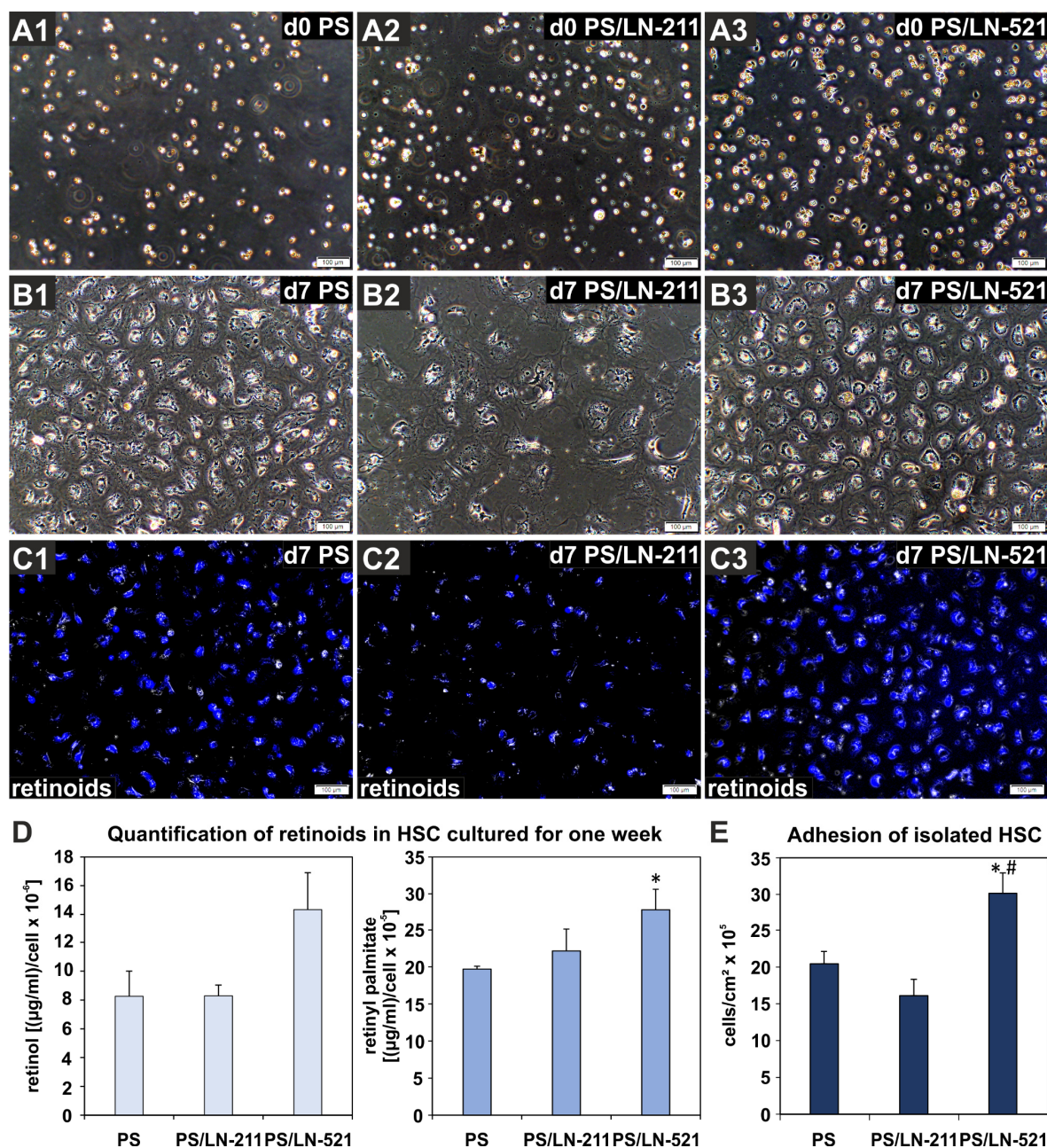


**Figure 9: Cell adhesion, morphology and retinoid storage of HSC cultured on uncoated or laminin-coated surfaces. (A1-3)** Directly after cell isolation (d0), the adhesion of HSC was improved on PS/LN-521 compared to PS/LN-211 or PS. **(B1-3)** After seven days of culture, HSC on PS and PS/LN-211 showed a myofibroblast-like cell morphology, whereas cells on PS/LN-521 appeared more homogeneous. **(C1-3)** In addition, retinoid-storing lipid droplets were retained in HSC on PS/LN-521 compared to cells on PS and PS/LN-211 as indicated by the characteristic retinoid fluorescence after UV light excitation (blue). Representative images are shown ( $n = 3$ ; scale bars A-C:  $100 \mu\text{m}$ ). **(D)** Retinol (left) and retinyl palmitate (right) contents of HSC cultured for one week on uncoated or laminin-coated PS were quantified by LC-MS/MS. Retinoid amounts normalized to cell number were elevated in HSC on PS/LN-521 compared to HSC cultured on PS and PS/LN-211. **(E)** A significantly higher number of HSC adhered on PS/LN-521 compared to PS and PS/LN-211 as ascertained four hours after cell seeding. Data are indicated as means  $\pm$  SEM ( $n = 3-5$ ; \*  $p < 0.05$  laminins vs. PS; #  $p < 0.05$  PS/LN-211 vs. PS/LN-521). Modified from Rohn *et al.* (2018).

After one week of culture, HSC on PS and PS/LN-211 showed less retinoid-containing lipid droplets and developed a myofibroblast-like cell morphology (Figure 9B, C), whereas cells cultured on PS/LN-521 increased in size but showed a homogeneous morphology and retained their retinoid droplets typical for freshly isolated HSC (Figure 9B3, C3). The presence of retinoids in HSC on PS/LN-521 was indicated by a strong retinoid autofluorescence after UV light excitation. To investigate this in more detail, the retinol and retinyl palmitate content of HSC was quantified by LC-MS/MS after seven days of culture. The LC-MS/MS analyses revealed that the overall retinoid amount was better preserved in HSC on PS/LN-521 compared to HSC on PS and PS/LN-211 (Figure 9D). The improved adhesion, the more homogeneous cell morphology as well as the maintenance of retinoids suggested a better preservation of HSC characteristics on PS/LN-521.

### 3.1.3. Reduced HSC activation on LN-521

The positive effect of LN-521 on HSC characteristics was further evaluated by qPCR analysis of genes associated with their quiescent and activated states that show significant alterations during one week of culture under serum-free conditions (Figure 10). Suitable markers for HSC quiescence were identified by comparative qPCR of freshly isolated and culture-activated HSC. *Gfap*, *Notch1*, *reelin*, *Sparcl1*, *Lrat*, *Ppar $\gamma$* , and e-cadherin were selected, since their expression decreased during HSC activation (Figure 10A). In contrast to this,  $\alpha$ -*Sma*, collagen I (*Col1a2*), collagen IV (*Col4a1*), *Notch3*, integrin  $\beta$ 1 (*Itgb1*), fibronectin (*Fn*), and nestin were identified as suitable indicators of HSC activation (Figure 10B). HSC cultured on uncoated and laminin-coated surfaces for one week under serum-free conditions showed no differences in mRNA expression of the myofibroblast marker  $\alpha$ -*Sma* (Figure 11A). Nevertheless, HSC  $\alpha$ -SMA protein levels were significantly reduced by  $32\% \pm 7\%$  in HSC cultured on PS/LN-521 compared to cells on PS, while there was no marked decrease in HSC on PS/LN-211 as analyzed by Western blot (Figure 11C, E). The gene expression of *Col1a2* was also not altered in HSC on PS/LN-521, but it was slightly lowered on PS/LN-211 compared to PS. In contrast, the expression of collagen IV mRNA was significantly downregulated by  $16\% \pm 3\%$  and its protein by  $32\% \pm 18\%$  in cells on PS/LN-521 compared to uncoated PS surface. In comparison to HSC cultured on PS, PS/LN-211 only minor reduced COL4 mRNA and protein amounts in HSC (Figure 11A, C, E).

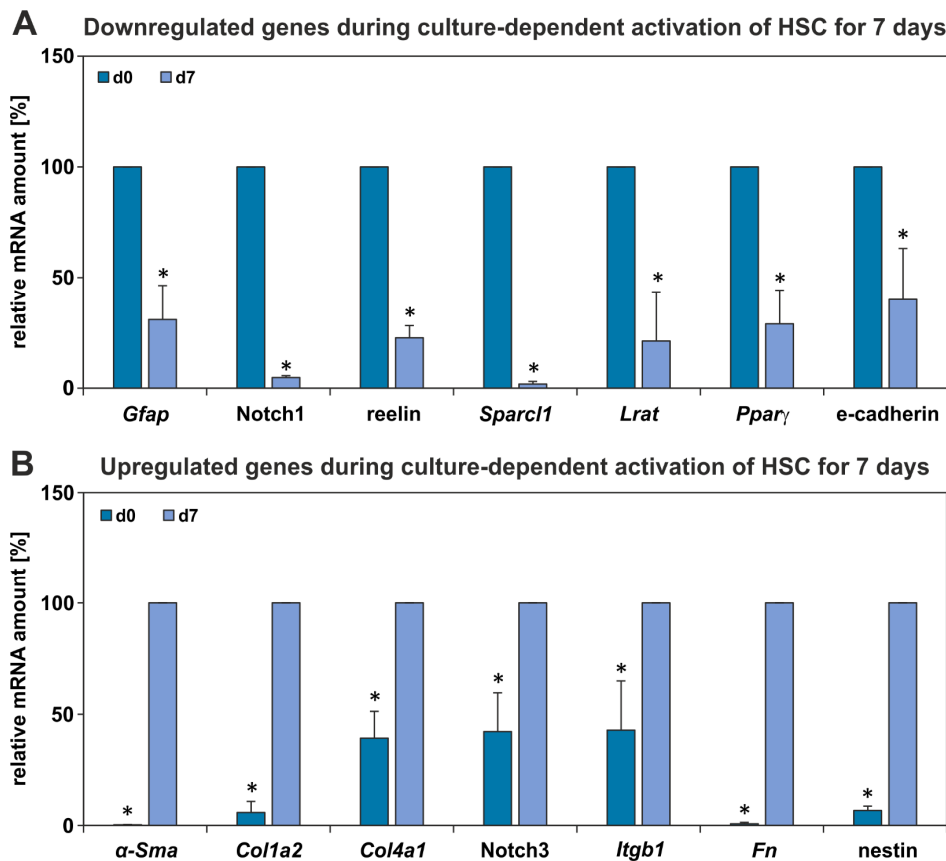


**Figure 10: Identification of genes showing significant expression changes during culture-dependent activation of HSC. (A)** Expression analyses by qPCR of HSC cultured for one week on PS (d7) revealed a significant downregulation of *Gfap*, *Notch1*, *reelin*, *Sparcl1*, *Lrat*, *Pparγ*, and *e-cadherin* compared to freshly isolated HSC (d0, four hours after cell seeding). **(B)** In contrast, mRNA levels of *α-Sma*, *Col1a2*, *Col4a1*, *Notch3*, *Itgb1*, *Fn*, and *nestin* were significantly upregulated in HSC after seven days on PS. The highest expression of each gene was set to 100%. The data are presented as means  $\pm$  SEM ( $n = 3$ ; \*  $p < 0.05$ ). Modified from Rohn *et al.* (2018).

Moreover, the activation markers Notch3 and ITGB1 showed a marked decrease in HSC on PS/LN-521 compared to cells on PS. Notch3 was significantly reduced by  $21\% \pm 8\%$  at mRNA level and by  $74\% \pm 6\%$  at protein level in HSC on PS/LN-521 (Figure 11A, C, E). In contrast, cells cultured on PS/LN-211 showed no altered Notch3 mRNA expression, but lowered Notch3 protein amount. The expression of ITGB1 was reduced in HSC on PS/LN-521 by  $10\% \pm 6\%$  at mRNA and by  $42\% \pm 17\%$  at protein level (Figure 11A, C, E). Also HSC on PS/LN-211 tended to decrease ITGB1 expression at mRNA and protein levels. In addition, *Fn* mRNA was significantly reduced by  $22\% \pm 6\%$  in HSC cultured on PS/LN-521 compared to HSC cultured on PS, which was also observed at protein level (Figure 11A, C, E). Furthermore, *Fn* mRNA expression was significantly lower in cells on PS/LN-521 compared to HSC on PS/LN-211. In contrast, HSC cultured on PS/LN-211 showed a slight upregulation of fibronectin at mRNA and protein level.

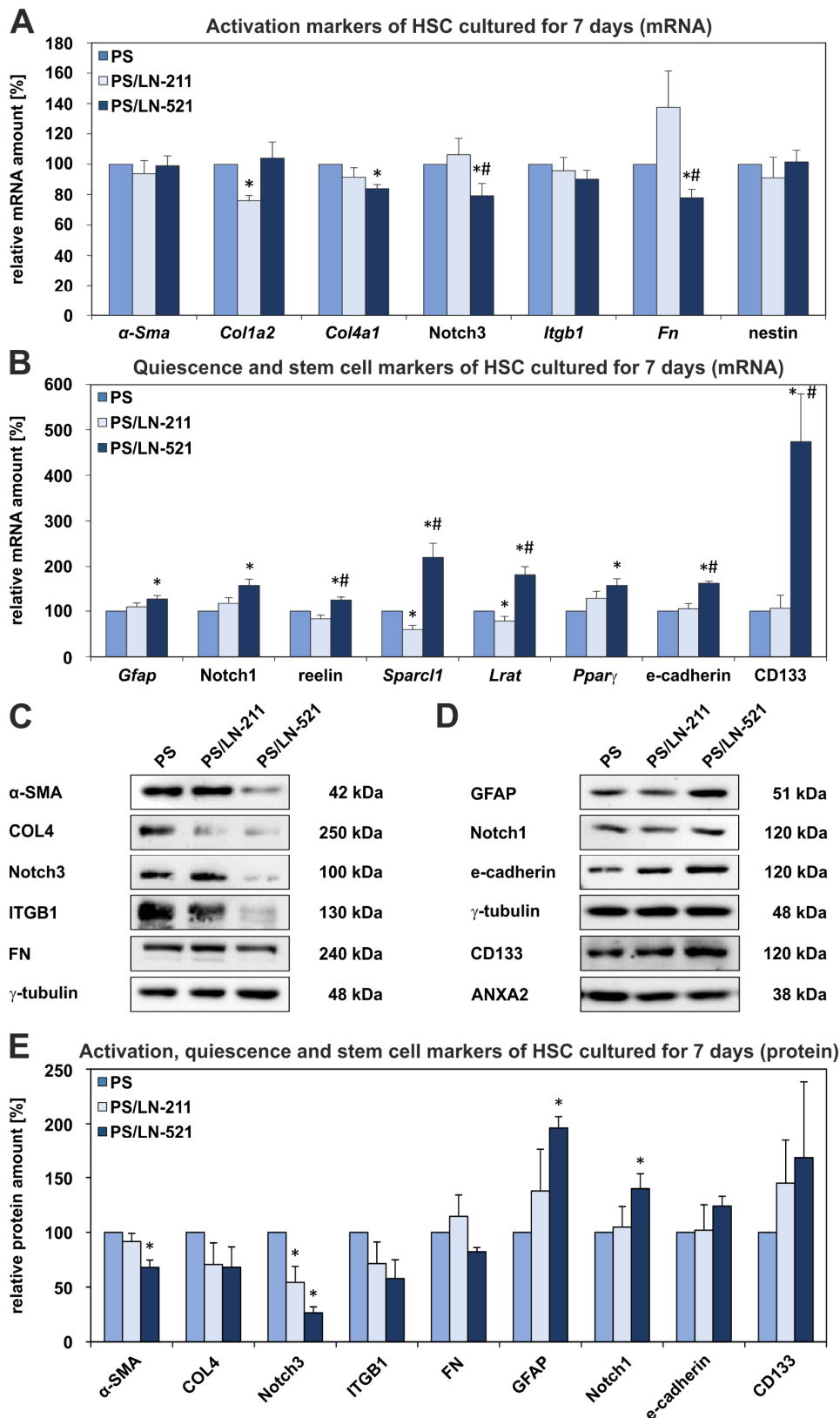


**Figure 11: PS/LN-521 promotes HSC quiescence.** (A) HSC cultured for seven days on PS/LN-521 showed a significant downregulation of *Col4a1*, *Notch3*, and *Fn* expression compared to cells cultured on uncoated PS and PS/LN-211 as demonstrated by qPCR. In contrast, the mRNA levels of  *$\alpha$ -Sma* and *nestin* were not differentially altered in HSC on different culture surfaces. (B) Furthermore, qPCR analyses revealed that HSC cultured on PS/LN-521 for one week showed significantly increased mRNA expression of quiescence markers. For instance, *Gfap*, *Notch1*, *reelin*, *Sparcl1*, *Lrat*, and *Ppar $\gamma$*  as well as of the stem cell-associated markers *e-cadherin* and *CD133* were increased compared to the HSC

**Figure 11 continued:** cultured on uncoated PS and PS/LN-211. The mRNA expression of HSC cultured for one week on PS was set to 100% for each independent experiment and data are presented as means  $\pm$  SEM ( $n = 10$ ; \*  $p < 0.05$  laminins vs. PS; #  $p < 0.05$  PS/LN-211 vs. PS/LN-521). **(C)** Representative Western blots of activation markers in HSC cultured for seven days on different surfaces. Whole cell lysates were analyzed and the protein  $\gamma$ -tubulin served as a loading control. **(D)** Representative Western blots of quiescence markers analyzed in lysates of HSC cultured under similar conditions for which  $\gamma$ -tubulin served as loading control. CD133 was detected in membrane protein fractions and Annexin II (ANXA2) was used as loading control. **(E)** Densitometric analyses of protein bands of activation markers in HSC cultured for seven days on laminin-coated and uncoated surfaces. The Western blot data supported qPCR results and showed reduced protein amounts of  $\alpha$ -SMA, COL4, Notch3, ITGB1, and FN in HSC on PS/LN-521. However, HSC cultured on PS/LN-211 also downregulated these markers compared to HSC on PS. The mean values of the quiescence and stem cell-associated markers GFAP, Notch1, e-cadherin, and CD133 were higher in HSC on PS/LN-521 compared to PS and PS/LN-211 as determined by Western blot analyses. Nevertheless, the protein amounts of quiescence markers were also slightly increased in HSC cultured on PS/LN-211 compared to cells on PS. The protein amount of HSC incubated for one week on PS was set to 100% for each independent experiment. The data are indicated as means  $\pm$  SEM ( $n = 3-8$ ; \*  $p < 0.05$ ). Modified from Rohn *et al.* (2018).

The results of qPCR and Western blot analyses were supported by immunofluorescence of HSC cultured for seven days on uncoated or laminin-coated PS using antibodies against  $\alpha$ -SMA and COL4. This indicated reduced expression of activation-associated markers in HSC on PS/LN-521 but not on PS/LN-211 (Figure 12A, B). In contrast to nestin mRNA amount, which showed no significant alterations in HSC on uncoated and laminin-coated surfaces (Figure 11A), the strong nestin fluorescence signal suggested higher nestin protein levels in HSC on PS/LN-521 compared to PS and PS/LN-211 (Figure 12C). The gene expression and protein levels of quiescence markers were also analyzed in HSC on all three culture surfaces by qPCR and Western blot. In accordance to the decreased expression of activation markers in HSC on LN-521-coated surfaces, HSC cultured on PS/LN-521 significantly increased the expression of quiescence markers compared to the culture on PS, whereas HSC cultured on PS/LN-211 showed no consistent upregulation of markers associated with HSC quiescence (Figure 11B, D, E). For instance, HSC on PS/LN-521 significantly increased mRNA levels of *Gfap* by 26%  $\pm$  8%, *Notch1* by 56%  $\pm$  14%, and *Ppar $\gamma$*  by 56%  $\pm$  15% (Figure 11B). These genes also showed an increased expression in HSC on PS/LN-211, but without reaching significance. Furthermore, mRNA expression of *reelin*, *Spar11*, and *Lrat* significantly increased only in cells which had been cultured on PS/LN-521 for one week, but were reduced in HSC on PS/LN-211. While *reelin* mRNA expression was downregulated in HSC on PS/LN-211, it was increased on PS/LN-521 by 24%  $\pm$  7%.

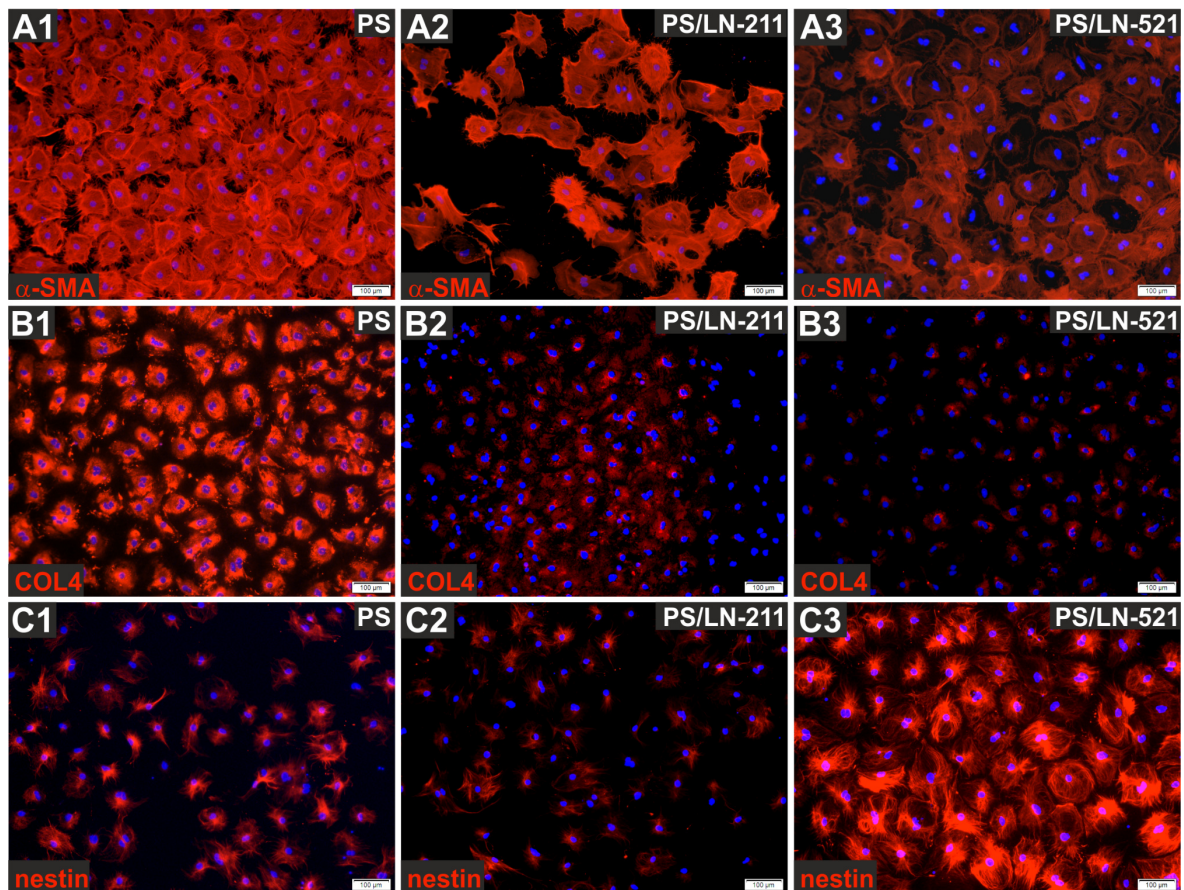


**Figure 12: Reduced activation in HSC cultured on PS/LN-521.** HSC incubated for one week on uncoated and laminin-coated PS surfaces were stained with antibodies against proteins associated with their activated state (red). The fluorescence signal of **(A1-3)**  $\alpha$ -SMA was lower in HSC on PS/LN-521 than in cells on PS and PS/LN-211, while **(B1-3)** COL4 protein was reduced in HSC on both laminins compared to HSC on PS. In contrast to nestin mRNA expression, **(C1-3)** nestin protein fluorescence signal intensity was stronger in HSC on PS/LN-521 compared to PS and PS/LN-211. Cell nuclei were stained by DAPI (blue;  $n = 3$ ). Representative images are shown ( $n = 3$ ; scale bars: 100  $\mu\text{m}$ ). Modified from Rohn *et al.* (2018).

Similar results were found with the mRNA of *Sparcl1*, which was lowered in cells on PS/LN-211 by  $41\% \pm 9\%$ , but increased in HSC on PS/LN-521 by  $120\% \pm 31\%$ . Additionally, HSC on PS/LN-211 significantly reduced *Lrat* expression, whereas it was significantly elevated by  $80\% \pm 20\%$  on PS/LN-521. Lastly, the expression of the stem-cell associated markers e-cadherin and CD133 was not altered in HSC on PS/LN-211, but significantly increased in cells on PS/LN-521 by  $61\% \pm 4\%$  and  $374\% \pm 105\%$ , respectively. The mRNA expression of all analyzed quiescence markers was significantly upregulated in HSC on PS/LN-521 compared to PS. In addition, reelin, *Sparcl1*, *Lrat*, e-cadherin, and CD133 also showed higher mRNA levels in HSC on PS/LN-521 compared to PS/LN-211 (Figure 11B). Moreover, mean

values of e-cadherin and CD133 protein amounts were higher on PS/LN-521 than on PS (Figure 11D, E).

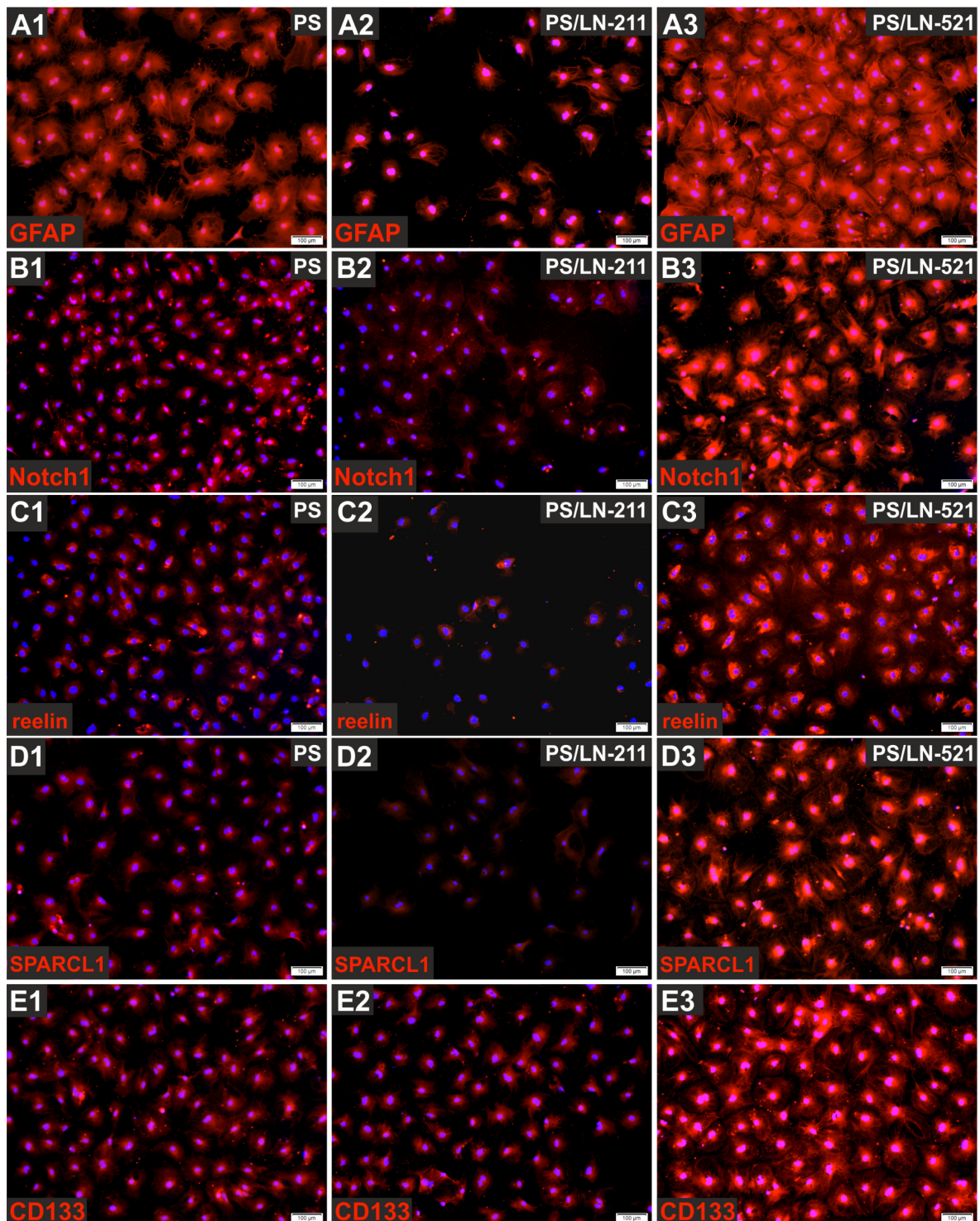


**Figure 13: Support of quiescence in HSC cultured on PS/LN-521.** Immunofluorescence staining with antibodies against (A1-3) GFAP, (B1-3) Notch1, (C1-3) reelin, (D1-3) SPARCL1, and (E1-3) CD133 in HSC cultured on PS, PS/LN-211 or PS/LN-521 for seven days demonstrated stronger fluorescence signal intensities of all quiescence and stem cell-associated markers in cells on PS/LN-521 compared to PS and PS/LN-211. Cell nuclei were stained by DAPI (blue). Representative images are shown (n = 3; scale bars: 100 µm). Modified from Rohn *et al.* (2018).

Overall, there were no significant differences between e-cadherin and CD133 expression in HSC on PS/LN-211 and PS. Immunofluorescence analysis of HSC on the different surfaces using antibodies against GFAP, Notch1, reelin, SPARCL1, and CD133 indicated a stronger fluorescence signal and, thus, a higher protein amount in HSC cultured for seven days on PS/LN-521 compared to PS/LN-211 and PS (Figure 13A-E). Hence, immunofluorescence images supported qPCR and Western blot data and also demonstrated the promotion of HSC quiescence on PS/LN-521. There was no obvious difference in the fluorescence intensities of CD133 in HSC on PS and PS/LN-211 (Figure 13E1, E2). Since e-cadherin, CD133, and nestin are expressed by embryonic and mesenchymal stem cells, culture of HSC on PS/LN-521 maintained not only quiescence but also stem cell characteristics of HSC. Western blot analyses supported the qPCR data and revealed a significant increase of GFAP by  $96\% \pm 10\%$  and of Notch1 by  $40\% \pm 14\%$  (Figure 11D, E).

To identify receptors that could be involved in laminin-mediated regulation of HSC quiescence and activation, mRNA expression analyses of integrin subunits (*Itga3*, *Itga6*, *Itgb1*, *Itgb4*) as well as of syndecan-1 (*Sdc1*), dystroglycan-1 (*Dag1*), and LAMA5-specific *Lu/Bcam* were conducted in HSC cultured for one week on uncoated or laminin-coated surfaces (Figure 14A). Furthermore, immunofluorescence analysis was performed in HSC on all three culture surfaces with antibodies against ITGB4 and LU/BCAM (Figure 14B-G). The qPCR and immunofluorescence analyses demonstrated a significant increase of ITGB4 in HSC cultured for one week on PS/LN-521 compared to PS and PS/LN-211 (Figure 14A-D). In contrast, *Itga6* and *Lu/BCAM* mRNA expression only tended to increase in HSC cultured on PS/LN-521 in comparison to PS and PS/LN-211 (Figure 14A). LU/BCAM also showed a stronger immunofluorescence signal in HSC on PS/LN-521 than on PS and PS/LN-211 (Figure 14E-G). In addition, LU/BCAM was detected in sinusoids of normal rat liver and additionally in areas of ductular reaction (2AAF/PHx liver regeneration model) where it co-localized with desmin-positive HSC (Figure 14H-J). These results suggest an involvement of integrins containing the subunit ITGB4 and of LU/BCAM in the maintenance of HSC.

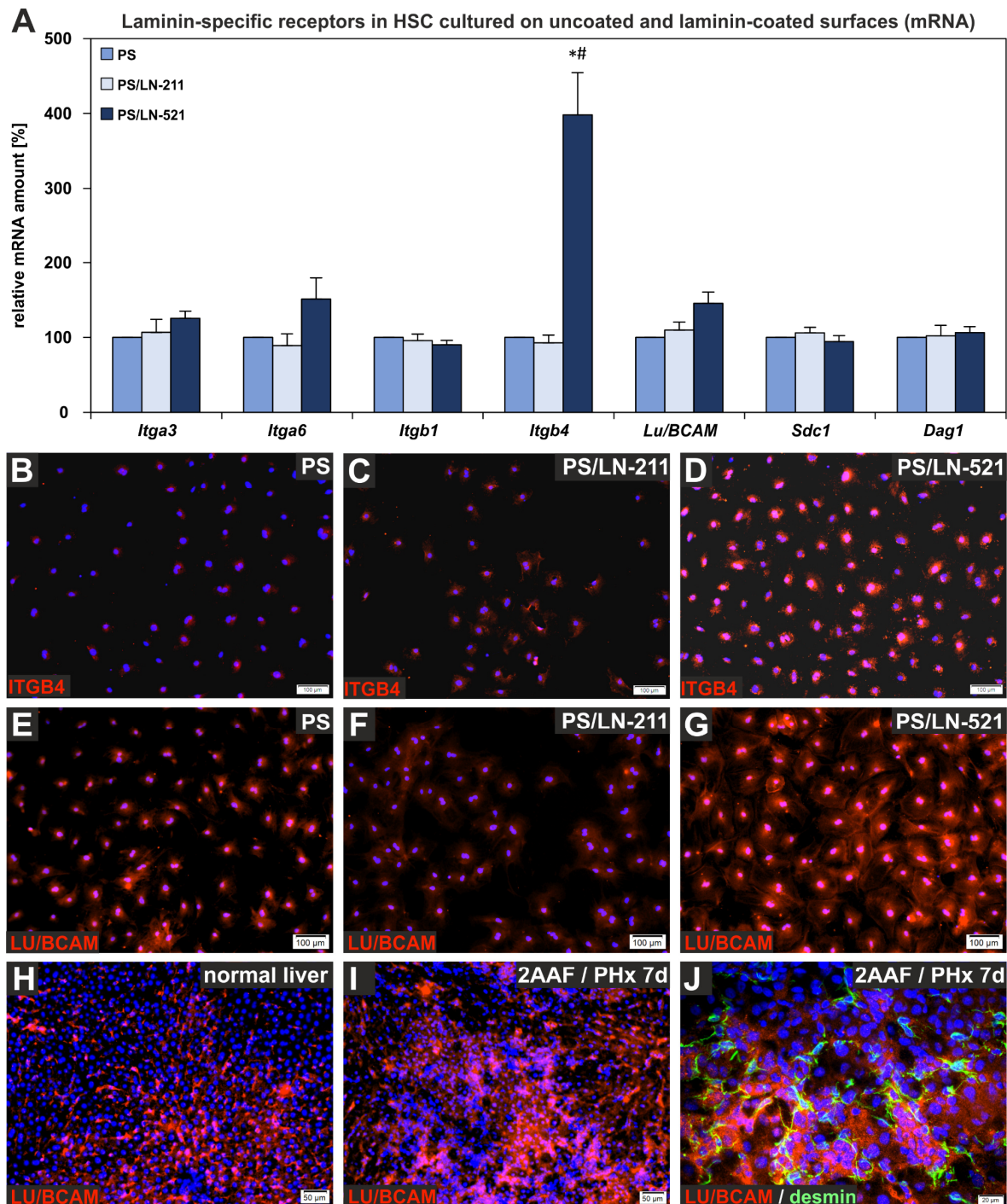


**Figure 14: Analyses of receptors capable to bind laminins in isolated HSC and in rat liver.** (A) The expression of *Itgb4* was significantly increased and of *Itga6* and *Lu/BCAM* slightly upregulated in HSC cultured on PS/LN-521 for one week compared to PS and PS/LN-211 as analyzed by qPCR. The mRNA expression of other laminin-specific receptors such as *Sdc1* and *Dag1* was not influenced by culture on laminins. Expression levels of HSC on PS were set to 100% for each independent experiment. The data are presented as means  $\pm$  SEM ( $n = 6-9$ ; \*  $p < 0.05$  laminins vs. PS; #  $p < 0.05$  PS/LN-211 vs. PS/LN-521). Immunofluorescence of (B-D) ITGB4 and (E-G) LU/BCAM (red) verified qPCR data and showed stronger fluorescence signals in HSC cultured for seven days on PS/LN-521 than on PS and PS/LN-211. Furthermore, LU/BCAM (red) was detected in liver sinusoids of (H) normal rat liver and additionally in areas of ductular reaction in the (I) 2AAF/PHx liver regeneration model where it co-localized with (J) desmin-positive (green) HSC seven days (7d) after injury. Cell nuclei were stained by DAPI (blue). Representative images are shown ( $n = 3$ ; scale bars B-G: 100  $\mu$ m, H-I: 50  $\mu$ m, J: 20  $\mu$ m). Modified from Rohn *et al.* (2018).

### 3.1.4. LN-521-coated nanostructured surfaces provide a biomimetic stem cell microenvironment

Coating of PS surfaces with laminin leads to random binding of laminin molecules. Therefore, LN-211 and LN-521 were bound to nanostructured surfaces in order to obtain defined distances between single laminin molecules and to improve the three-dimensional protein presentation. Bio-functionalized surfaces (FS) on which laminins were bound to gold dots with defined distances of either 70 nm, 100 nm or 150 nm were generated (Figure 15A, D). A PEG layer prevented binding of laminin between the single gold dots and, thus, also attachment of cells to the uncoated surface. To validate proper laminin binding to the gold dots, scanning electron microscopy images were acquired, which revealed that mostly one laminin molecule bound to one gold dot (Figure 15B, C).

Freshly isolated HSC were seeded on FS and cell number was ascertained after 24 hours (Figure 16A). Similar to laminin-coated PS (Figure 9E), also a higher number of HSC adhered to FS coated with LN-521 (FS/LN-521) than to FS coated with LN-211 (FS/LN-211). Moreover, the number of adherent HSC was inversely proportional to the distance between gold dots. After culture on bio-functionalized nanostructured surfaces for one week, HSC on FS/LN-521 retained most of their retinoid-containing lipid droplets as indicated by a strong retinoid fluorescence after UV light excitation, while cells on FS/LN-211 had lost most of their lipid droplets (Figure 15E, F). However, HSC on FS/LN-211 tended to form spheroids that showed a strong retinoid fluorescence (Figure 15E, insert). During culture time, spheroids started to detach from the surfaces and lowered the sample numbers for mRNA expression analysis.

Immunofluorescence of HSC cultured for one week on bio-functionalized surfaces with antibodies against SPARCL1 showed a stronger fluorescence signal on FS/LN-521 than on FS/LN-211 suggesting maintenance of their quiescent state (Figure 16B, C). HSC on FS/LN-211 formed spheroids, which showed strong SPARCL1 immunofluorescence (Figure 16B, insert). The immunofluorescence data were supported by qPCR analyses that revealed that the expression of the quiescence markers *Sparcl1*, *Lrat*, and *reelin* was generally higher on FS/LN-521 than on FS/LN-211 (Figure 16D-F). Interestingly, the mRNA levels of quiescence markers

in HSC cultured on FS/LN-521 were even comparable to freshly isolated HSC (Figure 16D-F, grey dashed lines).

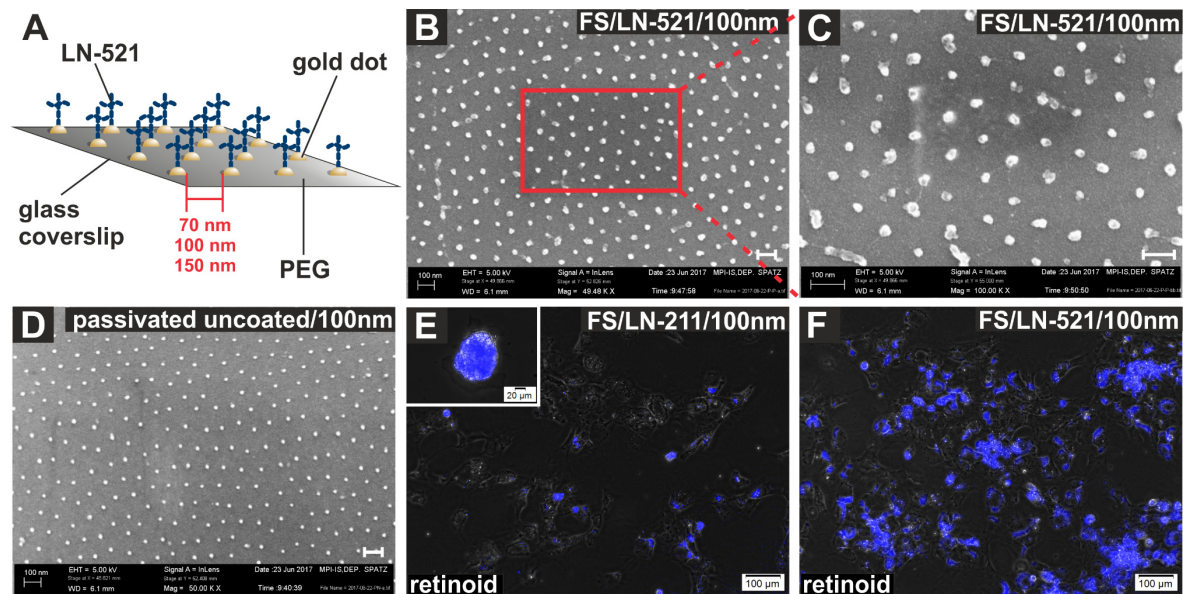


**Figure 15: Laminin-functionalized nanostructured surfaces.** (A) Schematic overview of nanostructured laminin-coated surface (FS), which was obtained by binding of laminin molecules via their cysteines to the gold dots. Gold dots were placed at a distance of 70 nm, 100 nm or 150 nm. The area between gold dots was passivated with poly(ethylene glycol) (PEG) in order to ensure laminin binding only to gold dots and, thus, HSC adhesion only to laminin. Orientation of laminin molecules was not controlled. (B-D) Representative scanning electron microscopy images of (B, C) PEG- and LN-521-coated and (D) only PEG-coated nanostructured surfaces with a defined spacing of 100 nm between single gold dots (scale bars B-D: 100 nm)<sup>2</sup>. (E) HSC on FS/LN-211 contained less retinoid-containing lipid droplets compared to (F) HSC on FS/LN-521 as demonstrated by higher retinoid fluorescence after UV light excitation (blue). However, in some areas on FS/LN-211 HSC formed spheroids with strong retinoid fluorescence (E insert). Representative images of HSC on FS with spacing of 100 nm (n = 3; scale bars E, F: 100  $\mu$ m and E insert: 20  $\mu$ m). Modified from Rohn *et al.* (2018).

Furthermore, defined spacing of LN-521 molecules on FS/LN-521 led to an elevated expression of quiescence markers compared to PS/LN-521. For instance, *Sparcl1* mRNA expression was significantly increased by about 2500-3500% when HSC were cultured on FS/LN-521 with different spacing (70 nm, 100 nm, 150 nm) compared to PS/LN-521 (Figure 16D). Moreover, upregulation of *Lrat* and *reelin* mRNA expression amounted to 200% in HSC on FS/LN-521 in comparison to cells cultured on PS/LN-521 (Figure 16E, F). Interestingly, *Sparcl1*, *Lrat*, and *reelin* showed also a slight increase on FS/LN-211 compared to PS/LN-211.

<sup>2</sup> Scanning electron images were acquired by the group of Professor Dr. Joachim P. Spatz (Max-Planck-Institute for Medical Research, Heidelberg, Germany).

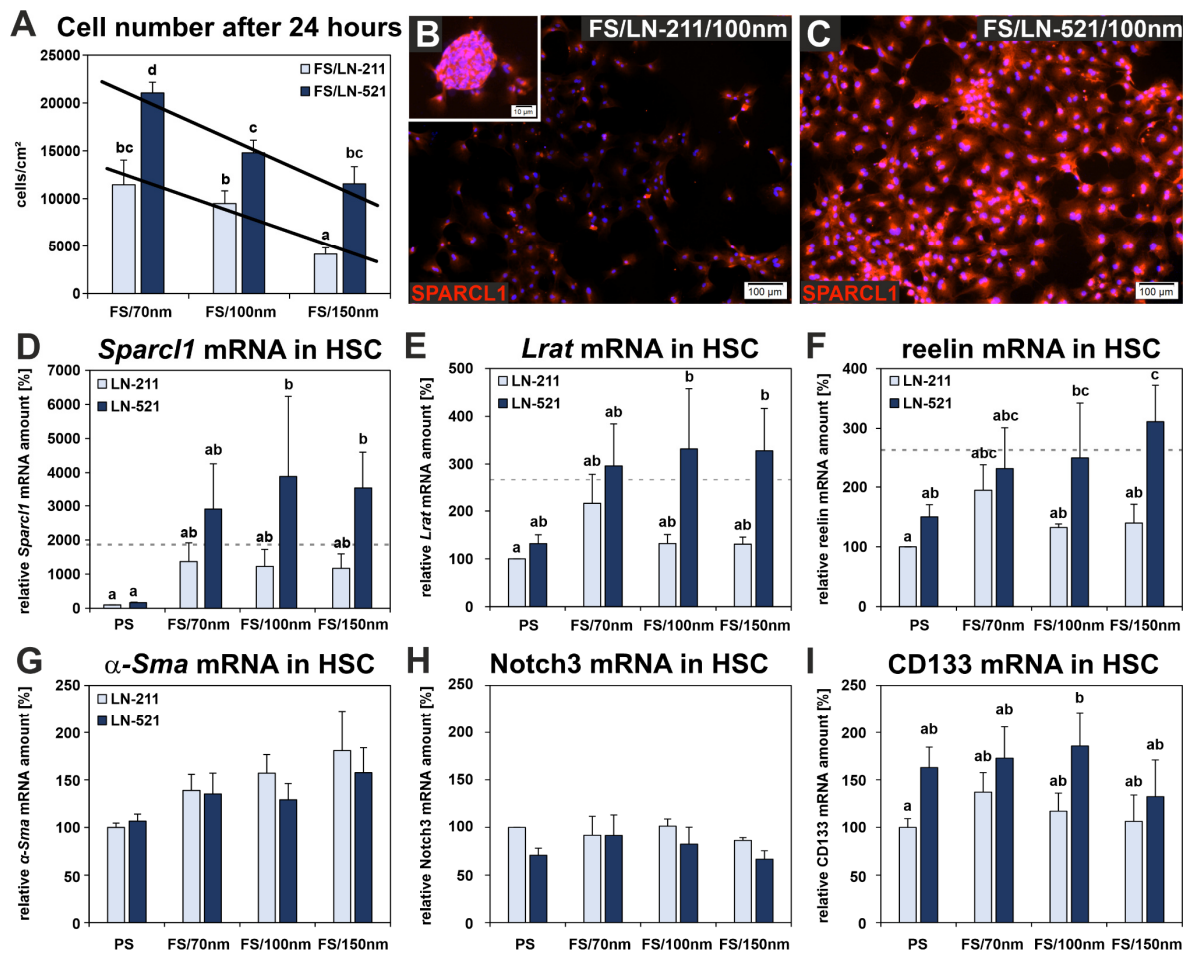


**Figure 16: Improved HSC quiescence on laminin-functionalized nanostructured surfaces.** (A) Significantly more cells adhered to LN-521 compared to LN-211-coated FS as ascertained 24 hours after cell seeding. Moreover, the cell number inversely correlated with increased distance between gold-dots. For a better overview, sub-groups of multiple comparison tests are indicated by letters (a, b, c, d). If data share similar letters, no significant difference was observed ( $n = 5$ ;  $p < 0.05$ ;  $R^2_{LN-211} = 0.93$  and  $R^2_{LN-521} = 0.97$ ). (B, C) Representative immunofluorescence images of HSC on FS (100 nm gold dot distance) using antibodies against SPARCL1 (red). HSC on (B) FS/LN-211 showed weaker SPARCL1 immunofluorescence than on (C) FS/LN-521. Cell spheroids were found on FS/LN-211 with strong SPARCL1 fluorescence (B insert). Cell nuclei were stained by DAPI (blue). Representative images are shown ( $n = 3$ ; scale bars B, C: 100  $\mu\text{m}$  and B insert: 10  $\mu\text{m}$ ). (D-F) Expression analyses by qPCR of HSC on PS and FS coated with different laminins after one week of culture revealed a marked upregulation of the quiescence markers (D) *Sparcl1*, (E) *Lrat*, and (F) *reelin* in HSC on FS/LN-521 compared to PS/LN-521. Moreover, the expression of quiescence-associated markers in HSC on FS/LN-211 was generally lower than in cells on FS/LN-521 surfaces. The grey dashed lines indicate average expression levels in quiescent HSC cultured for four hours after isolation on uncoated PS (0d,  $n = 3$ ). (G, H) Comparative expression analyses of HSC on PS and FS coated with different laminins by qPCR after one week of culture indicated that activation-associated markers were not significantly altered. (I) Furthermore, the stem cell-associated marker CD133 tended to increase on all LN-521-coated compared to LN-211-coated surfaces. PS/LN-211 was set to 100% for each independent experiment and data are indicated as means  $\pm$  SEM. Sub-groups of multiple comparison tests are indicated by letters (a, b, c). If data share similar letters, no significant difference was observed ( $n = 5$  except for FS/LN-211/100nm  $n = 4$  and FS/LN-211/150nm  $n = 3$ ;  $p < 0.05$ ). Modified from Rohn *et al.* (2018).

Nevertheless, the activation markers  $\alpha$ -Sma and Notch3 as well as the stem cell-associated marker CD133 showed no differential mRNA expression in HSC on laminin-coated FS compared to laminin-coated PS for both laminin trimers (Figure 16G-I). In contrast to the number of adhered cells, the mRNA expression was independent of the spacing between the laminin-coated gold dots (Figure 16D-I).

To ensure low variation of the mRNA expression data obtained from HSC isolated from different rats, cells were cultured on uncoated PS and uncoated nanostructured gold surfaces without passivation (no PEG coating) and with different spacing (70 nm, 100 nm, 150 nm). Thereby, HSC showed no significant differences regarding the mRNA expression levels of *Lrat*, *reelin*, *Sparcl1*,  $\alpha$ -Sma, Notch3, and CD133 on all four uncoated surfaces (Figure 17A). Only Notch3 showed slightly elevated expression in HSC on uncoated nanostructured surfaces compared to uncoated PS but without reaching significance (Figure 17A).

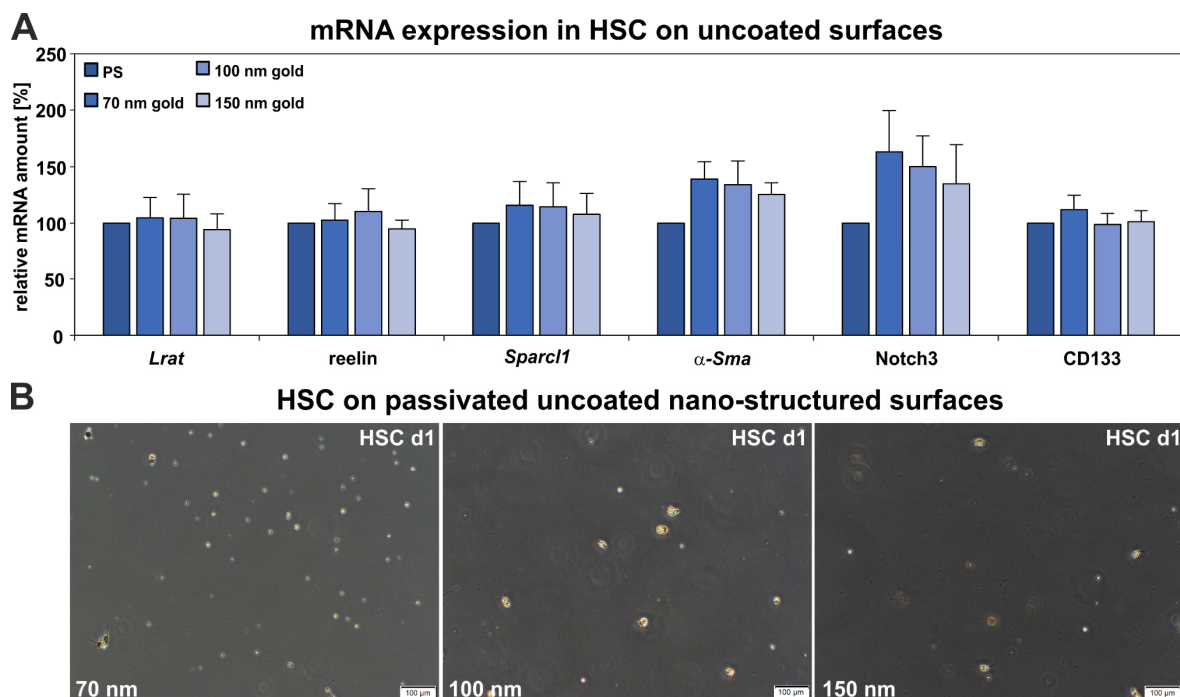


**Figure 17: Gene expression analyses of HSC on uncoated culture surfaces. (A)** HSC were seeded on uncoated PS and nanostructured gold surfaces without PEG coating. After one week of culture the mRNA expression of quiescence and activation markers was analyzed by qPCR. No significant differences between cells on diverse uncoated surfaces were observed for *Lrat*, *reelin*, *Sparcl1*,  $\alpha$ -Sma, Notch3, and CD133 mRNA expressions. Uncoated PS was set to 100% for each independent experiment. The data are indicated as means  $\pm$  SEM ( $n = 5$ ). **(B)** HSC did not adhere to passivated (PEG) uncoated nanostructured surfaces regardless of gold dot spacing (70 nm, 100 nm, 150 nm) as shown one day after cell isolation. Bright spots are non-adherent cells (scale bars: 100  $\mu$ m).

Furthermore, complete coating of PEG was confirmed by seeding freshly isolated HSC on passivated nanostructured surfaces without laminin-functionalization and with varying spacing between gold dots (70 nm, 100 nm, 150 nm). On these surfaces HSC did not adhere. Non-adherent roundish cells could be detected (Figure 17B).

Overall, defined coating of LN-521 (FS/LN-521) markedly improved supportive effects of LN-521 on the quiescent state of HSC in comparison to a random coated PS surface (PS/LN-521). However, culture on functionalized nanostructured surfaces did not alter the expression of activation and stem cell-associated markers in HSC. Furthermore, mRNA expression levels were independent on spacing between laminin molecules. However, cell adhesion decreased with increasing distance between the gold dots.

### 3.1.5. Reversal of HSC activation on LN-521

To analyze whether HSC-derived myofibroblast-like cells can re-establish their quiescent state on LN-521, HSC were culture-activated under serum-free conditions on PS for one week. During this time, HSC had lost most of their lipid droplets. HSC-derived myofibroblast-like cells were re-plated on laminin-coated and uncoated PS surfaces and cultured for another week under serum-free conditions. HSC on PS and PS/LN-211 exhibited an irregular myofibroblast-like morphology, while cells on PS/LN-521 appeared more homogeneous (Figure 18A-C). Quantitative PCR and immunofluorescence analyses were carried out in order to analyze the activation state of HSC-derived myofibroblasts. Interestingly, mRNA expression of  *$\alpha$ -Sma* showed a significant decrease by  $19\% \pm 7\%$  on PS/LN-211 and by  $41\% \pm 9\%$  on PS/LN-521 in myofibroblast-like cells incubated for seven days on laminin-coated in comparison to uncoated PS surfaces (Figure 18D). Immunofluorescence of  $\alpha$ -SMA supported the mRNA expression data and revealed higher  $\alpha$ -SMA fluorescence intensities in cells on PS and PS/LN-211 than on PS/LN-521 (Figure 18E-G). Moreover, the expression of quiescence markers such as *Gfap*, *Notch1*, *reelin*, *Sparcl1*, and *Lrat* tended to increase in cells on PS/LN-521 (Figure 18D). However, only *Gfap* expression was significantly upregulated in HSC-derived myofibroblasts on PS/LN-521 compared to uncoated PS.

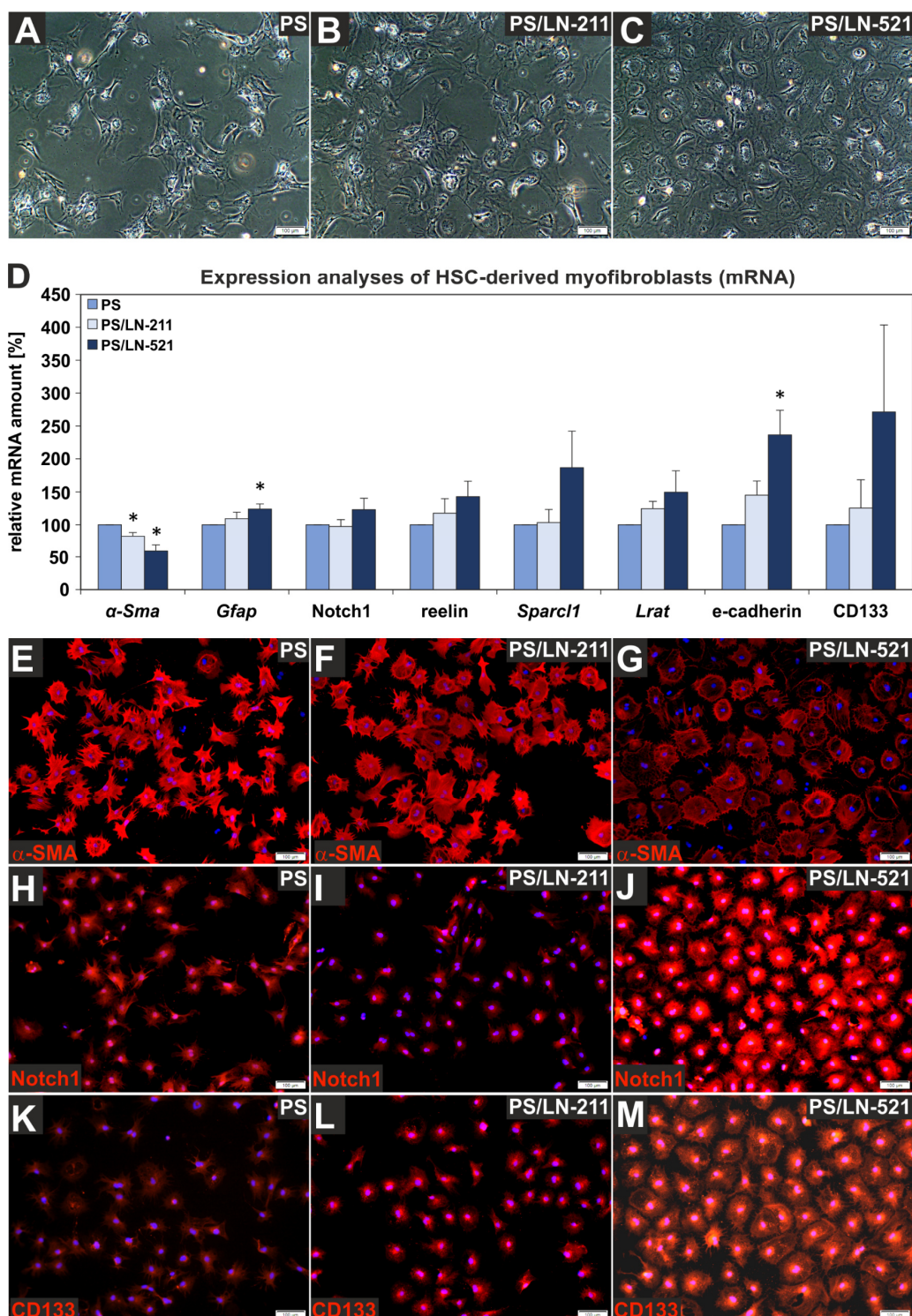


**Figure 18: Re-establishment of a quiescent-like state in stellate cell-derived myofibroblasts on PS/LN-521.** HSC-derived myofibroblast-like cells were obtained by culture-activation under serum-free conditions for one week on PS. Myofibroblasts were replated on laminin-coated and uncoated surfaces and cultured for additional seven days in serum-free medium. HSC-derived myofibroblast-like cells cultured on (A) PS and (B) PS/LN-211 showed a myofibroblast-like cell morphology, whereas cells on (C) PS/LN-521 appeared more homogeneous, although most lipid droplets have been lost during the activation phase. (D) Expression analyses of myofibroblast-like cells on uncoated and laminin-coated PS were performed by qPCR with respect to activation-, quiescence- and stem cell-associated markers. Reduced  $\alpha$ -Sma and elevated Gfap gene expressions were observed in myofibroblast-like cells on PS/LN-521. Reelin, Sparcl1, and Lrat mRNA expressions were also slightly increased on PS/LN-521 compared to PS and PS/LN-211.

**Figure 18 continued:** Furthermore, the expression of the stem cell-associated markers e-cadherin and CD133 was upregulated in HSC on PS/LN-521. No differential expression was observed when HSC on PS/LN-211 and on PS were compared. The expression of HSC-derived myofibroblast-like cells cultured on PS for one week was set to 100% for each independent experiment and data are indicated as means  $\pm$  SEM ( $n = 6$ ; \*  $p < 0.05$ ). **(E-M)** Immunofluorescence staining using antibodies against  $\alpha$ -SMA revealed a weaker fluorescence intensity in HSC on PS/LN-521 than on PS and PS/LN-211, while Notch1 and CD133 fluorescence intensities indicated the highest protein levels in HSC on PS/LN-521. Cell nuclei were stained by DAPI (blue). Representative images are shown ( $n = 3$ ; scale bars A-M: 100  $\mu$ m). Modified from Rohn *et al.* (2018).

In contrast, PS/LN-211 did not alter mRNA expression in re-seeded myofibroblasts when compared to PS (Figure 18D). In addition, the stem-cell associated marker e-cadherin was significantly elevated by  $136\% \pm 37\%$  in myofibroblast-like cells on PS/LN-521 and tended to increase in these cells on PS/LN-211 but without reaching significance. Furthermore, CD133 mRNA expression was increased by  $171\% \pm 132\%$  in cells on PS/LN-521 but showed a high variation (Figure 18D). In contrast, CD133 expression was not altered in HSC on PS/LN-211. Immunofluorescence signal intensities of Notch1 (Figure 18H-J) and CD133 (Figure 18K-M) were markedly stronger in HSC-derived myofibroblasts on PS/LN-521 compared to cells on uncoated PS and PS/LN-211. Overall, the expression of activation, quiescence, and stem cell-associated markers suggested the re-establishment of a quiescent-like state in HSC on PS/LN-521. However, HSC quiescence could not be restored completely.

In conclusion, the results presented in section 3.1 indicate that LAMA5 is present in liver sinusoids and that LN-521 promotes the quiescent state of isolated stellate cells from rat liver.

### 3.2. Aging alters HSC and their niche

Aging processes influence the cellular function and tissue integrity. To investigate whether there are also alterations in HSC and their niche during aging, HSC, blood serum, whole liver tissue, and the hepatic matrix of young (2 months) and old (22 months) rats were compared at mRNA and protein levels (Figure 19).

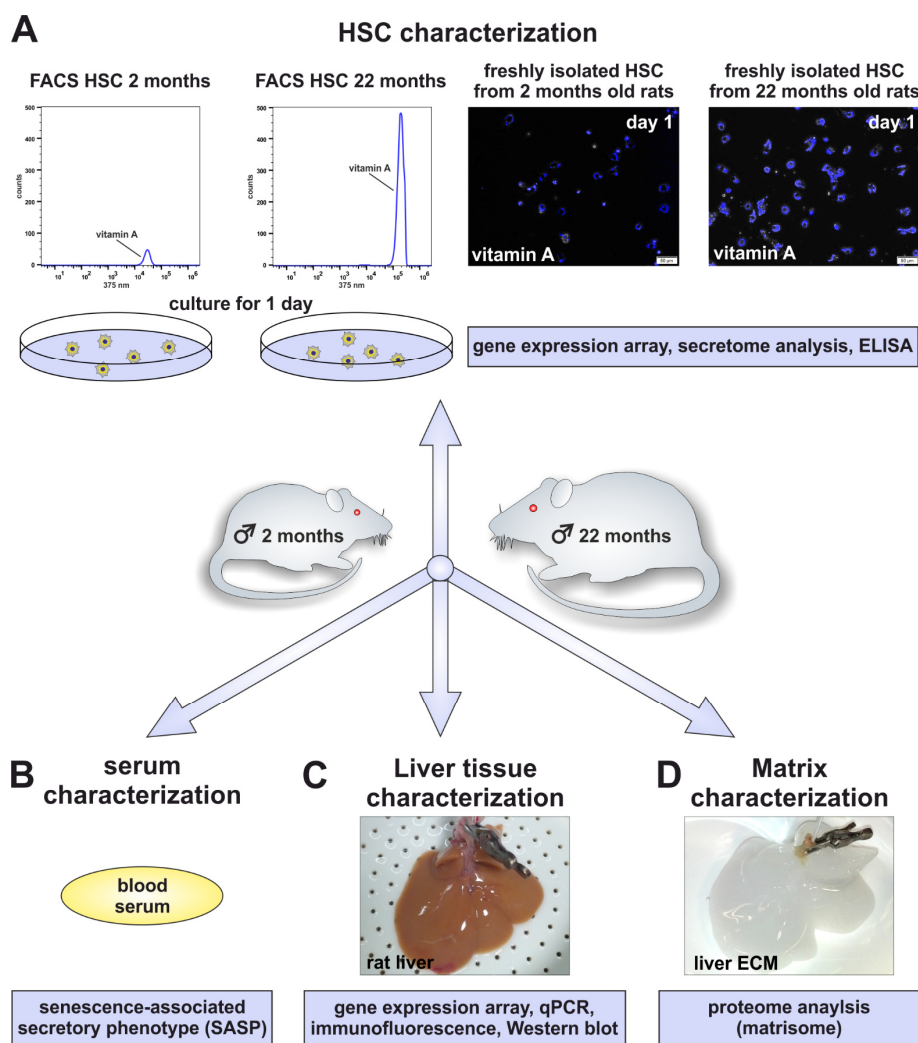


**Figure 19: Study design for the comparison of HSC, blood serum, whole liver tissue, and hepatic matrix of young and old rats.** HSC from 2-months and 22-months-old rats were isolated and purified by FACS using their characteristic retinoid fluorescence. After 24 hours, the HSC showed typical cell morphology and vitamin A fluorescence after UV light excitation (blue). The HSC from young rats contained fewer retinoids compared to cells isolated from old rats. Differences in HSC from young and old rats were investigated by gene expression arrays ( $n = 3$ ). The culture medium of the HSC was analyzed by cytokine protein arrays and ELISA with respect to a senescence-associated secretory phenotype (SASP). **(B)** SASP factors were also investigated in the blood sera ( $n = 4-6$ ). **(C)** Whole liver tissues of young and old rats were also analyzed by gene expression arrays ( $n = 3$ ). The array results were verified by qPCR analysis, immunofluorescence, and Western blot to identify age-related alterations in the rat liver ( $n = 3-10$ ). **(D)** Finally, the liver tissues from both age groups were decellularized by perfusion with detergents and analyzed by proteome analysis to quantify the ECM protein composition ( $n = 3$ ). Modified from Rohn *et al.* (under revision).

Therefore, HSC were isolated from 2-months and 22-months-old rats and sorted via FACS with the help of their characteristic retinoid fluorescence. The vitamin A fluorescence was higher in HSC from old rats as demonstrated by the corresponding histograms, indicating a higher retinoid content in HSC from old compared to HSC from young rats (Figure 19A). At the following day, cells were washed and their purity was assessed by the retinoid fluorescence after UV light excitation (Figure 19A). Subsequently, HSC were either collected for analysis by gene expression arrays or fresh serum-free medium was added. After two days of culture under serum-free conditions, medium was collected and further analyzed with respect to secreted cytokines, chemokines, and growth factors released by HSC into the culture supernatant using protein arrays (Figure 19A). Blood sera from young and old rats were analyzed in a similar way (Figure 19B). Selected cytokines and chemokines associated with senescence were also quantified by ELISA in the conditioned culture medium of HSC. Moreover, whole liver tissue from 2-months and 22-months-old rats was investigated at mRNA level by gene expression arrays and by qPCR as well as at protein level by immunofluorescence and Western blot (Figure 19C). Finally, livers from young and old rats were decellularized by perfusion with detergents and the remaining hepatic matrix was analyzed by a mass spectrometric analysis to quantify age-related alterations of the ECM (Figure 19D).

### **3.2.1. Quality control of gene expression microarray raw data**

Microarray raw data were first analyzed regarding their quality (Figure 20). The signal intensities of microarray raw data of isolated HSC and whole liver tissue from three young and three old rats were comparable (Figure 20A, B) and could therefore be included in comparative gene expression analysis. Microarray data of HSC showed marked differences between both age groups when Pearson correlation was calculated (Figure 20C). In contrast, there were no obvious differences in Pearson correlation analysis when liver tissues of young and old rats were compared (Figure 20D). Nevertheless, in principle component analysis (PCA) HSC and liver tissue samples from 2-months and 22-months-old rats clustered together according to their respective age group (Figure 20E, F). In addition, data of old rats showed a higher variation in PCA indicating individual aging processes.

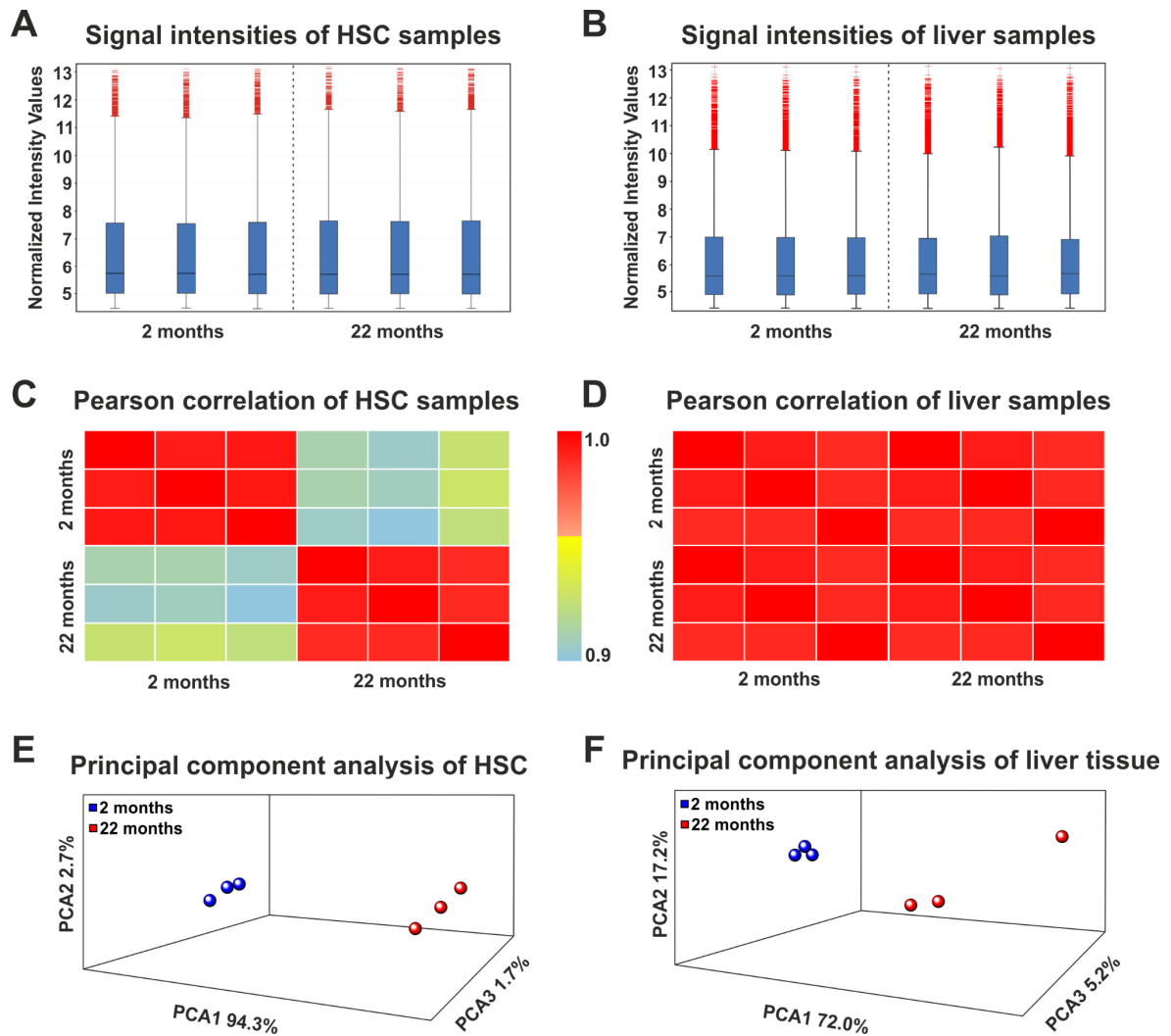


**Figure 20: Quality control of microarray raw data.** Microarray signal intensities of (A) isolated HSC and (B) liver samples from young and old rats were compared and showed equal quality necessary for comparison. Pearson correlation analyses of the microarray data revealed significant differences between (C) HSC, whereas no obvious differences were observed in case of (D) liver tissue from young and old rats. (E) Principal component analysis (PCA) of gene expression data of (E) isolated HSC and (F) liver tissue from 2-months (blue) and 22-months-old (red) rats. Samples clustered according to age groups. However, data of liver tissue from old rats showed a higher variation. Each dot represents a data set from a single animal ( $n = 3$  for each age group). Figure from Rohn *et al.* (under revision).

### 3.2.2. Altered ECM composition in aged rat liver

Hierarchical cluster analysis of gene expression microarray data from whole liver tissue of young and old rats was performed (Figure 21A). Only 130 genes out of 30,429 analyzed genes showed a significantly different expression when a fold change larger than 2 and a p-value smaller than 0.05 was applied. In detail, 63 genes were significantly upregulated and 67 genes significantly downregulated in liver tissue from old compared to young rats (Figure 21A, B).

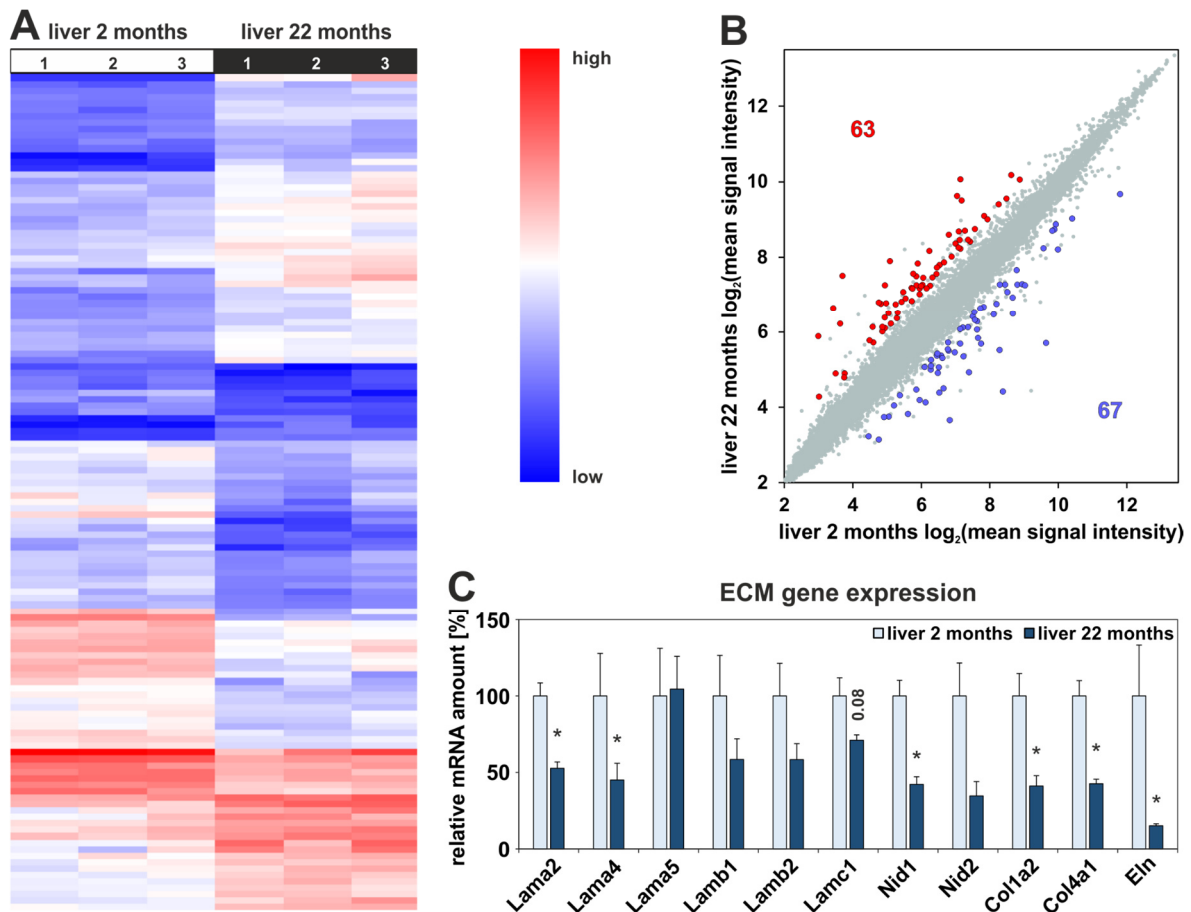


**Figure 21: Altered ECM protein-associated gene expression in aged rat liver.** (A) Hierarchical cluster analysis of differentially expressed genes in whole liver tissue revealed that 130 genes were differentially expressed in young and old rat liver tissue. Low intensities are indicated by a blue color, while high intensities are indicated by a red color. (B) Scatter plot of gene expression in whole liver tissue from both age groups demonstrate that 63 genes were significantly upregulated (red), while 67 genes were significantly downregulated (blue) in liver tissue from 22-months compared to 2-months-old rats ( $n = 3$  per age group, fold change  $> 2$ , ANOVA  $p < 0.05$ ). (C) Expression analyses of genes encoding for ECM proteins by qPCR revealed a significant downregulation of *Lama2*, *Lama4*, *Nid1*, *Col1a2*, *Col4a1*, and *Eln* in aged rat liver. All other ECM-associated genes investigated tended to decrease in aged liver tissue except for *Lama5*. Mean expression of liver tissue samples from young rats was set to 100%. The data are presented as means  $\pm$  SEM ( $n = 8-10$ , \*  $p < 0.05$ ). Modified from Rohn *et al.* (under revision).

Interestingly, genes of the aged liver showing significantly reduced expression were associated with the ECM (Table 6). This observation was verified by qPCR analyses using a higher number of samples and inclusion of additional rats. The qPCR data revealed marked downregulation of the ECM-associated genes *Lama2*, *Lama4*, *Lamc1*, *Nid1*, *Col1a2*, *Col4a1*, *Eln* (Figure 21C), and *Fn* (Figure 25A) in whole liver tissue from old compared to young rats. Besides all other ECM-associated genes analyzed by qPCR, only *Lama5* mRNA expression showed no reduction in whole liver tissue of aged rats (Figure 21C).

**Table 6: Differential expression of genes encoding for ECM proteins and integrin subunits in liver tissue from aged rats.** Gene expression alterations in liver tissue from young (2 months) and old (22 months) rats were investigated by Affymetrix micorarrays (n = 3 for each age group). All significantly altered ECM-associated genes, showed a reduction in aged rat liver. Among integrins, only integrin  $\alpha_5$  (*Itga5*) was markedly reduced. Modified from Rohn *et al.* (under revision).

Process	Gene Symbol	Fold Change <sup>1</sup>	ANOVA p-value <sup>2</sup>
ECM-associated	Lama2	-1.31	0.026214
	Nid1	-1.82	0.000481
	Col1a1	-1.23	0.002631
	Col1a2	-2.92	0.014069
	Col3a1	-2.50	0.001962
	Col4a1	-1.54	0.011863
	Col5a1	-1.41	0.028843
	Col14a1	-1.20	0.010225
	Eln	-1.55	0.022032
	Fn1	-1.05	0.047903
integrins	Itga1	-1.09	0.026565
	Itga5	-1.65	0.002914
	Itga6	-1.37	0.049957
	Itgb4	1.17	0.044354

<sup>1</sup>Negative fold change indicates lower expression, while positive values indicate higher expression in samples from aged rats

<sup>2</sup>p < 0.05 considered significant

Immunofluorescence analysis of liver sections with antibodies against LAMA5, COL1, and COL4 revealed no obvious differences in fluorescence signal intensities of different age groups (Figure 22A-F). ECM protein amounts in rat liver matrix from 2-months and 22-months-old rats were quantified by proteome analysis. Here, an overall reduction of matrix proteins in the aged rat liver was observed (Figure 22G). In detail, the protein amounts of different laminin chains (LAMA2, LAMA4, LAMB2, LAMC1), NID2, various collagens (COL1A1, COL1A2, COL3A1, COL6A1, COL6A2, COL14A1), ELN, and FN were reduced in liver matrix of old rats (Figure 22G). In contrast, COL4A2 (209 ± 78%), COL4A5 (332 ± 185%), COL6A5 (325 ± 103%), and COL6A6 (182 ± 27%) protein amounts tended to increase in old compared to young rat liver matrix, but only the latter one was significantly elevated (n = 3; p < 0.05). Immunofluorescence staining of liver sections with antibodies against FN revealed that its fluorescence signal could be only detected around larger vessels and was nearly absent in the remaining parenchyma of old compared to young rats (Figure 23A, B). In line with this, the fluorescence signal intensity of the FN receptor subunit ITGA5 appeared to be reduced in liver sections from 22-months-old rats

(Figure 23C, D). In contrast, immunofluorescence staining with antibodies against the respective heterodimer ITGB1 indicated no obvious alterations in the protein amount of old rat liver (Figure 23E, F). While ITGA5 was more prominent in liver sinusoids, ITGB1 could be detected in whole liver tissue (Figure 23C-F).

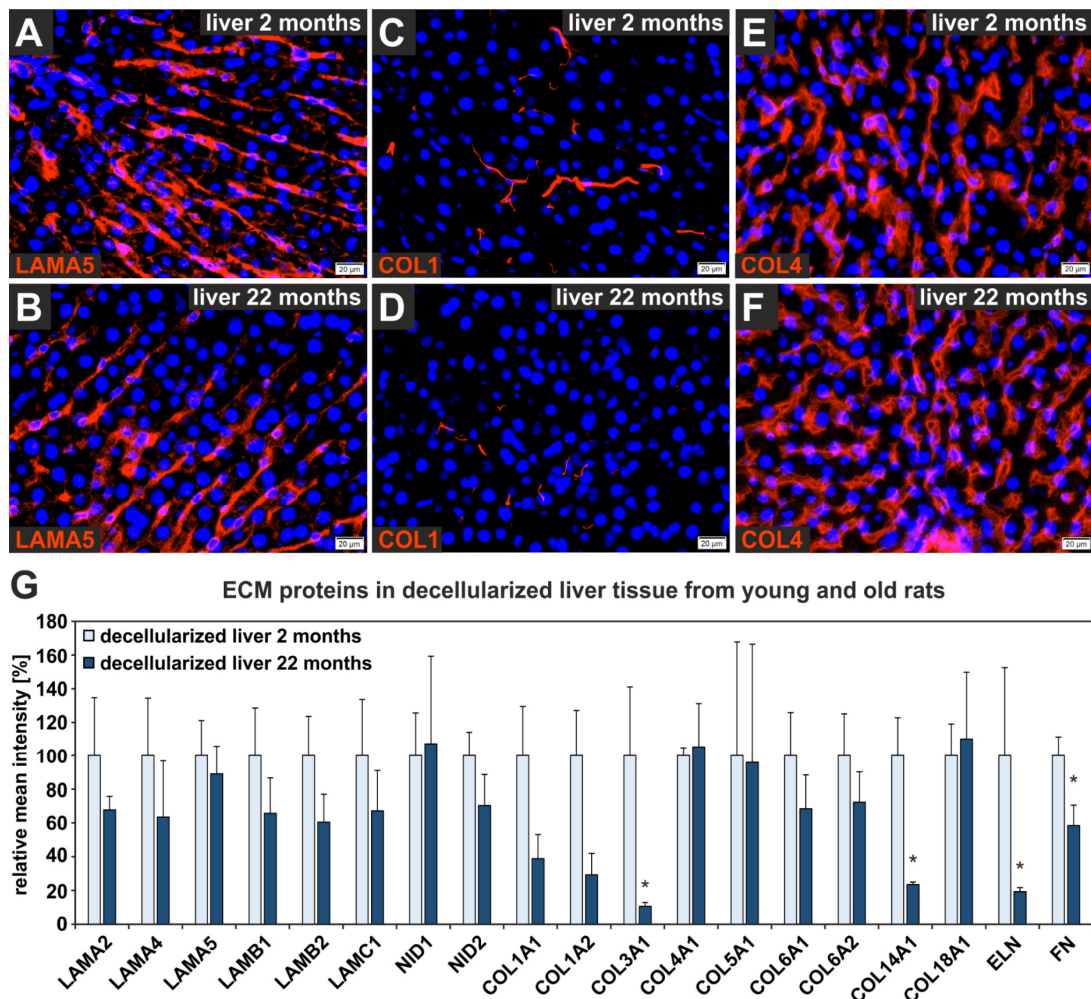


**Figure 22: Altered ECM protein composition in aged rat liver.** Immunofluorescence staining of liver tissue sections from young and old rats with antibodies against (A, B) LAMA5, (C, D) COL1, and (E, F) COL4 (red) showed no obvious changes in fluorescence intensity in the aged rat liver. The cell nuclei were stained by DAPI (blue; scale bars: 20  $\mu$ m). Representative images are shown (n = 3). (G) Matrisome analysis of hepatic ECM revealed an overall reduction of several laminin chains (LAMA2, LAMA4, LAMB2, LAMC1), NID2, and different collagens (COL1A1, COL1A2, COL3A1, COL6A1, COL6A2, COL14A1) in liver matrix from old rats. Furthermore, ELN and FN were significantly reduced in the liver matrix of 22-months compared to 2-months-old rats indicating altered ECM composition in the aged liver. Mean intensities of samples from young rats were set to 100%. The data are presented as means  $\pm$  SEM (n = 3, \* p < 0.05). Modified from Rohn *et al.* (under revision).

In addition, densitometric quantification of protein bands obtained by Western blot also revealed a significant decrease of ITGA5 protein amount by  $31 \pm 8\%$  in liver tissue of old rats, while ITGB1 only showed a trend towards reduction (Figure 23G, H).

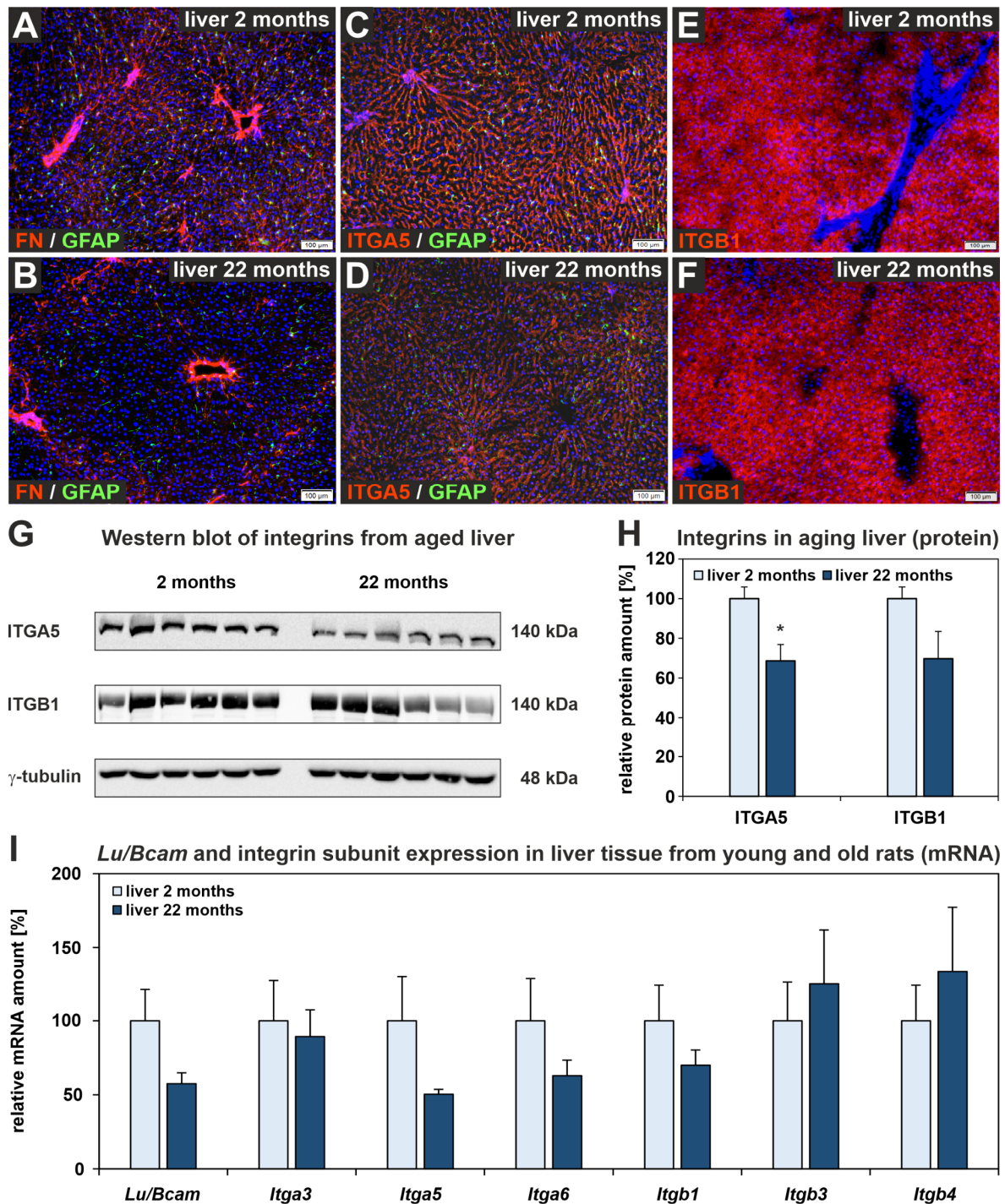


**Figure 23: FN and ECM receptors in aged rat liver.** Co-staining of liver sections from young and old rats with antibodies against (A, B) FN (red) and (C, D) ITGA5 (red) with the HSC marker GFAP (green) revealed a weaker fluorescence signal in old rat liver. (B, D) Immunofluorescence of (E, F) ITGB1 (red) in young and old rat liver indicated no obvious alterations in the protein amount. Cell nuclei were stained by DAPI (blue; scale bars: 100  $\mu$ m). Representative images are shown (n = 3). (G) Western blot analyses of whole liver samples from young and old rats with antibodies against ITGA5 and ITGB1 as well as  $\gamma$ -tubulin as a loading control. (H) Densitometric analysis of Western blots revealed a significant decrease of ITGA5, whereas ITGB1 only tended to decrease in liver tissue of old rats. (I) *Lu/Bcam* and integrin subunit mRNA expression analyses by qPCR revealed a reduced average expression of *Lu/Bcam*, *Itga5*, and *Itga6* by about 40% in old compared to young rat liver tissue. Values of young rats from qPCR and Western blot were set to 100%. The data are indicated as means  $\pm$  SEM (n = 6 for both age groups; \* p < 0.05). Modified from Rohn *et al.* (under revision).

In line with the protein data, the mRNA amount of *Itga5* was also significantly downregulated in HSC and liver tissue from old rats as analyzed by microarray (Table 6). The mean expression value of *Itga5* was markedly reduced in qPCR analysis of whole liver tissue but reached no significance (Figure 23I). A similar result was obtained for *Itgb1* mRNA expression (Table 6, Figure 23I).

### 3.2.3. Impaired HSC characteristics in aged rat liver

Hierarchical cluster analysis of gene expression microarray data from HSC of young and old rats cultured for 24 hours revealed a significant differential expression of 1,426 genes out of 30,429 analyzed genes (Figure 24A). Here, the expression of 753 genes significantly increased, whereas the expression of 673 genes significantly decreased in HSC from 22-months-old rats when a fold change larger than 2 and a p-value smaller than 0.05 was applied (Figure 24B).

To identify altered biological processes in HSC isolated from aged rat liver, a gene ontology (GO) term analysis of all significantly differential expressed genes was performed. Interestingly, biological processes associated with “development” and “differentiation” as well as with “aging”, “inflammation”, “stress”, and “cell death” were mainly altered in HSC by aging (Figure 24D). Furthermore, “cell migration”, “extracellular matrix organization”, “cell adhesion”, and “integrin-mediated signaling pathway” were among the GO terms of differential expressed genes in HSC from old rats (Figure 24D). In line with the GO terms, genes encoding for ECM proteins (e.g. collagens, laminins, *, *, and *) as well as several integrin subunits (e.g.  *and *) were significantly downregulated in HSC from old rats (Figure 24C, Table 7). Furthermore, the expression of genes associated with ECM remodeling and cell migration such as matrix metalloproteinase 13 (*) (Table 7) and  *(Table 11) increased. In addition, microarray data of focal adhesion elements such as vinculin (*) and talin (*, *) were significantly reduced in HSC from old rats (<http://www.ebi.ac.uk/arrayexpress>; accession number: E-MTAB-7423). All these results together suggested weakened cellular adhesion and integrin-mediated signaling as well as reduced ECM production in HSC from aged rat liver, which in turn could lead to an impaired cell-ECM interaction in their stem cell niche and increased migration during aging.**********

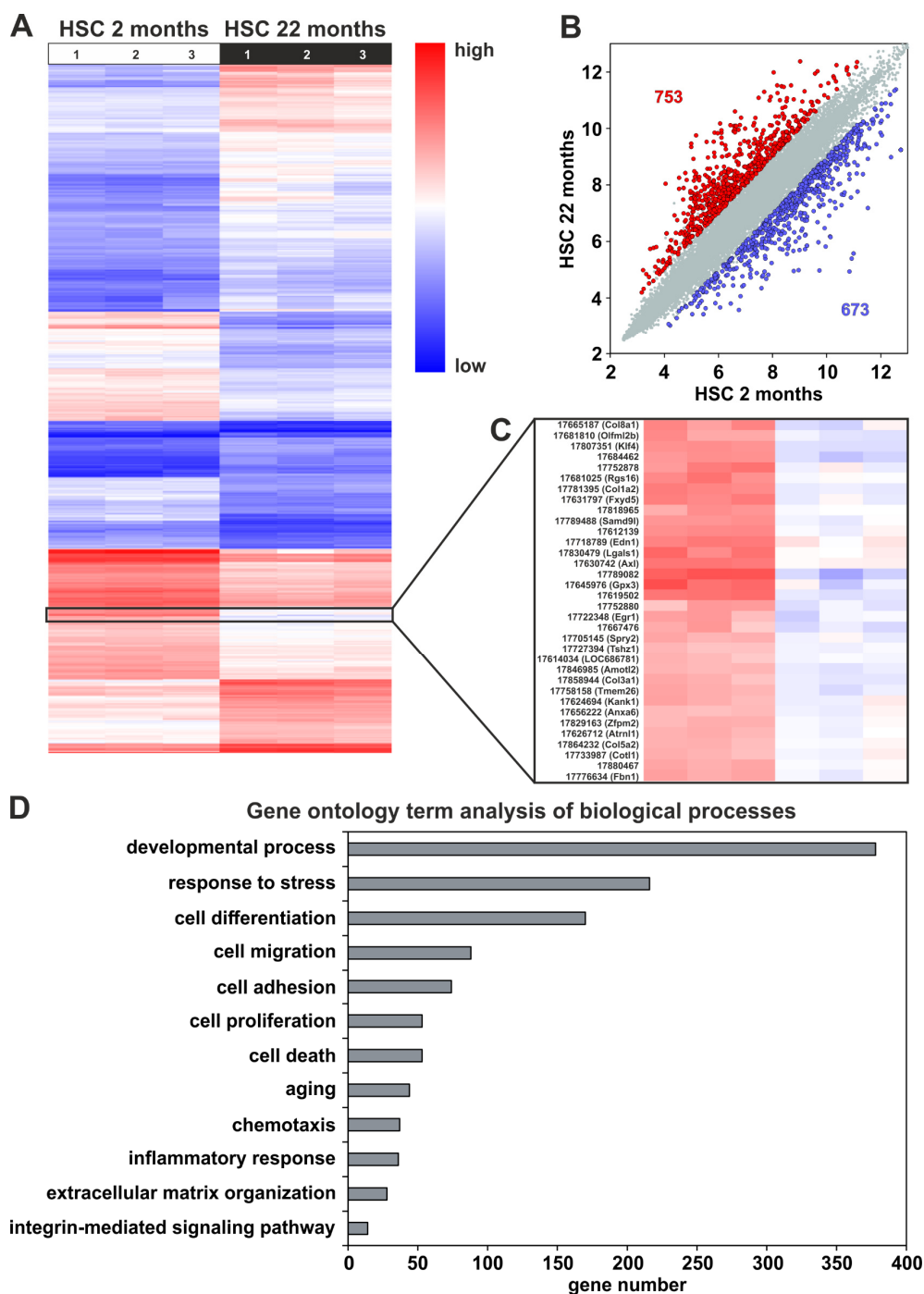


**Figure 24: Gene expression alterations in HSC from aged rat liver. (A)** Hierarchical cluster analysis of differential expressed genes in HSC from young and old rats revealed that 1,426 genes out of 30,429 genes analyzed were differentially expressed. **(B)** Scatter plot of gene expression arrays showed 753 upregulated genes (red) and 673 downregulated genes (blue) in HSC from aged rats ( $n = 3$  per age group, fold change  $> 2$ , ANOVA  $p < 0.05$ ). **(C)** The expression of different collagens (*Col8a1*, *Col1a2*, *Col3a1*, *Col5a2*) decreased in HSC from old rats. **(D)** Gene ontology (GO) term analysis of biological processes involving differentially expressed genes in HSC from aged liver. Analysis was performed with the software GOzilla (October 2018; fold enrichment  $> 1.5$ ;  $p < 0.05$ ). Modified from Rohn *et al.* (under revision).

Microarray data of HSC from young and old rats was further screened regarding the expression of markers associated with HSC quiescence and activation (Table 8).

**Table 7: Differential expression of genes encoding for ECM-associated proteins and integrins in HSC from aged rat liver.** HSC isolated from young (2 months) and old (22 months) rat livers were investigated by Affymetrix gene expression arrays (n = 3 for each group). The expression of *Mmp13* increased significantly on mRNA level, while *Lama2*, *Lamc1*, *Nid1*, *Nid2*, collagens, *Fn*, *Itga5*, and *Itgb1* decreased in HSC from old rats. Modified from Rohn *et al.* (under revision).

Process	Gene Symbol	Fold Change <sup>1</sup>	ANOVA p-value <sup>2</sup>
ECM-associated	Mmp2	-2.68	0.004478
	Mmp28	-1.67	0.004404
	Mmp17	1.21	0.029466
	Mmp16	1.24	0.025820
	Mmp3	1.74	0.000433
	Mmp11	2.37	0.001967
	Mmp13	15.38	0.000619
	Lama2	-3.15	0.000760
	Lamc1	-1.38	0.006252
	Lama4	2.92	0.009783
	Nid2	-3.37	0.002714
	Nid1	-1.58	0.000652
	Col8a1	-9.65	0.002631
	Col12a1	-7.79	0.000108
	Col1a2	-7.47	0.000010
	Col3a1	-4.35	0.000293
	Col1a1	-3.90	0.000268
	Col5a2	-3.23	0.000345
	Col4a1	-2.39	0.000551
	Col4a2	-2.14	0.000920
	Col5a1	-2.12	0.000001
	Col14a1	-1.95	0.017937
Col6a3	-1.88	0.021628	
Col6a2	-1.56	0.007514	
Fn	-7.89	0.000032	
integrins	Itga2	-2.54	0.005192
	Itga9	-2.12	0.027800
	Itga5	-1.96	0.000357
	Itga6	-1.72	0.027102
	Itga3	-1.50	0.010345
	Itgb1	-1.48	0.000374
	Itga1	-1.29	0.004938
	Itga4	-1.24	0.024648
	Itgax	2.18	0.011056
	Itgb2	2.34	0.003577
	Itgb8	4.88	0.001907

<sup>1</sup>Negative fold change indicates lower expression, while positive values indicate higher expression in samples from aged rats

<sup>2</sup>p < 0.05 considered significant

Interestingly, even though typical quiescence markers such as *Sparcl1*, periostin, *Pparγ*, and reelin as well as activation markers such as *Fn*, nestin, and desmin decreased, the myofibroblast marker  $\alpha$ -*Sma* was not altered (Table 8).

**Table 8: Differential expression of genes associated with quiescence or activation in HSC from old rats.** HSC isolated from young (2 months) and old (22 months) rat livers were investigated by Affymetrix gene expression arrays (n = 3 for each group). The quiescence markers *Sparcl1*, periostin, *Pparγ*, and reelin as well as the activation markers *Fn*, nestin, and desmin were significantly reduced in HSC from old compared to young rats. In contrast, *Gfap* and  $\alpha$ -*Sma* remained unchanged on mRNA level in array analysis. Modified from Rohn *et al.* (under revision).

Process	Gene Symbol	Fold Change <sup>1</sup>	ANOVA p-value <sup>2</sup>
HSC quiescence / activation-associated	Fn	-7.89	0.000032
	nestin	-2.96	0.008251
	Sparcl1	-2.84	0.000004
	desmin	-2.22	0.002086
	periostin	-2.18	0.002297
	Pparγ	-1.60	0.024991
	reelin	-1.47	0.007415
	$\alpha$ -Sma (Acta2)	1.04	0.666481
	Gfap	1.20	0.098913

<sup>1</sup>Negative fold change indicates lower expression, while positive values indicate higher expression in samples from aged rats

<sup>2</sup>p < 0.05 considered significant

The mRNA expression of typical quiescence and activation markers of HSC was further investigated by qPCR analysis of whole liver tissue from young and old rats (Figure 25A). The average mRNA levels of genes that are associated with the quiescent state in HSC (*Gfap*, *Sparcl1*, *Lrat*) tended to decrease in aged liver tissue, but reached no significance (Figure 25A). In addition, typical activation markers such as desmin or  $\alpha$ -*Sma* showed no differential expression in HSC from young and old rats. Quite the contrary, the activation markers nestin and *Fn* even decreased in aged liver tissue. The expression data were further supported by immunofluorescence staining and Western blot analyses of liver tissue from 2-months and 22-months-old rats. Samples from old rat livers showed weaker fluorescence intensities (Figure 25B) and reduced protein amounts of GFAP and FN in old rat liver (Figure 25C). In line with the mRNA data, also desmin and  $\alpha$ -SMA protein amounts were not altered in liver tissue from 22-months-old rats (Figure 25B, C). Reduction of quiescence but also of several activation markers indicated impaired HSC characteristics in the aged rat liver.

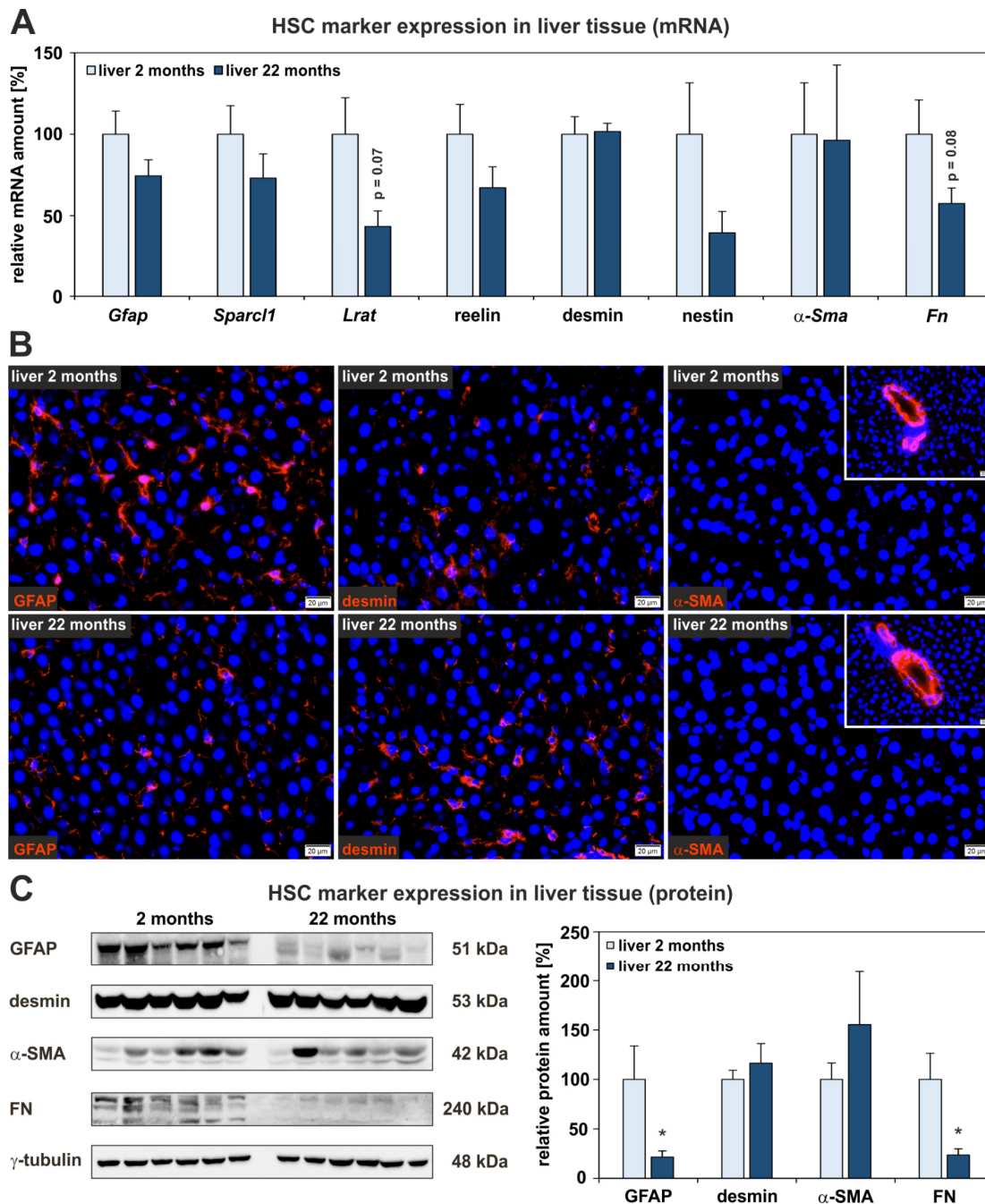


**Figure 25: Expression of HSC-associated markers in aged rat liver.** The mean expression of genes typically expressed in quiescent HSC (*Gfap*, *Sparcl1*, *Lrat*, *reelin*) tended to decrease in old compared to young rat liver without reaching significance as investigated by qPCR of whole liver samples. Furthermore, *Fn* showed reduced expression in aged liver tissue, whereas other activation markers of HSC (*desmin*, *nestin*, *α-Sma*) were not significantly changed. Mean expression of HSC markers in liver tissue samples from young rats was set to 100%. The data are presented as means  $\pm$  SEM ( $n = 10$  for 2-months-old rats,  $n = 9$  for 22-months-old rats, \*  $p < 0.05$ ). **(B)** Immunofluorescence analysis of liver tissue sections (red) revealed less GFAP-positive HSC in liver tissue from old rats, while *desmin* and *α-SMA* fluorescence showed no obvious differences. The cell nuclei were stained by DAPI (blue;  $n = 3$  per age group; scale bars:  $20 \mu\text{m}$ ). **(C)** Western blot analyses of liver tissue from young and old rats demonstrated significantly reduced GFAP and FN protein amounts in old rat liver, while *desmin* and *α-SMA* protein levels were not affected by aging. Mean values of liver tissue samples from young rats were set to 100%. The data are presented as means  $\pm$  SEM ( $n = 10$  for 2-months-old rats,  $n = 9$  for 22-months-old rats, \*  $p < 0.05$ ). Modified from Rohn *et al.* (under revision).

### 3.2.4. Differentiation of HSC in aged rat liver

Since HSC from aged rat liver had downregulated quiescence markers and possess a developmental potential, the gene expression array data were screened regarding genes that indicate differentiation (Table 9).

**Table 9: Expression of differentiation-associated markers in HSC from old rat liver.** HSC isolated from young (2 months) and old (22 months) rat livers were investigated by Affymetrix arrays (n = 3 for each group). The adipocyte-associated marker fatty acid binding protein 4 (*Fabp4*) increased markedly. No further signs of differentiation were observed in HSC from aged rat liver. However, HSC from old rats increased the expression of genes associated with endodermal specification (*Gata4*, *Sox17*, *Hhex*).

Process	Gene Symbol	Fold Change <sup>1</sup>	ANOVA p-value <sup>2</sup>
adipogenic differentiation	Lpl	-7.24	0.00174
	Pparγ	-1.60	0.02499
	Slc2a4 (Glut4)	-1.27	0.03516
	Adipoq	-1.10	0.03161
	Lep	1.03	0.67908
	Cfd	1.04	0.91551
	Cebpa	1.07	0.51103
	Add1	1.15	0.00175
	Fabp4	15.96	0.00054
osteogenic differentiation	Runx2	-4.03	0.00001
	Bmpr2	-1.58	0.00388
	Bmpr1a	-1.49	0.06399
	Alpi	-1.19	0.04846
	Vdr	-1.15	0.12317
	Pth1r	-1.03	0.58455
	Bmpr1b	-1.02	0.24965
chondrogenic differentiation	Prelp	-2.79	0.00068
	Bgn	-1.36	0.00070
	Acan	-1.06	0.15446
	Lum	2.50	0.10504
hepatic differentiation	Alb	-2.58	0.08396
	Krt18	-1.17	0.89669
	Hnf4a	-1.17	0.02725
	Epcam	-1.06	0.09450
	Krt19	-1.05	0.16024
	Cyp7a1	-1.00	0.74333
	Afp	1.00	0.83777
	Lgr5	1.00	0.76229
endodermal specification	Gata4	1.20	0.04052
	Hhex	2.43	0.00863
	Sox17	6.05	0.00604

<sup>1</sup>Negative fold change indicates lower expression, while positive values indicate higher expression in samples from aged rats

<sup>2</sup>p < 0.05 considered significant

Among marker genes suitable to indicate cell lineage determination, only fatty acid binding protein 4 (*Fabp4*) associated with adipogenic cell differentiation increased significantly (Table 9). However, other genes typically expressed by adipocytes were not elevated or even decreased such as *Lpl* suggesting that a differentiation along this lineage had not occurred or remained incomplete. Although molecular markers of mature hepatocytes were not induced, genes that indicate endodermal specification such as *Gata4*, *Sox17*, *Hhex*, and *Cxcr4* significantly increased in HSC from old rat liver (Table 9, Table 11).

Even though more than 450 genes involved in biological processes associated with “development” and “differentiation” were differentially expressed in HSC isolated from aged rat livers (Figure 24D), the data available thus far were not strong enough to provide clear evidence for cell differentiation.

### 3.2.5. SASP factors in HSC and serum from aged rats

To assess the state of senescence in old rat liver, microarray data of HSC and whole liver tissue from 2-months and 22-months-old rats were analyzed regarding typical senescence markers (Table 10). Thereby, *p21/Cdkn1a* and *p53/TP53* showed significantly upregulated mRNA levels, whereas the expression of *p16/Cdkn2a*, senescence marker protein 30/regucalcin (*Smp30/Rgn*), and *Glb1* was not significantly altered in HSC from aged rats (Table 10). In whole liver tissue a significantly increased expression of *p21/Cdkn1a* was found, while *Smp30/Rgn*, which is known to be significantly downregulated in aged liver (Fujita *et al.*, 1992), significantly decreased in 22-months-old rats (Table 10). The latter was further analyzed by qPCR that confirmed the significant downregulation of *Smp30/Rgn* mRNA amounts in aged liver tissue (Figure 26A). However, the expression of *p21/Cdkn1a* assessed by qPCR only showed a slight increase in liver tissue from old rats without reaching significance (Table 10). Furthermore, neither by microarray nor by qPCR a differential expression of *p16/Cdkn2a* and *p53* in livers from 2-months and 22-months-old rats could be detected (Table 10, Figure 26A).

Cellular senescence is further characterized by the secretion of a certain pattern of chemokines, cytokines, and growth factors, which together compose the SASP factors (Coppé *et al.*, 2010). A significant rise of these factors was detected in HSC from old compared to young rats as analyzed by gene expression arrays (Table 11).

For instance, diverse growth factors, such as transforming growth factor  $\beta$  (*Tgfb1*, *Tgfb2*, *Tgfb3*), fibroblast growth factor 2 (*Fgf2*), connective tissue growth factor (*Ctgf*), and *Hgf*, were significantly downregulated, while several inflammatory factors, such as interleukin-6 (*Il6*), interleukin-1 $\alpha$  (*Il1a*), tumor necrosis factor receptors (*Tnfrsf1a*, *Tnfrsf1b*), and colony stimulating factors (*Csf2*, *Csf3*), were significantly increased in HSC from old rats (Table 11).

**Table 10: Expression of senescence markers in HSC and liver tissue from young and old rats.** HSC isolated from young (2 months) and old (22 months) rat livers were investigated by Affymetrix arrays (n = 3 for each group). The senescence markers *p21/Cdkn1a* and *p53/Tp53* were significantly increased in HSC from aged rats. Moreover, *p21/Cdkn1a* expression was also significantly upregulated in whole liver tissue of aged rats, while *Smp30/Rgn* and *Glb1* were significantly downregulated as expected for aging processes.

Sample	Gene Symbol	Fold Change <sup>1</sup>	ANOVA p-value <sup>2</sup>
HSC	p16/Cdkn2a	1.02	0.681115
	p21/Cdkn1a	3.97	0.000081
	p53/Tp53	1.79	0.000013
	Smp30/Rgn	-1.04	0.384313
	Glb1	1.06	0.297601
liver tissue	p16/Cdkn2a	1.04	0.377872
	p21/Cdkn1a	1.81	0.025747
	p53/Tp53	1.22	0.374742
	Smp30/Rgn	-1.29	0.010480
	Glb1	-1.27	0.018824

<sup>1</sup>Negative fold change indicates lower expression, while positive values indicate higher expression in samples from aged rats

<sup>2</sup>p < 0.05 considered significant

To further quantify SASP factors at protein level, blood sera from young and old rats were analyzed by a rat cytokine antibody array. Overall, no differences in the cytokine concentrations could be measured except for CXCL7, which was significantly decreased in the sera from old rats (Figure 26B). In addition, conditioned culture medium from HSC of young and old rats was investigated by the cytokine array. Unfortunately, the sensitivity of the array was very low. Only CXCL1 and TIMP1 could be detected in all culture supernatant samples and, thus, could be quantified (Figure 27A, B). In accordance to microarray data, mean CXCL1 concentration was increased two-fold, while TIMP1 was not altered in culture supernatants of HSC from 22-months-old rats compared to medium samples of HSC from 2-months-old rats (Figure 27C, D; Table 11; <http://www.ebi.ac.uk/arrayexpress> accession number: E-MTAB-7423).

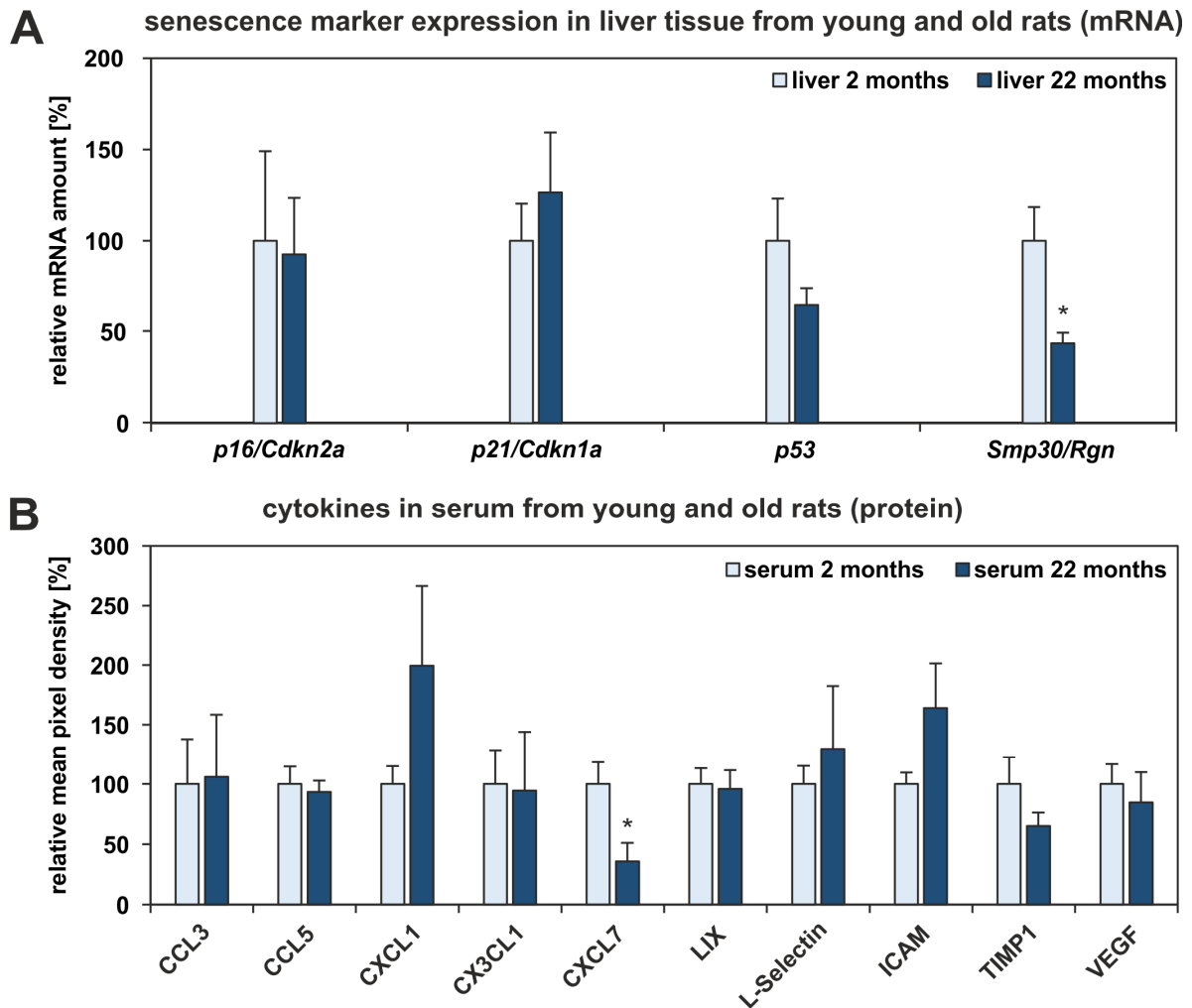


**Figure 26: Analysis of senescence-associated markers in whole liver tissue and blood serum from young and old rats. (A)** Expression analyses of senescence-associated markers in whole liver tissue from young and old rats revealed no significant alterations in the expression levels of *p16/Cdkn2a*, *p21/Cdkn1a*, and *p53* by qPCR. In contrast, *Smp30/Rgn* was significantly downregulated in the liver tissue of old rats. **(B)** The rat cytokine array revealed no obvious differences in cytokine concentration of the blood sera from young and old rats except for CXCL7, which was significantly reduced in the serum samples from 22-months-old rats. Mean values of samples from 2-months-old rats were set to 100% and data are presented as means  $\pm$  SEM ( $n = 4-6$ , \*  $p < 0.05$ ). Modified from Rohn *et al.* (under revision).

The SASP factors CXCL3 and IL6 were additionally analyzed by ELISA and their respective concentrations were both markedly higher in culture medium of HSC from old rats (Figure 27E, F). While the average CXCL3 concentration was increased ten-fold, the mean IL6 concentration showed a four-fold increase in culture supernatants of HSC from old rats.

**Table 11: Differential expression of SASP factors in HSC from aged rat liver.** HSC isolated from young (2 months) and old (22 months) rat livers were investigated by Affymetrix arrays (n = 3 for each group). Many genes associated with a SASP showed differential expression in HSC from old compared to young rats. For instance, the expression of many growth factors decreased, but inflammation- (e.g. *Il6*) and cell migration-associated (e.g. *Cxcr4*) genes were significantly upregulated. Modified from Rohn *et al.* (under revision).

Process	Gene Symbol	Fold Change <sup>1</sup>	ANOVA p-value <sup>2</sup>
Senescence-associated secretory phenotype (SASP) <sup>3</sup>	Tgfb3	-4.87	0.00547
	Tgfb2	-3.02	0.00121
	Timp2	-2.70	0.00015
	Tgfb1	-2.16	0.00033
	Fgf2	-1.75	0.00054
	Ctgf	-1.72	0.00012
	Hgf	-1.68	0.03020
	Il15	-1.64	0.02986
	Igfbp7	-1.10	0.00747
	Adipoq	-1.10	0.03161
	Ccl26	-1.06	0.04205
	Cxcl3	1.33	0.00091
	Il6st	1.46	0.00021
	Icam1	1.49	0.00853
	Ccl2	1.50	0.02335
	Cxcl12	1.56	0.02179
	Ctsb	1.56	0.00038
	Icam2	1.64	0.01713
	Tnfrsf1a	1.65	0.00060
	Tnfrsf1b	1.76	0.00376
	Ngf	1.91	0.00096
	Cxcl10	1.93	0.00122
	Cxcl9	1.93	0.02212
	Ereg	2.09	0.00989
	Cxcl5	2.28	0.00099
	Cxcl1	3.70	0.00050
	Il6	4.01	0.01542
	Ccl20	4.57	0.00833
	Cxcl13	7.75	0.00124
	Serpinb2	7.90	0.05005
	Csf2	8.87	0.00458
	Cxcr4	10.15	0.00076
	Cxcl2	10.16	0.00308
Il1a	14.13	0.00098	
Csf3	23.86	0.00169	

<sup>1</sup>Negative fold change indicates lower expression, while positive values indicate higher expression in samples from aged rats

<sup>2</sup>p < 0.05 considered significant

<sup>3</sup>According to Freund *et al.* (2010) and Coppé *et al.* (2010)

These observations were also in accordance with the results of the gene expression arrays (Table 11, <http://www.ebi.ac.uk/arrayexpress> accession number: E-MTAB-7423).

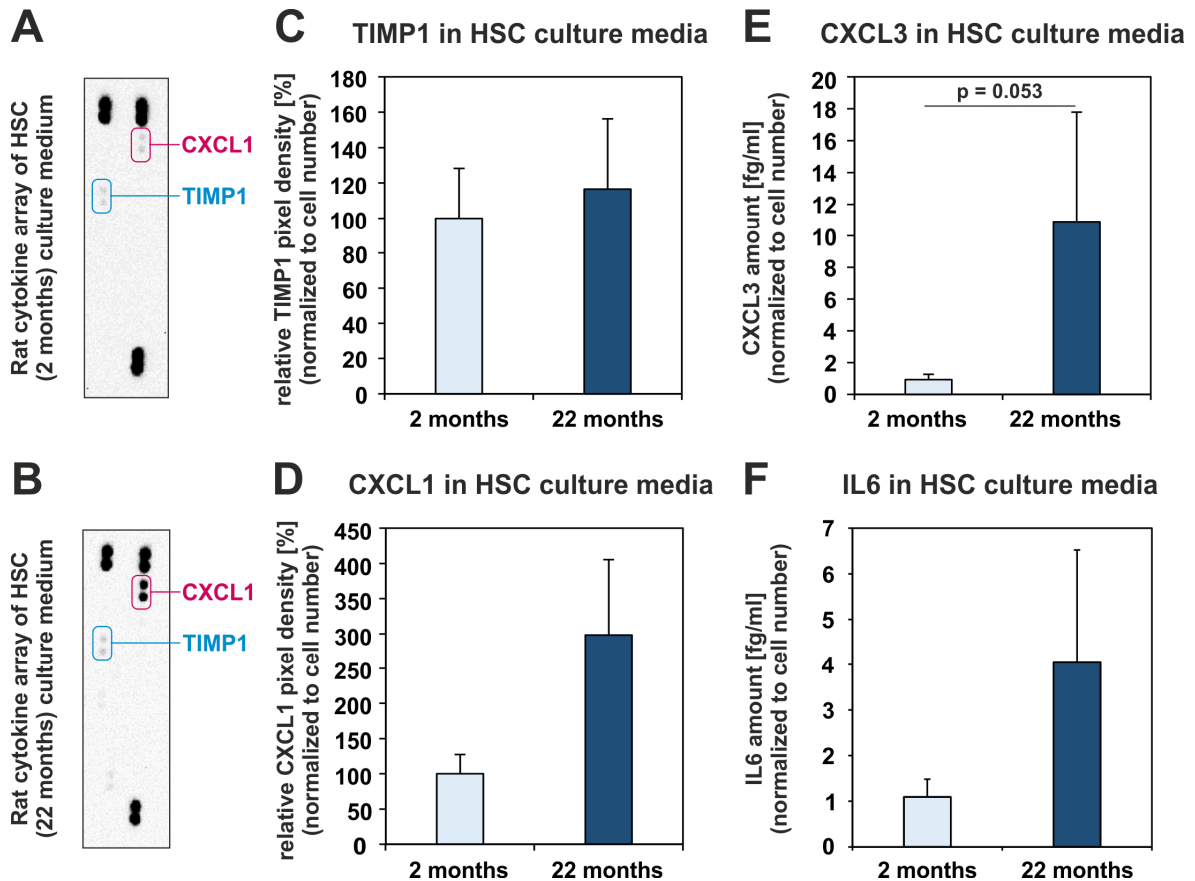


**Figure 27: Senescence- and inflammation-associated factors in conditioned culture medium of HSC.** (A, B) Cytokines released into culture medium by freshly isolated HSC from (A) young (2 months) and (B) old (22 months) rats were analyzed by protein arrays. Due to its low sensitivity only TIMP1 (blue) and CXCL1 (pink) could be detected in all culture supernatants. Representative immuno blots are presented. The uppermost four and bottommost two dots are reference spots. (C) TIMP1 concentration remained unchanged, (D) whereas CXCL1 markedly increased by three-fold in culture medium of HSC from old rats. (E) Analysis of CXCL3 by ELISA revealed a ten-fold increase in CXCL3 concentration in culture supernatants of HSC from old rats. (F) The IL6 concentration in culture media of HSC from old rats increased by four-fold as quantified by ELISA. Cytokine array and ELISA data were normalized to cell number. Mean values from young rats were set to 100% and data are presented as means  $\pm$  SEM (cytokine arrays: n = 3; ELISA: n = 5 for 2-months, n = 3 for 22-months-old rats). Modified from Rohn *et al.* (under revision).

### 3.2.6. Oxidative stress in liver tissue from aged rats

Gene expression array data of whole liver tissue from young and old rats were screened regarding oxidative stress response markers (Table 12). There were no signs of increased oxidative stress in liver tissue from old compared to young rats as investigated at mRNA level.

**Table 12: Expression of genes typically associated with oxidative stress response in liver tissue from young and old rats.** HSC isolated from young (2 months) and old (22 months) rat livers were investigated by Affymetrix arrays (n = 3 for each group). The array data indicated no obvious signs for increased oxidative stress in the aged rat liver.

Process	Gene Symbol	Fold Change <sup>1</sup>	ANOVA p-value <sup>2</sup>
Oxidative stress response <sup>3</sup>	Nox4	-1.43	0.232174
	Gpx7	-1.32	0.031716
	Ncf1 (p47phox)	-1.09	0.527824
	Duox1	1.03	0.950471
	nNos	1.12	0.158355
	Duox2	1.14	0.349387
	Nox3	1.24	0.013967
	Gadd45a	1.28	0.927826

<sup>1</sup>Negative fold change indicates lower expression, while positive values indicate higher expression in samples from aged rats

<sup>2</sup>p < 0.05 considered significant

<sup>3</sup>According to Sies (1993), Reinehr and Häussinger (2007), and Qvartskhava *et al.* (2019)

Furthermore, immunofluorescence staining of liver sections from young and old rats with antibodies against the phosphorylated p47<sup>phox</sup> subunit of the nicotinamide adenine dinucleotide phosphate (NADPH) oxidase (phospho-p47<sup>phox</sup>) and against 8-hydroxy-2'-deoxyguanosine, 8-hydroxyguanine, and 8-hydroxyguanosine (8-OHG), which detects oxidative damage to DNA and RNA, revealed only slightly increased fluorescence intensities in the aged rat liver indicating that no oxidative damage occurred during aging (Figure 28).

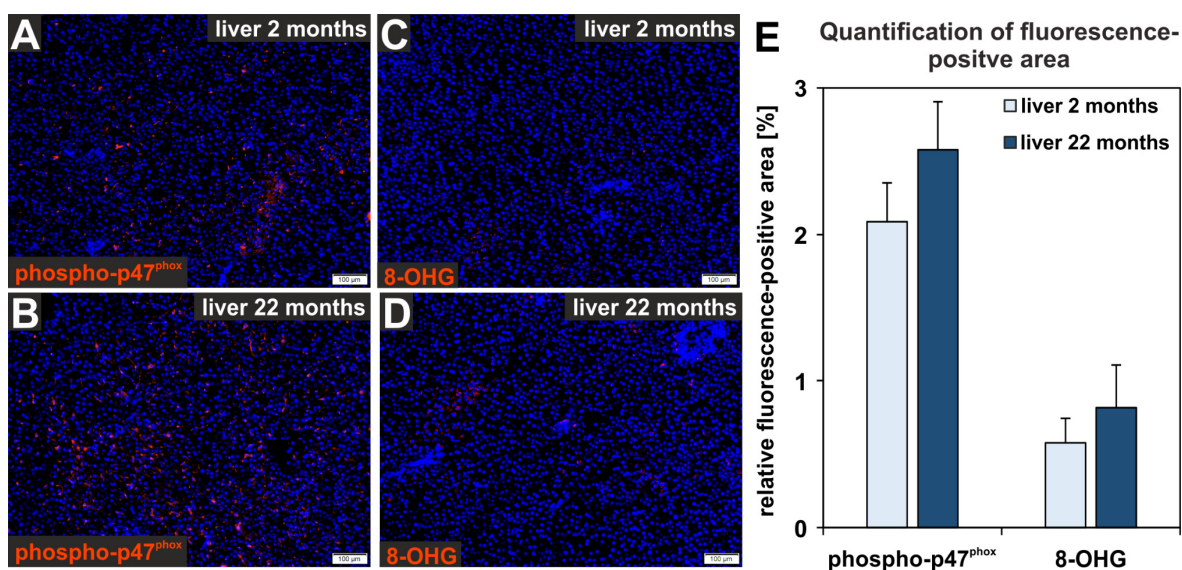


**Figure 28: Markers of oxidative stress in liver tissue from young and old rats.** Immunofluorescence staining of liver sections revealed that neither (A, B) phospho-p47<sup>phox</sup> nor (C, D) 8-OHG (red) showed and increased fluorescence signal in the aged rat liver. (E) In aged liver tissue, no upregulation of phospho-p47<sup>phox</sup> and 8-OHG was detected by quantification of the fluorescence intensities of both oxidative stress markers. Cell nuclei were stained by DAPI (blue; n = 3 for each age group; scale bars A-D: 100 µm).

### 3.2.7. Influence of fluid shear stress and ECM composition on HSC function

Immunofluorescence staining of rat liver sections revealed the presence of HGF in liver sinusoids where it co-localized with FN (Figure 29A, B). HGF distribution in young rat liver was comparable to the distribution of COL4 (Figure 22E, Figure 29E). Furthermore, GFAP-expressing HSC were also positive for HGF immunofluorescence (Figure 29C, D). In accordance with FN and GFAP fluorescence signals, the fluorescence intensity of HGF was also weaker in liver tissue from old compared to young rats (Figure 29A-F). Western blot of matrix-bound pro-HGF using an antibody that specifically binds this HGF precursor protein supported the immunofluorescence and revealed significantly reduced pro-HGF amounts by about  $62 \pm 10\%$  in aged rat liver (Figure 29G, H). However, serum HGF levels were not altered by aging (Figure 29I).

When PHx was performed in 2-months-old rats, HGF immunofluorescence signal was weaker in the liver sections compared to control (Figure 30A, B). Quantification of the fluorescence intensities revealed a significant reduction of the HGF-positive hepatic sinusoidal tissue area by one quarter compared to the control without surgery as analyzed one day after PHx (Figure 30C-E). These results indicate HGF liberation from the matrix and by sinusoidal cells shortly after PHx.

In contrast to the situation after liver injury by PHx in which an unchanged blood volume has to pass a smaller number of liver sinusoids, there is an age-related reduction of hepatic blood flow as explained in sections 1.4 and 1.6. Therefore, it was investigated whether fluid mechanical forces such as shear stress influence HSC function by exposing them to low ( $2.9 \text{ dyn/cm}^2$ ), medium ( $15 \text{ dyn/cm}^2$ ), and high ( $29 \text{ dyn/cm}^2$ ) shear stresses under laminar pulsatile ( $2.5 \text{ Hz} / 150 \text{ bpm}$ ) flow for one hour.

Subsequently, HGF release into the culture medium and mRNA expression alterations were investigated by ELISA and qPCR, respectively. The results were compared to HSC under static condition ( $0 \text{ dyn/cm}^2$ ) before shear stress was applied. HGF release in response to shear stress significantly increased compared to static condition (Figure 31A).

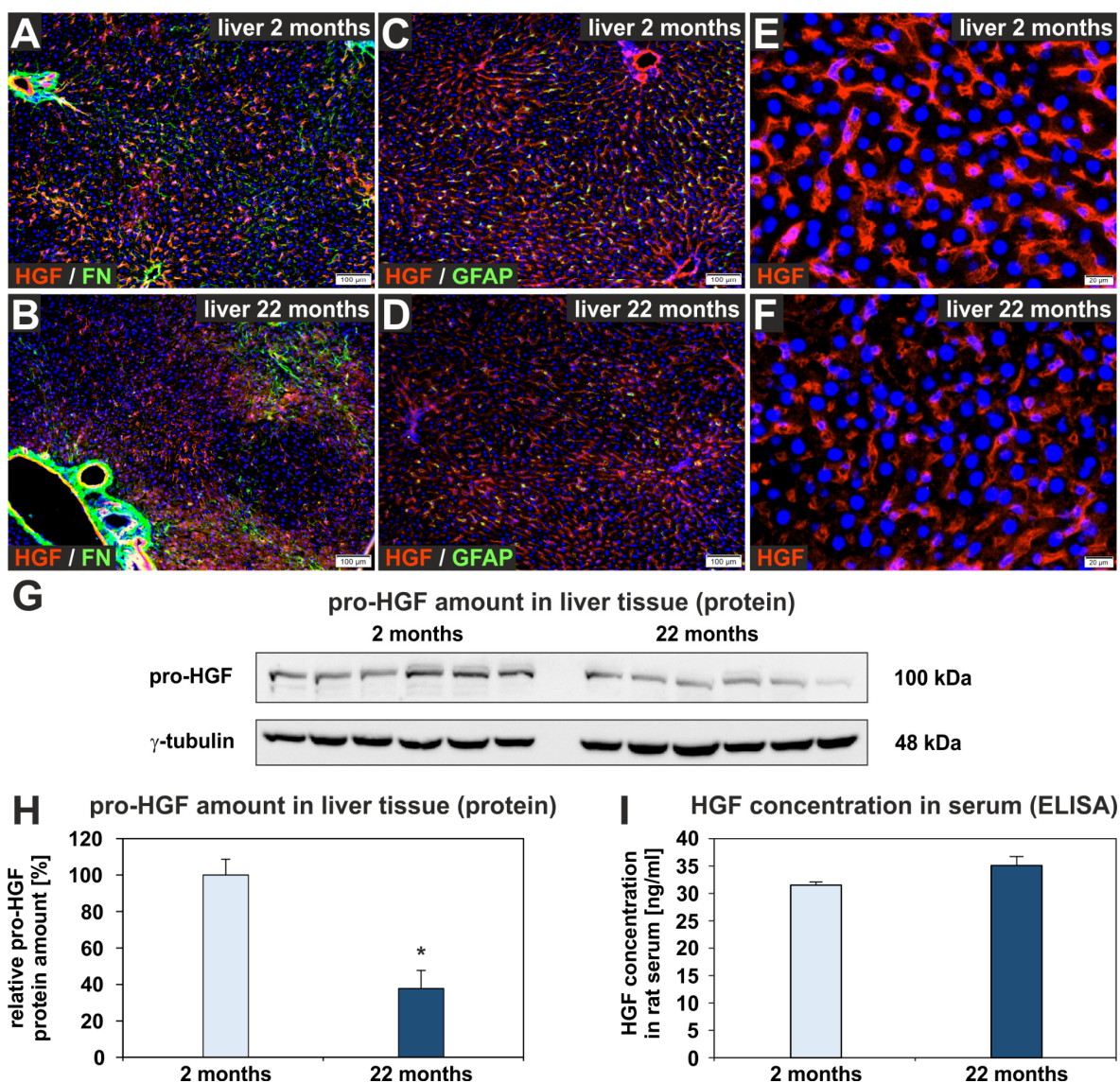


**Figure 29: HGF in liver tissue and blood serum from aged rats.** Immunofluorescence staining of liver sections revealed that HGF (red) could be detected in liver sinusoids where it co-localized with (A, B) FN (green) and (C, D) GFAP (green). (E, F) In accordance with FN and GFAP protein amounts also the HGF immunofluorescence intensity declined in aged rat liver. Cell nuclei were stained by DAPI (blue;  $n = 3$  for each age group; scale bars A-D: 100  $\mu\text{m}$  and E, F: 20  $\mu\text{m}$ ). (G) Representative Western blot of pro-HGF in liver tissue from 2-months and 22-months-old rats.  $\gamma$ -Tubulin was used as loading control. (H) Western blot analyses of liver tissue from young and old rats revealed age-related significantly reduced pro-HGF amounts ( $n = 6$  for each age group; \*  $p < 0.05$ ). (I) HGF concentration in blood sera from young and old rats analyzed by ELISA did not differ significantly ( $n = 4$  for both age groups). Modified from Rohn *et al.* (under revision).

These results were supported by HGF immunofluorescence analysis of HSC before and after fluid flow that showed a lower fluorescence intensity in HSC after exposure to shear stress (Figure 31B, C).

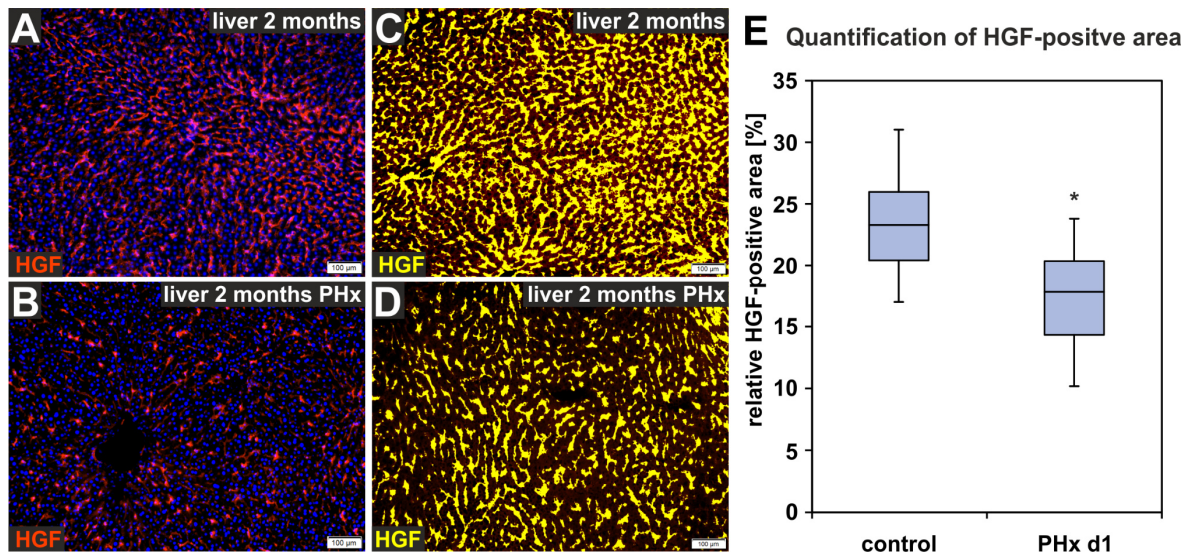


**Figure 30: HGF in regenerating rat liver.** (A, B) One day (d1) after PHx, HGF (red) immunofluorescence was markedly reduced in liver sinusoids of injured compared to normal rat liver. (C, D) HGF-positive tissue area (yellow) was quantified with the cellSens Dimension 1.16 software (Olympus). (E) Quantification of HGF-positive tissue area from six different positions per liver section revealed significantly downregulated HGF levels in liver sinusoids of rats that had undergone PHx compared to control rats. Cell nuclei were stained by DAPI (blue;  $n = 3$  for both conditions; scale bars: 100  $\mu\text{m}$ ). Modified from Rohn *et al.* (under revision).

In addition, expression levels of several ECM-associated genes (*Col1a4*, *Lamb1*, *Lamb2*, *Lamc1*) and of the integrin subunit *Itga5* were significantly increased by about 80% in HSC exposed to shear stress (Figure 32A, B). Interestingly, these were exactly those genes whose expression was significantly downregulated in HSC from aged rat liver (Table 7). However, not all analyzed ECM-encoding genes increased in HSC after applying shear stress. Furthermore, shear stress significantly downregulated the expression of *Il6* by about 65% (Figure 32C) which is opposed to the significant upregulation of *Il6* during aging (Table 11). In contrast to *Itga5*, the expression of *Itga6* and *Itgb1* was not altered by fluid flow, while *Itgb3* and *Itgb4* expression tended to decrease (Figure 32B). Even though fluid shear stress induced the release of HGF (Figure 31B-F), the mRNA expression of *Hgf* in HSC was only minor affected by shear stress (Figure 32C). Neither *Hgf* mRNA levels nor HGF protein release were significantly altered by variation of shear stress (2.9  $\text{dyn}/\text{cm}^2$ , 15  $\text{dyn}/\text{cm}^2$ , 29  $\text{dyn}/\text{cm}^2$ ). Overall, these results indicate that HGF release can be induced in HSC by mechanical stimuli.

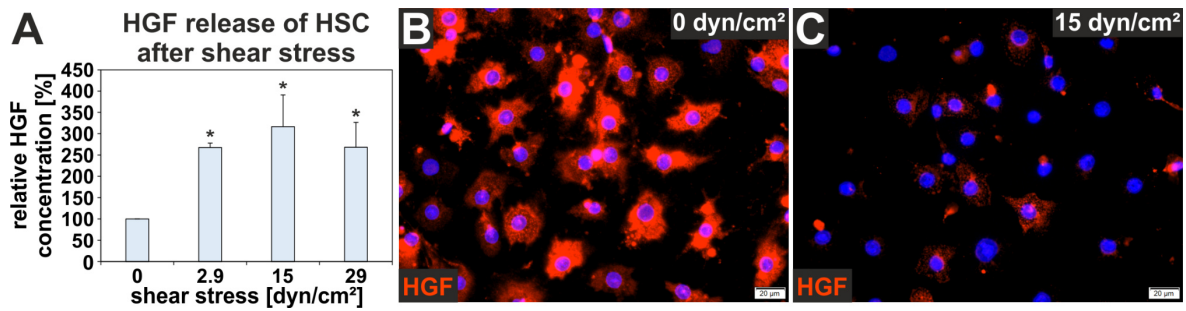


**Figure 31: Fluid shear stress induces HGF release by HSC.** (A) Fluid shear stress applied for one hour significantly increased HGF concentration in culture supernatants of HSC as analyzed by ELISA. HGF amount in culture media from static condition (0 dyn/cm<sup>2</sup>) was set to 100% for each independent experiment. The data are presented as means  $\pm$  SEM ( $n = 4$ ; \*  $p < 0.05$ ). Immunofluorescence analyses of HGF (red) in HSC showed a strong fluorescence intensity under (B) static condition (0 dyn/cm<sup>2</sup>), while after the exposure to (C) fluid shear stress (15 dyn/cm<sup>2</sup>) the intracellular HGF storages markedly decreased. Cell nuclei were stained by DAPI (blue;  $n = 3$ ; scale bars: 20  $\mu$ m). Modified from Rohn *et al.* (under revision).

In addition to fluid mechanical forces, the effect of ECM proteins on HGF expression and release was analyzed since the composition of the hepatic ECM exhibited age-related alterations (Figure 21, Figure 22) and it was shown that matrix proteins influence HSC function (see section 3.1). Therefore, HSC from mid-aged rats were seeded on PS dishes coated with different ECM proteins (LN-211, LN-521, COL4, FN) and cultured for one week under serum-free conditions. Expression of *Hgf* in HSC on uncoated and ECM protein-coated PS surfaces was analyzed by qPCR and HGF protein release into the conditioned culture medium by an ELISA. Interestingly, *Hgf* mRNA levels and HGF protein release were significantly upregulated in HSC cultured on LN-521 compared to cells on uncoated PS and LN-211, respectively (Figure 33). HGF expression and release were also elevated on FN (Figure 33A, C), while cells maintained on LN-211 and COL4 showed no altered *Hgf* expression compared to HSC on uncoated dishes (Figure 33A). Furthermore, the expression of *Il6* was significantly upregulated when HSC were cultured on LN-211 compared to uncoated PS and markedly elevated compared to cells on LN-521, COL4, and FN (Figure 33A).

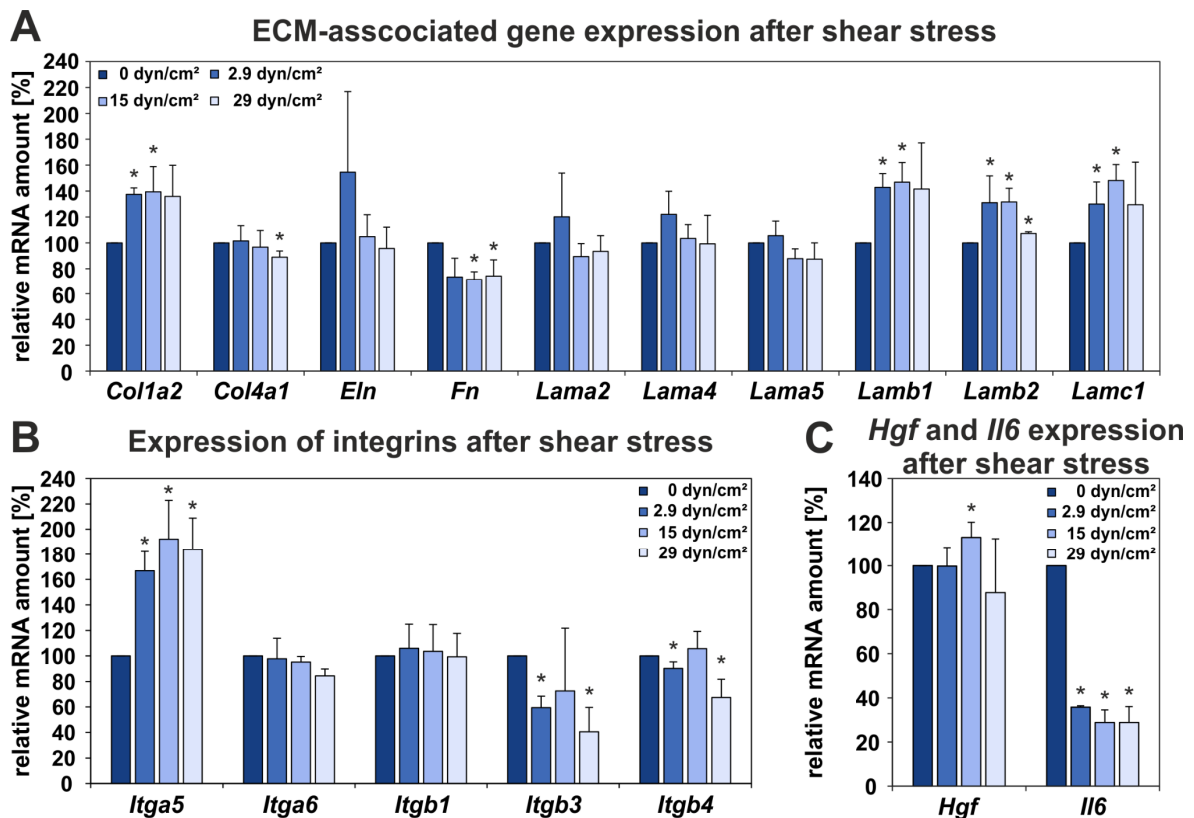


**Figure 32: Fluid shear stress influences HSC function.** Fluid shear stress applied for one hour significantly upregulated the expression of (A) several genes associated with the ECM (*Col1a2*, *Lamb1*, *Lamb2*, *Lamc1*) and of (B) *Itga5* in HSC. In contrast, *Itgb3* and *Itgb4* tended to decrease, while *Itga6* and *Itgb1* expression remained unchanged in HSC after exposure to shear stress. (C) *Il6* was significantly downregulated when HSC were exposed to laminar pulsatile flow. The mRNA expression of HSC under static condition (0 dyn/cm<sup>2</sup>) was set to 100% for each independent experiment and data are presented as means  $\pm$  SEM (n = 3; \* p < 0.05). Modified from Rohn *et al.* (under revision).

To provide a more defined laminin coating, a nanostructured culture surface was used on which laminin molecules were bound to gold dots with a defined spacing (70 nm, 100 nm, 150 nm). Culture on these nanostructured surfaces functionalized with LN-521 significantly upregulated *Hgf* expression in HSC and the mRNA amount reached its highest level when a gold dot spacing of 150 nm (FS/150nm) was used (Figure 33B). In contrast, *Hgf* expression in HSC cultured on LN-211 coated surfaces did not differ significantly (Figure 33B).

Dependence of *Hgf* and *Il6* expression and HGF release on ECM protein coating indicate that the ECM composition influences HSC function. Additionally, these observations were in line with the results in section 3.1, which indicated support of HSC characteristics by culture on LN-521-coated surfaces.

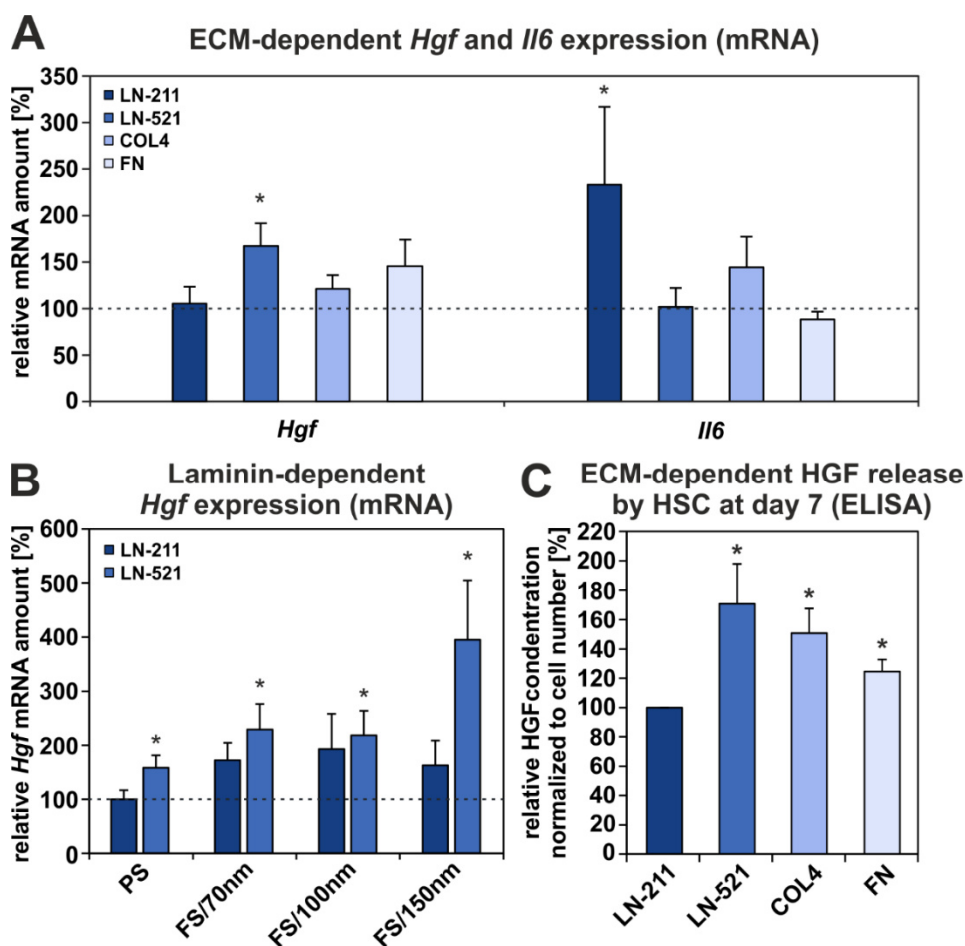


**Figure 33: LN-521 supports HSC function.** (A) Expression of *Hgf* and *Il6* in HSC was observed to be dependent on ECM protein coating of culture dishes (LN-211, LN-521, COL4, or FN). *Hgf* expression was significantly upregulated in HSC on LN-521 and tended to increase on FN after one week of culture under serum-free conditions. Moreover, *Il6* expression was significantly higher in HSC on LN-211 compared to uncoated surfaces. The mRNA expression of HSC cultured for one week on uncoated dishes was set to 100% (dashed line) for each experiment ( $n = 8$  for PS, LN-211, and LN-521;  $n = 6$  for COL4;  $n = 4$  for FN;  $* p < 0.05$ ). (B) Nanostructured surfaces functionalized with LN-521 further upregulated *Hgf* expression compared to laminin-coated and uncoated PS especially when a gold dot spacing of 150 nm (FS/150nm) was used. The mRNA expression of HSC cultured for one week on uncoated dishes was set to 100% (dashed line) for each experiment ( $n = 5$ ;  $*p < 0.05$ ). (C) Relative HGF concentration in conditioned culture medium normalized to cell number from HSC (mid-aged rats) on different ECM protein-coated surfaces (LN-211, LN-521, COL4, FN) analyzed by ELISA on day seven after isolation. HSC cultured on LN-521, COL4, and FN released significantly more HGF compared to cells on LN-211. HGF concentration of HSC on LN-211 was set to 100% for each independent experiment. The data are presented as means  $\pm$  SEM ( $n = 4$ ,  $* p < 0.05$ ). Modified from Rohn *et al.* (under revision).

### 3.2.8. *Itga5* and *Itgb1* knockouts in HSC impair mechanosensing

ITGA5 protein amount showed a significant reduction in HSC and liver tissue from aged rats (Figure 23, Table 6, Table 7) and its expression could be induced when HSC were exposed to shear stress under laminar pulsatile flow for one hour (Figure

32B). Western blot and immunofluorescence analyses of HSC on day one after isolation showed presence of ITGA5 suggesting that this integrin subunit is already present in their quiescent state (Figure 34A-D). Based on this observation it was investigated whether ITGA5 might function as a mechanosensor in HSC. Therefore, this integrin subunit was knocked out by CRISPR-Cas9 with two different gRNA. HSC were incubated under standard culture conditions for three days and the knockout efficiency was investigated. Densitometric analysis of Western blots revealed that the knockout efficiency of gRNA 1 was  $73 \pm 14\%$ , while gRNA 2 yielded a higher knockout efficiency of  $87 \pm 5\%$  (Figure 35A, B). Both gRNA led to a significant reduction in ITGA5 protein amounts in HSC.

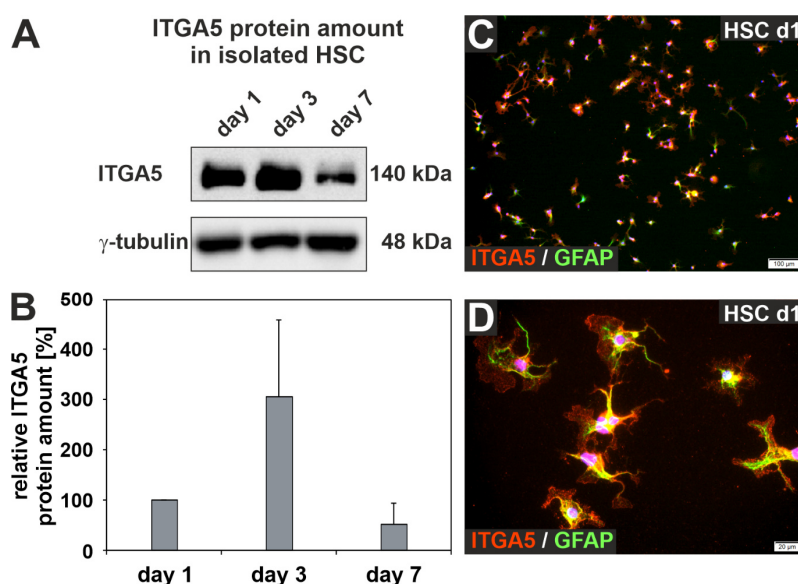


**Figure 34: Expression of ITGA5 in HSC.** (A, B) ITGA5 was expressed by isolated HSC as analyzed by Western blot. ITGA5 protein amount in HSC on day 1 was set to 100%. The data are presented as means  $\pm$  SEM ( $n = 3$ ; \*  $p < 0.05$ ). (C, D) HSC one day after isolation (d1) were positive for ITGA5 (red) and GFAP (green). Cell nuclei were stained with DAPI (blue; scale bars: C 100  $\mu$ m, D 20  $\mu$ m). Modified from Rohn *et al.* (under revision).

The CRISPR/Cas9-mediated *Itga5* knockout using the more efficient gRNA 2 led to a significant reduction of HGF released into the culture medium by HSC under static condition compared to culture supernatants from the mock control (Figure 35C). When HSC without ITGA5 were exposed to medium shear stress of 15 dyn/cm<sup>2</sup>, HGF was still released into the culture supernatant but the total amount of HGF decreased markedly with increasing knockout efficiency suggesting the involvement of ITGA5 in HGF release by HSC (Figure 35C). Since HSC lacking ITGA5 showed an impaired cell adhesion (Figure 35D), HGF concentration was normalized to cell number. The significantly lower number of adherent cells in case of HSC with *Itga5* knockout compared to mock control (Figure 35D) indicated that ITGA5 is important for focal adhesion in HSC. The reduction of HGF release as well as the decreased number of adherent cells correlated to the *Itga5* knockout efficiencies.

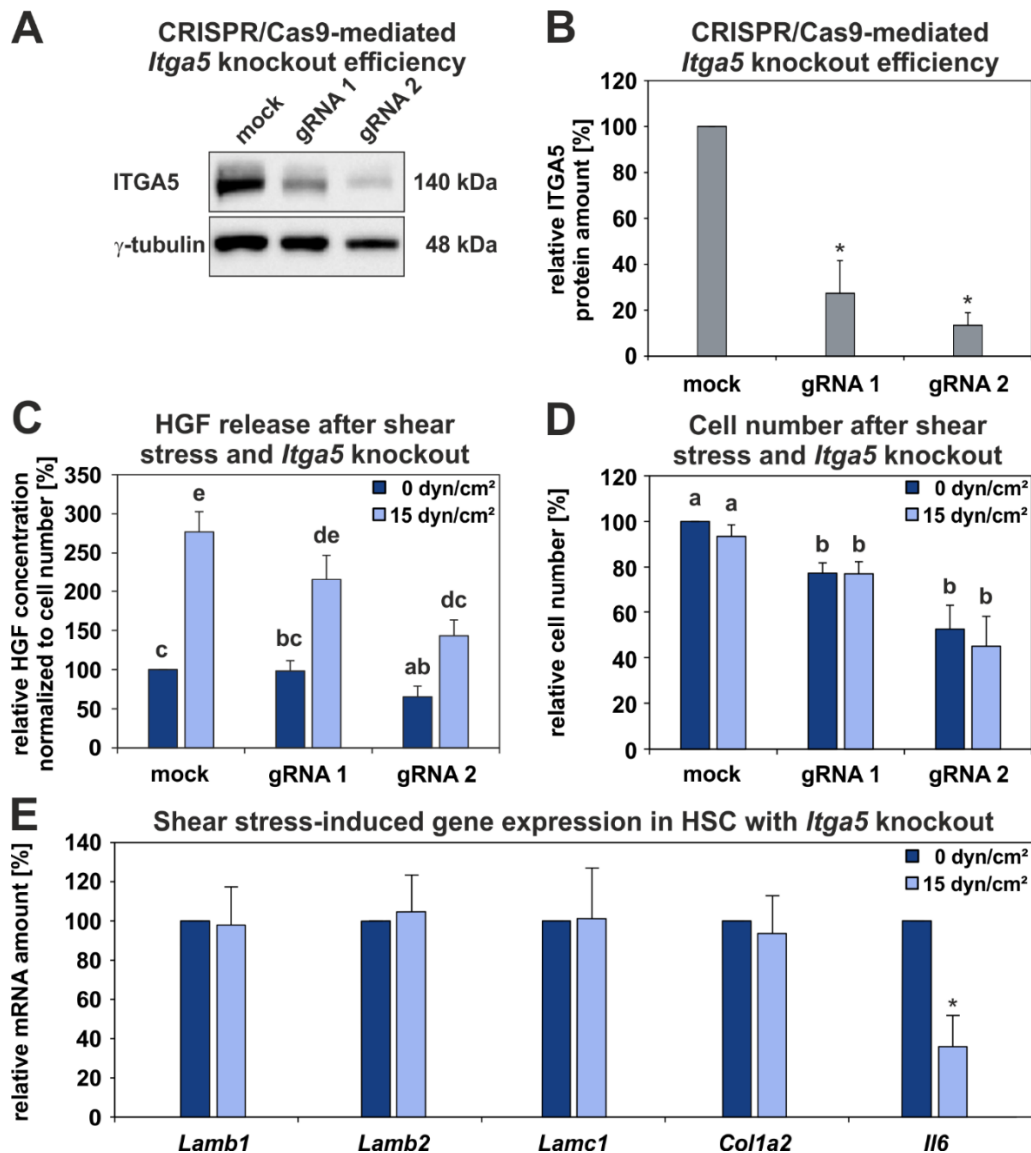


**Figure 35: Influence of shear stress on HSC with CRISPR/Cas9-mediated *Itga5* knockout.** (A, B) Western blot analyses of CRISPR/Cas9-mediated *Itga5* knockout in HSC after three days of culture. The efficiencies of two different gRNA were compared to ITGA5 protein amount in mock controls. The gRNA 1 yielded a lower knockout efficiency than gRNA 2.  $\gamma$ -tubulin served as a loading control. ITGA5 protein amount from mock was set to 100% for each independent experiment ( $n = 3$ ; \*  $p < 0.05$ ). (C) Relative HGF concentration analyzed by ELISA and normalized to cell number in culture supernatants from HSC with *Itga5* knockout after shear stress compared to mock. The HGF release into the culture supernatants by HSC with *Itga5* knockout was markedly lower compared to mock in response to shear stress. HGF concentration from mock static condition was set to 100% for each independent experiment. Significant differences are indicated by letters (a, b, c, d, e) and groups sharing the same letters did not differ significantly ( $n = 5$ ;  $p < 0.05$ ). (D) Relative cell number was assessed before and after shear stress experiments and revealed a correlation between *Itga5* knockout efficiency and HSC number. Cell number from mock static condition was set to 100% for each independent experiment and data are presented as means  $\pm$  SEM ( $n = 5$ ; a, b:  $p < 0.05$ ; groups sharing the same letters did not differ significantly) (E) Genes differentially expressed by HSC under shear stress (see Figure 32A) remained unchanged in HSC with *Itga5* knockout (gRNA 1). Only the *Il6* mRNA levels were significantly downregulated as observed in genetically unmodified HSC (see Figure 32C). The mRNA amount of the static condition was set to 100% for each independent experiment. The data are presented as means  $\pm$  SEM ( $n = 3$ ; \*  $p < 0.05$ ). Modified from Rohn *et al.* (under revision).

Finally, the expression of genes that could be induced in genetically unmodified HSC by shear stress (Figure 32A, C) were analyzed in HSC with *Itga5* knockout (gRNA 1) by qPCR. Interestingly, there were no alterations in the mRNA expression of ECM-associated genes (*Lamb1*, *Lamb2*, *Lamc1*, *Col1a2*), while the expression of *Il6* was still significantly reduced by  $64 \pm 16\%$  in HSC with *Itga5* knockout after exposure to shear stress (Figure 35E). The mRNA yield obtained from HSC with *Itga5* knockout using gRNA 2 was insufficient for qPCR-based expression analysis.

The expression of *Itgb1* was also reduced in HSC from aged rats (Table 7). In contrast to ITGA5, ITGB1 protein is not detectable in HSC shortly after isolation but appears early during activation as described previously (Kordes *et al.*, 2013). ITGA5 dimerizes with ITGB1 to form a functional integrin heterodimer (Tamkun *et al.*, 1986; Nagae *et al.*, 2012). Therefore, CRISPR/Cas9-mediated *Itgb1* knockout was also performed in freshly isolated HSC (gRNA 3), resulting in a knockout efficiency of about 98% (Figure 36A, B). After three days of culture, when HSC are positive for ITGB1 protein (Kordes *et al.*, 2013), HSC with *Itgb1* knockout were either collected to assess the knockout efficiency or exposed to medium shear stress (15 dyn/cm<sup>2</sup>) under serum-free conditions as described above. HSC with *Itgb1* knockout released significantly less HGF into the culture medium compared to mock control under static (0 dyn/cm<sup>2</sup>) and under shear stress conditions as analyzed by ELISA (Figure 36C). In addition, the *Itgb1* knockout impaired adhesion of HSC significantly (Figure 36D). Since ITGA5 and ITGB1 decrease in HSC, as observed in aged rat liver, significantly diminished HGF release, an important function of these integrin subunits in mechanosensing of HSC could be assumed. The mRNA yield obtained from HSC with *Itgb1* knockout was insufficient for qPCR-based expression analysis.

In conclusion, the results presented in section 3.2 indicate that HSC from old rat liver lose their typical characteristics and show signs of senescence. Furthermore, the interaction with important elements of their niche such as ECM composition and sensing of mechanical stimuli seem to be severely affected by aging. ITGA5 and ITGB1 apparently play an important role for the focal adhesion, mechanosensing, and signal transduction in HSC. Especially these integrin subunits are reduced in HSC and liver tissue from aged rats suggesting an impaired cell-ECM interaction as well as impaired mechanosensing in the liver during aging.

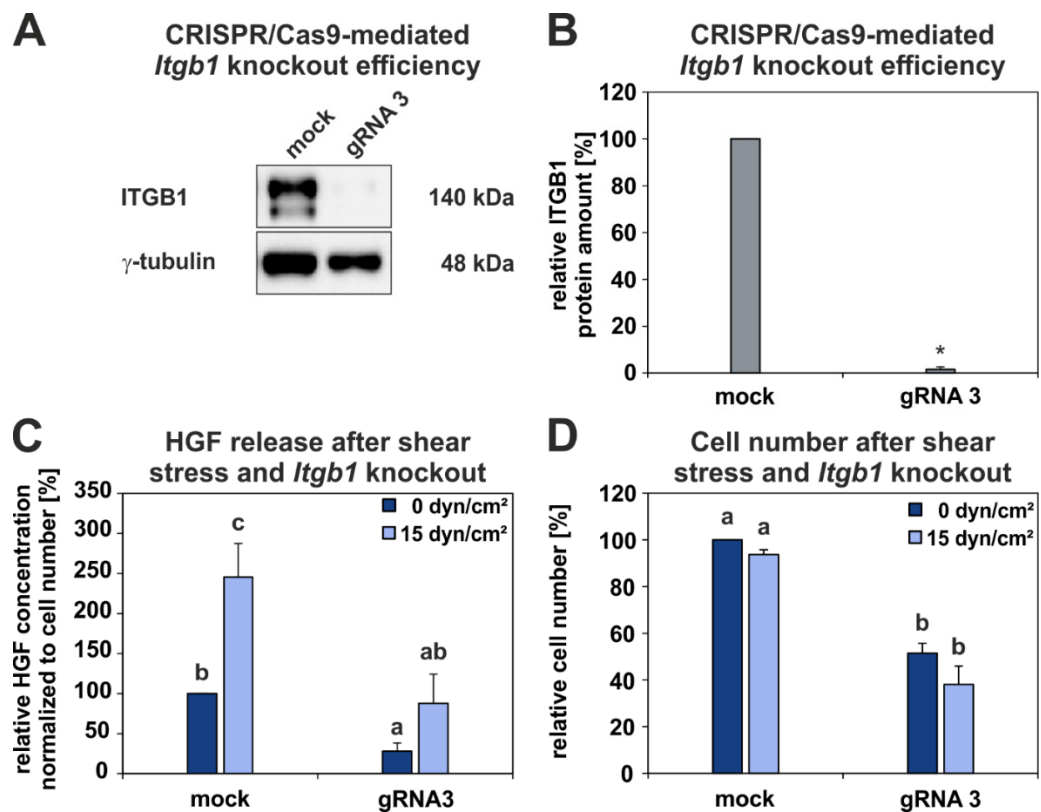


**Figure 36: Influence of shear stress on HSC with CRISPR/Cas9-mediated *Itgb1* knockout.** ITGB1 is not detectable in HSC during their quiescent state but appears early during their activation (Kordes *et al.*, 2013). **(A, B)** Western blot analyses of ITGB1 in HSC with CRISPR/Cas9-mediated *Itgb1* knockout. The efficiency of gRNA 3 was assessed in comparison to the ITGB1 protein amount of the mock control, which was set to 100% for each independent experiment.  $\gamma$ -tubulin served as a loading control ( $n = 3$ ;  $*p < 0.05$ ). **(C)** HSC with *Itgb1* knockout were exposed to medium shear stress (15 dyn/cm<sup>2</sup>) for one hour and the HGF concentration of the culture supernatant was measured by ELISA and normalized to cell number. The HGF concentration from mock static condition (0 dyn/cm<sup>2</sup>) was set to 100% for each independent experiment. The data are indicated as means  $\pm$  SEM ( $n = 3$ ; a, b, c:  $p < 0.05$ ; groups sharing the same letters did not differ significantly). **(D)** Relative cell number determined before and after application of shear stress. Knockout of *Itgb1* in freshly isolated HSC significantly reduced the number of adherent cells. The cell number from mock static condition was set to 100% for each independent experiment. The data are indicated as means  $\pm$  SEM ( $n = 3$ ; a, b:  $p < 0.05$ ; groups sharing the same letters did not differ significantly). Figure from Rohn *et al.* (under revision).

## 4. Discussion

This study provides new insights into fundamental mechanisms responsible for liver homeostasis involving MSC. The composition of the hepatic ECM as well as fluid mechanical forces were identified as key factors that govern the behavior of HSC and are altered during liver injury and aging. Particularly, the LAMA5 chain and shear stress were found to be important stem cell niche factors that support HSC maintenance and function. Evidence was provided that LAMA5 also supports stem cell characteristics of HSC and that this laminin chain is present in their stem cell niche, the space of Disse. Furthermore, it has previously been shown that the hepatic blood flow and the fenestration of the endothelium are reduced during aging (Le Couteur and McLean, 1998; McLean *et al.*, 2003) suggesting that HSC in the aged liver are exposed to lower shear stress. This study provides an interesting link between shear stress and HSC function since ECM-associated gene expression and HGF release were observed to be dependent on fluid flow. Moreover, it could be shown that important matrix proteins are reduced in the hepatic ECM from aged rats, which might lead to an impaired cell-ECM interaction. This interpretation is further supported by the observation that ITGA5 and ITGB1, which are significantly downregulated in HSC from aged rats, are involved in mechanosensing as well as -transduction leading to the increased expression of ECM protein-encoding genes. Finally, HSC from the aged rat liver were observed to develop a SASP, which could be explained (I) by reduced contact of HSC to their surrounding ECM and (II) by lowered ITGA5 and ITGB1 expression and shear stress as discussed in the following.

### 4.1. LN-521 promotes quiescence in HSC

In normal rat liver, LAMA5 was detected as a component of the basement membrane-like structure in liver sinusoids where it was co-localized with GFAP-positive HSC. Moreover, LAMA5 was found to be the most abundant  $\alpha$  chain in the rat liver matrix as determined by proteome analysis of decellularized liver tissue from normal rats. Furthermore, LAMB2 and LAMC1 were the dominant  $\beta$  and  $\gamma$  chains in hepatic ECM. These results confirmed an earlier study by Li *et al.* (2016) that describes LAMA5, LAMB2, and LAMC1 as major laminins of the normal rat liver matrix. These three laminin chains together compose the LN-521 trimer. During liver

regeneration associated with the appearance of putative progenitor cells, LAMA5 was also present in areas of ductular reaction indicated by CK19-positive cells. Chiu *et al.* (2009) made a similar observation in another rat liver injury model leading to proliferating putative progenitor cells associated with LAMA5 after 2AAF/carbon tetrachloride treatment. While LAMA5 was observed, LAMA2 – another laminin  $\alpha$  chain reported to occur in stem cell niches (Kazanis *et al.*, 2010) – was nearly undetectable in liver sinusoids and in areas of ductular reaction. Furthermore, LAMA2 was not detectable by proteome analysis of normal rat liver matrix. Since the LAMA2 and LAMA5 protein chains showed a distinct distribution in the 2AAF/PHx liver injury model, different functions of the two laminin  $\alpha$  chains during liver regeneration could be assumed. Overall, the observations of this work indicate an important role of LAMA5 during liver homeostasis and regeneration. Since LAMA5 was observed to be co-localized with GFAP-expressing HSC, the influence of the LAMA5-containing LN-521 on HSC was investigated.

Under standard culture conditions on PS, HSC activate and develop into myofibroblast-like cells. Thereby, HSC lose their retinoid-containing lipid droplets and reduce the expression of GFAP, while they upregulate the expression of  $\alpha$ -SMA and fibrillar collagens (Sawitza *et al.*, 2009; Reister *et al.*, 2011; Coll *et al.*, 2015; Schumacher *et al.*, 2017). Interestingly, adhesion and quiescence was promoted when HSC were cultured on LN-521-coated surfaces. Here, HSC maintained their retinoid-containing lipid droplets and significantly increased the expression of *Gfap*, *Notch1*, *reelin*, *Sparcl1*, *Lrat*, and *Ppary* compared to cells cultured on uncoated or on LN-211-coated surfaces which, in contrast, showed a myofibroblast-like cell morphology. It has been shown previously that LAMA5 is present in stem cell niches (Klaffky *et al.*, 2001) and that laminins containing this  $\alpha$  chain support stem cell characteristics *in vitro* (Laperle *et al.*, 2015). Since HSC are liver-resident MSC (Kordes *et al.*, 2013) that require a stem cell niche to preserve their characteristics (Sawitza *et al.*, 2009; Kordes and Häussinger, 2013; Kordes and Häussinger, 2019), it could be concluded from the results of this study that LAMA5 is an important niche element in the space of Disse. This is further supported by the increased expression of the stem cell-associated markers CD133, *Notch1*, *e-cadherin*, and *nestin* in HSC on LN-521. Even though the expression of the two activation markers  *$\alpha$ -Sma* and *nestin* were not altered at the mRNA level in HSC on different culture surfaces, the protein amount of  $\alpha$ -SMA was lower and that of *nestin* was higher when HSC were

cultured on LN-521 suggesting the presence of additional inversely regulated control mechanisms for translation. Furthermore, the culture of HSC on LN-521 did not only maintain quiescence but also re-established a quiescent-like state in stellate cell-derived myofibroblasts. However, quiescence could not be completely restored since only the expression of  $\alpha$ -Sma, Gfap, and e-cadherin was significantly altered among all analyzed markers. Nevertheless, re-establishing of a quiescent state in activated HSC has been shown to occur *in vivo* when the underlying etiological agent is removed in a mouse model for liver fibrosis (Kisseleva *et al.*, 2012). Therefore, additional factors such as retinoids, a softer culture substrate or co-culture with other hepatic cell types might be essential for complete re-establishment of quiescence in stellate cell-derived myofibroblasts.

For a defined laminin coating as well as for a better three-dimensional presentation of the laminin molecules a nanostructured surface was generated. On this laminin-functionalized surface a defined distance between single laminin molecules was provided since laminin was only bound to gold dots with defined spacing. This approach further improved HSC maintenance as demonstrated by the significantly upregulated mRNA expression of the quiescence markers *Sparcl1*, *Lrat*, and reelin in HSC on FS/LN-521. Surprisingly, HSC formed spheroids on FS/LN-211, which maintained retinoid-containing lipid droplets and expressed the quiescence marker SPARCL1. Huang *et al.* (2011) demonstrated spontaneous spheroid formation of MSC on biomaterials. These three-dimensional spheroids had been shown to maintain stem cell characteristics (Frith *et al.*, 2009). However, culture of HSC on FS/LN-521 further improved HSC quiescence compared to cells on PS/LN-521 and FS/LN-211. Interestingly, the number of adherent cells was inversely proportional to the spacing between the gold dots. In a different approach using another protein, namely a cyclic peptide of arginine-glycine-aspartic acid, for functionalization of nanostructured surfaces, Huang *et al.* (2009) also demonstrated that the adhesion of osteoblasts negatively correlates to the distance between the gold dots. Nevertheless, mRNA levels in HSC were not significantly affected by varying spacing which might be due to the small variation of the distance between gold dots in relation to the laminin molecule size of 100 nm (Doi *et al.*, 2002). Therefore, it was not possible to use a spacing below 70 nm because to prevent binding of one laminin molecule to several gold dots. On the contrary, a spacing larger than 150 nm would have exposed HSC to a larger PEG area and, thus, would have impaired cell

adhesion. However, the laminin-functionalized nanostructured surface further improved the supporting effect of LN-521 on HSC maintenance in a way that expression levels of quiescent HSC were obtained. This could be explained with a more natural and flexible presentation of the laminin proteins bound to the gold dots which provides better access of the cells to the laminin structure.

Different receptors might be responsible for the binding of HSC to LN-521 and for transducing signals, which lead to the maintenance of quiescence. This study investigated the expression of diverse laminin-specific receptors. Especially ITGB4 and LU/BCAM were found to be elevated on mRNA and protein level in HSC on PS/LN-521 compared to cells on PS and PS/LN-211. In contrast, the laminin-specific receptors SDC1 and DAG1 showed no altered mRNA expression in HSC on PS/LN-521 compared to PS. DAG1 has a higher binding affinity to LAMA1 and LAMA2 but lower to other laminin chains (Durbeej, 2010). However, DAG1 was not upregulated in HSC cultured on PS/LN-211. In case of ITGB4 it has been claimed previously that this integrin subunit is involved in the adhesion of human pluripotent stem cells to LN-521 (Kanninen *et al.*, 2016) and, furthermore, that ITGB4 together with ITGA6 might be responsible for the binding of K562 leukemic cells to LAMA5 (Kikkawa *et al.*, 2000). In line with this, the mean expression of *Itga6* was slightly increased in HSC cultured on PS/LN-521 suggesting an involvement of integrin  $\alpha_6\beta_4$  in the maintenance of HSC quiescence on LN-521. Moreover, LU/BCAM is a receptor that specifically mediates the binding to the LAMA5 chain (Mankelov *et al.*, 2007) and its presence has been described in ductular reaction during liver regeneration associated with progenitor cells (Miura *et al.*, 2018). In the present study, this LAMA5-specific receptor was also detected in liver sinusoids of normal rat liver and additionally in areas of ductular reaction in the 2AAF/PHx liver regeneration model. Furthermore, HSC on PS/LN-521 showed a stronger LU/BCAM immunofluorescence than cells on PS and PS/LN-211. Based on these results it is concluded that either integrin  $\alpha_6\beta_4$  and/or LU/BCAM are involved in the adhesion of HSC to LN-521.

Taken together, the results of this study demonstrate that LAMA5 is the most abundant  $\alpha$  chain in normal rat liver matrix. Furthermore, this  $\alpha$  chain is detectable in the sinusoids of normal rat liver where GFAP-positive HSC reside (Figure 37). As shown for other stem cell types, LN-521 also supports the quiescent state of isolated rat HSC, which are liver-resident MSC. This effect can be further improved with a

defined spacing between laminin molecules on LN-521-functionalized gold dots that provide a better three-dimensional presentation of the laminin trimer.

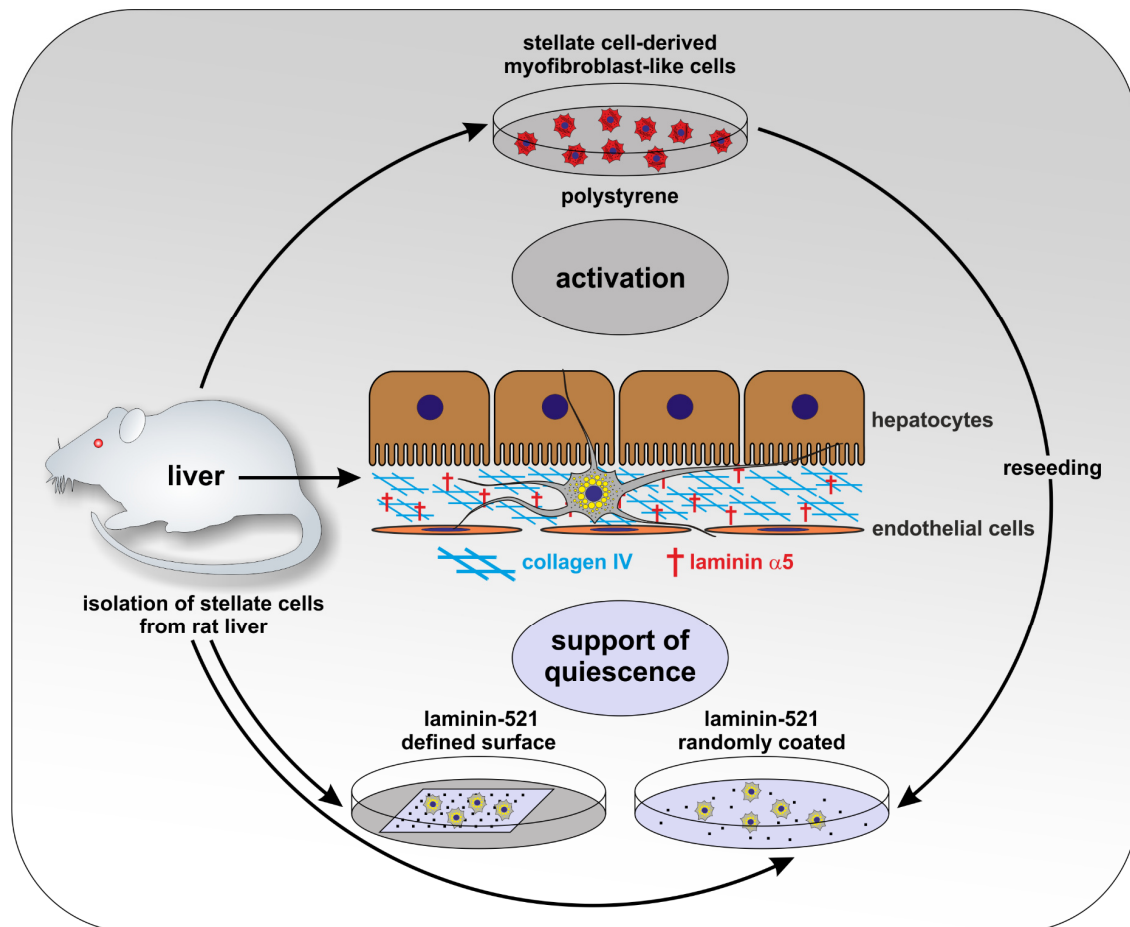


**Figure 37: Laminin  $\alpha 5$  is an element of the HSC niche.** In normal rat liver, LAMA5 chain was observed together with collagen IV in the liver sinusoids harboring HSC. The quiescent state of HSC was maintained when they were cultured on LN-521-coated plastic. This effect could be further improved by defining the distance between single LN-521 molecules on a bio-functionalized nanostructured surface. Furthermore, LN-521 could re-establish a quiescent-like state in HSC-derived myofibroblasts. Modified from Rohn *et al.* (2018).

LN-521 could not only preserve HSC quiescence but also re-established a quiescent-like state in stellate cell-derived myofibroblasts although HSC activation could not be completely prevented since the mRNA expression of  $\alpha$ -Sma and *Col1a2* was still on a high level when activated HSC were cultured on LN-521. It has been shown previously that the expression of these genes is induced in HSC by the culture on a stiff surface (Wells, 2005). Since surface stiffness of PS culture dishes is not lowered by LN-521 coating, the expression of activation markers remained elevated. However, the signs of HSC activation were markedly reduced by culture on LN-521. Overall, these results demonstrate that LAMA5 is a key factor in the microenvironment of HSC in the space of Disse.

#### 4.1. Mechanosensing of stellate cells from aged liver is impaired

A large set of genes and proteins was significantly altered in HSC and liver tissue from aged rats. Among them the expression of diverse genes associated with HSC quiescence such as *Sparcl1*, *Pparg*, *Gfap*, and *Lrat* was markedly downregulated. However, HSC from aged rats had more retinoid-containing lipid droplets which was in line with previous observations (Warren *et al.*, 2011). Markers that are typically expressed in activated HSC, such as *Col1a2*, *Col3a1*, *Col4a1*, *,  $\alpha$ -*Sma*, and desmin, were not differentially expressed or even reduced in HSC from aged livers. The reduced expression of ECM-encoding genes in HSC isolated from aged rats was summarized in the GO term “extracellular matrix organization”. These results indicate that the downregulated expression of quiescence-associated markers in HSC from old rats cannot be related to their myofibroblast-like phenotype in acute and chronic injured liver since ECM-encoding gene expression was also significantly reduced. Similar observations were made by other groups that demonstrated that senescence in activated HSC leads to decreased ECM deposition (Schnabl *et al.*, 2003; Krizhanovsky *et al.*, 2008) and reduced liver fibrosis in mice (Krizhanovsky *et al.*, 2008). HSC from aged rats had lost their typical expression pattern and biological processes associated with the GO terms “development” and “differentiation” were significantly altered. However, HSC did not show clear signs of cell lineage determination. Further GO term analysis of significantly altered genes in HSC from young and old rats revealed that the biological processes “cell migration”, “cell adhesion”, and “integrin-mediated signaling pathway” were affected by aging. A significant upregulation of *Cxcr4* and *Mmp13* expression and downregulation of *Vcl*, *Tln*, and *Itga5* expression indicated increased migration and impaired focal adhesion of HSC isolated from old rats and, thus, suggested impaired cell-ECM contact. Furthermore, biological processes associated with “inflammatory response” were altered in HSC from aged rat liver. This was in line with the increased expression and release of various cytokines by HSC from old rats such as CXCL1, CXCL3, and IL6. This specific pattern of SASP factors has been described to determine senescent cells (Coppé *et al.*, 2008; Coppé *et al.*, 2010; Freund *et al.*, 2010), which induce senescence in neighboring cells in a paracrine manner (Acosta *et al.*, 2013). Therefore, HSC from aged rats showed clear signs of senescence.*

Comparison of senescence-associated factors in whole liver tissue from young and old rats revealed only an increased expression of *p21/Cdkn1a* and a downregulated expression of *Smp30/Rgn*. Fujita *et al.* (1992) also reported on the reduction of SMP30/RGN in the aged rat liver. In contrast to isolated HSC, analyses of liver tissue and serum samples obtained no signs of increased inflammatory processes during aging. Moreover, no increase in oxidative stress could be detected in liver tissue from old compared to young rats. These results indicate that the rats included in this study aged under healthy conditions since inflammation and oxidative stress-associated tissue damage is mostly associated with a diseased state (Reuter *et al.*, 2010).

In addition to the increase of inflammatory factors, HSC from old rat liver significantly decreased the expression of various growth factors such as *Ctgf* and *Hgf* – both crucial for proper liver regeneration (Nakamura *et al.*, 1984; Yang *et al.*, 2013). The main alteration in human and rodent liver during aging is its decreased regenerative potential (Biondo-Simões Mde *et al.*, 2006; Timchenko, 2009; Zhu *et al.*, 2014; Enkhbold *et al.*, 2015). As a possible mechanism reduced HGF and c-Met expression had been suggested (Zhu *et al.*, 2014). Since HSC are critically involved in liver regeneration by the release of growth factors as proliferative stimuli for neighboring cells or by direct differentiation into hepatocytes and cholangiocytes, the loss of quiescence, increase of SASP factors, and reduction of growth factors (Figure 38) in HSC from old rat livers could explain the impaired regeneration capacity of the aged liver.

As described in section 1.4, HGF is necessary for proper liver regeneration. Already one hour after PHx, HGF reaches its maximum plasma concentration, which declines during the first 24 hours after surgery but remains elevated for more than three days (Lindroos *et al.*, 1991), while synthesis of new HGF starts three hours after injury (Michalopoulos, 2007). Two mechanisms leading to the fast HGF release had been proposed. First, HGF was claimed to be bound to the ECM as pro-HGF (Masumoto and Yamamoto, 1991) from where it is rapidly released and activated due to matrix degradation by MMPs shortly after liver injury (Kim *et al.*, 1997). Second, fluid mechanical forces acting on SEC by an increased blood flow induces the release of HGF (Lorenz *et al.*, 2018). In line with this, a pronounced reduction of HGF in liver sinusoids one day after PHx was observed in the present study. Since an age-related hepatic ECM reduction was demonstrated in this work, less HGF

might be bound to the matrix and is, therefore, available for liver regeneration. This is confirmed by the observation that the matrix-bound pro-HGF amount was significantly reduced in liver tissue from aged rats which further indicated a decreased HGF protein pool even though the *Hgf* mRNA levels remained unchanged in whole liver tissue.

One pronounced effect of aging in the liver is the decrease of blood flow by 20-55% as well as a reduced fenestration of the endothelium (Le Couteur and McLean, 1998; McLean *et al.*, 2003). Both observations could lead to a decreased fluid flow reaching HSC in the space of Disse and, thus, to reduced shear stress since the blood flow is positively proportional to shear stress (see formula in section 1.7). Interestingly, exposure of HSC from mid-aged rats to laminar pulsatile fluid flow led to an increased expression of ECM-encoding genes (i.e. *Col1a2*, *Lamb1*, *Lamb2*, *Lamc1*) that were downregulated in HSC of the aged rat liver. Furthermore, *Itga5* and *Il6* expression were significantly up- and downregulated, respectively, in response to shear stress suggesting that fluid mechanical forces can counteract some age-related processes. The results of this study are in line with previous observations in which reduced fluid mechanical forces led to decreased ECM protein deposition and *Itga5* expression, while increased shear stress downregulated *Il6* expression in endothelial cells (Urbich *et al.*, 2000; Lund *et al.*, 2010; Espinosa *et al.*, 2018). Since the liver represents a blood reservoir (Lautt and Greenway, 1976), it is especially exposed to blood flow alterations. The present study demonstrates that the function of HSC as liver-resident MSC is particularly affected by fluid shear stress and that there are universal mechanisms applying to different cell types concerning the response to these mechanical stimuli.

Furthermore, in this work evidence is provided that fluid mechanical forces also trigger the release of HGF by HSC as demonstrated for SEC (Lorenz *et al.*, 2018). However, *Hgf* expression in HSC was only slightly influenced by shear stress, but was significantly increased by LN-521. Overall, no significant differences between low, medium, and high shear stresses were observed at *Hgf* mRNA or released HGF protein level. This could be explained by the limitations of the perfusion system in which the lowest possible shear stress is 2.9 dyn/cm<sup>2</sup>. Noh *et al.* (2012) calculated that liver SEC are exposed to a shear stress of 3.7 dyn/cm<sup>2</sup>. In contrast to SEC, HSC are not directly exposed to the blood stream and the physiologic shear stress in the space of Disse might be lower. Nevertheless, this study provides an

interesting correlation between shear stress and HSC function. Furthermore, these results indicate that SEC in concert with HSC release HGF upon increased shear stress exposure due to enhanced blood flow shortly after PHx.

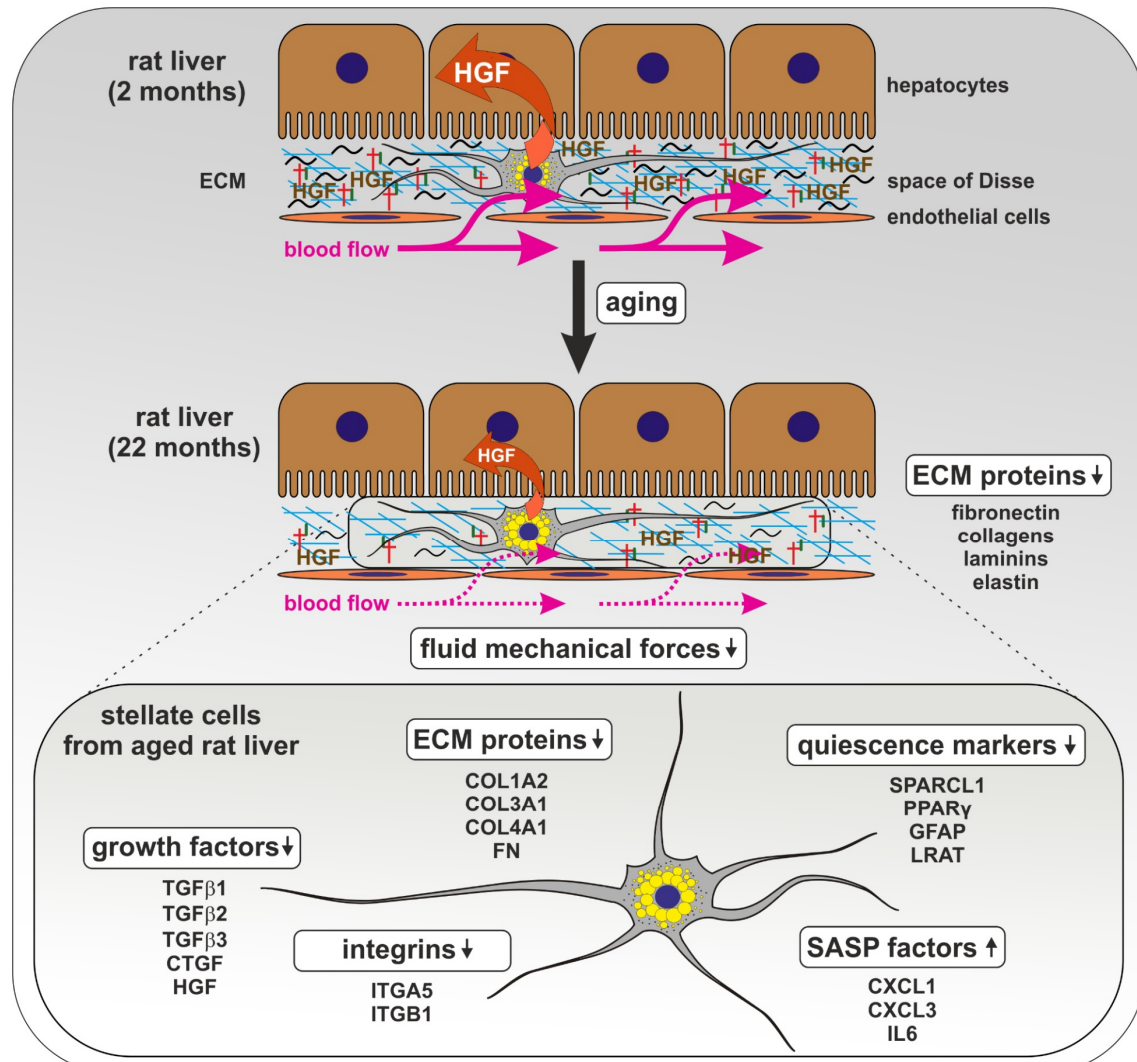


**Figure 38: The HSC niche is impaired by aging leading to senescence and loss of typical characteristics in HSC.** The hepatic ECM composition is altered due to aging. For instance, fibronectin, different collagens as well as laminins, and elastin are reduced in the aged rat liver. Thereby, also the HGF binding capacity of the matrix is lowered. Furthermore, during aging the fluid flow in the space of Disse is decreased since hepatic blood flow and fenestration of the endothelium are reduced. HSC from old rats exhibit a senescence-associated secretory phenotype (SASP) and typical characteristics such as growth factor synthesis (e.g. HGF) and expression of quiescence-associated markers are impaired. Moreover, HSC from old liver tissue reduce the fibronectin binding subunits ITGA5 and ITGB1 that are involved in cell adhesion and growth factor release. Modified from Rohn *et al.* (under revision).

Interestingly, stretching of HSC for one hour by about 30% also leads to an elevated HGF concentration in the culture supernatant of about 250% compared to unstretched HSC (Rohn *et al.*, under revision). This relative increase is comparable to the HGF amount released by HSC after the exposure to shear stress (Figure

31A). These observations suggest that different mechanical stimuli exerted by blood flow alterations trigger the release of HGF by HSC.

Although prevalence of liver fibrosis increases with advanced age (Mahrouf-Yorgov *et al.*, 2011), the results of the present study revealed that ECM proteins declined in the aged rat liver matrix (Figure 38) including fibrillar collagen types I (COL1A1, COL1A2) and III (COL3A1). Since MMP13 is known to cleave these fibrillar collagens (Freije *et al.*, 1994) and HSC from old rats significantly increase *Mmp13* and reduce *Ctgf* expression, it could be assumed that HSC are involved in the age-related matrix degradation in the liver. Even though LAMA5 protein amount was not altered during aging, the two other laminin chains of the LN-521 trimer (LAMB2, LAMC1) were reduced indicating an impaired stellate cell niche, since LN-521 was shown to play an important role for their maintenance and function as demonstrated in section 3.1 (Rohn *et al.*, 2018).

In addition to diverse collagens and laminins, especially ELN and FN were significantly downregulated in the aged rat liver. The reduction of FN in liver tissue from old rats had also been described in an earlier study by Singh and Kanungo (1993). Interestingly, FN was more prominent around larger vessels and nearly undetectable in the remaining liver parenchyma of old rats. In line with this, ITGA5 was significantly reduced in old compared to young rat liver. ITGA5 together with ITGB1 forms the FN receptor integrin  $\alpha_5\beta_1$  (Tamkun *et al.*, 1986; Takagi, 2004; Nagae *et al.*, 2012) and the mRNA expression of both integrin subunits were markedly downregulated in HSC from old rats. Interestingly, ITGA5 was prominent in liver sinusoids, while the  $\beta_1$  subunit was detectable in whole liver tissue suggesting a unique role of ITGA5 for sinusoidal cells in normal rat liver. This integrin subunit is essential for embryonic development and its relevance becomes obvious by an abnormal development of mesodermal structures in *Itga5* knockout mice (Yang *et al.*, 1993).

CRISPR/Cas9-mediated knockout of *Itga5* and *Itgb1* in isolated HSC decreased HGF release and impaired cell adhesion. Furthermore, *Itga5* knockout in HSC abolished the shear stress-induced expression of matrix-associated genes. Integrins do not only mediate cell adhesion but can also act as mechanosensors and -transducers (Häussinger *et al.*, 2003; vom Dahl *et al.*, 2003; Katsumi *et al.*, 2004; Schliess *et al.*, 2004). For instance, in hepatocytes cell volume changes are

transmitted via integrins to downstream signaling pathways (Häussinger *et al.*, 2006; Reinehr *et al.*, 2010). In the present study, the heterodimer integrin  $\alpha_5\beta_1$  was identified as an important mechanosensor in HSC involved in growth factor release, cell adhesion, and control of ECM synthesis. Since ITGA5 and ITGB1 decrease in old rat liver tissue, the aforementioned functions are impaired in the aged liver. Interestingly, the signaling pathways activated by physical forces via integrins are dependent on the specific ECM proteins to which the cells are attached (Katsumi *et al.*, 2004). For instance, ERK2 signaling is activated when fibroblasts are cultured on FN, JNK1 signaling on FN and laminin, whereas the incubation on collagen does not activate any MAP kinase (Katsumi *et al.*, 2004). Nevertheless, activation of diverse signaling pathways might vary in different cell types. However, these findings highlight the sensitive interaction between different elements of the microenvironment that show severe alterations in the aged liver as demonstrated in this study, such as sensing of mechanical stimuli and the matrix composition.

It has been shown previously that in endothelial cells mechanosensing by integrins containing the  $\beta_1$  subunit is involved in lymph vessel expansion and liver growth during embryogenesis as well as in liver maintenance (Planas-Paz *et al.*, 2012; Lorenz *et al.*, 2018). In quiescent HSC only ITGB1 mRNA but not its protein can be detected as demonstrated one day after isolation (Kordes *et al.*, 2013). As soon as they activate, HSC markedly increase ITGB1 protein amount (Kordes *et al.*, 2013). In contrast, this study confirmed the presence of ITGA5 protein in quiescent as well as in activated HSC. This raises the question whether another integrin  $\beta$  subunit interacts with ITGA5 to form a mechanosensor in quiescent HSC. However, the shear stress experiments presented in this study were performed three days after HSC isolation. At this time point HSC have already been activated (Schumacher *et al.*, 2017). Therefore, activation of HSC, as it is the case during liver disease and regeneration, might be essential for proper mechanosensing via the integrin  $\alpha_5\beta_1$  dimer. Batra *et al.* (2012a) demonstrated that integrin  $\alpha_5\beta_1$ -mediated signaling due to mechanical forces induced the opening of the hemichannel connexin 43 in osteocytes leading to the release of factors which are essential for bone formation and remodeling, such as calcium and prostaglandin E<sub>2</sub> (Batra *et al.*, 2012b). In normal liver, connexin 43 is mainly expressed by stellate cells (Fischer *et al.*, 2005) and it is significantly downregulated in HSC but not in whole liver tissue from aged rats (<http://www.ebi.ac.uk/arrayexpress>, accession number: E-MTAB-7423)

suggesting that direct cell-cell communication between HSC and neighboring liver cells might be impaired. However, connexin 43 is responsible for the shuttling of molecules smaller than 1.2 kDa between neighboring cells (Batra *et al.*, 2012b). In contrast, HGF is released into the extracellular space and its molecular weight is 82.9 kDa (<https://www.uniprot.org/uniprot/P17945>). Thus, it is not clear yet how ITGA5 is involved in the release of HGF and whether HGF also passes through a channel or is released by fusion of intracellular vesicles with the cell membrane.

Batra *et al.* (2012a) also observed that integrin  $\alpha_5\beta_1$ -mediated opening of hemichannels did not depend on binding to FN and the authors suggested an alternative function of ITGA5. A similar observation has been made in this study, since *Itga5* knockout in HSC led to impaired cell adhesion on COL4-coated surfaces indicating that integrins containing the ITGA5 subunit do not only bind to FN but are important for cellular adhesion in general. Since this work demonstrates an important link between ITGA5, focal adhesion, HGF release, and shear stress, a significant decrease of ITGA5 in HSC from aged liver could lead to an impaired anchorage to the basement membrane-like structure in the space of Disse and to reduced mechanosensitivity in HSC from old liver. Consequently, HSC lose their typical characteristics such as the supply of neighboring cells with growth factors.

Overall, this study demonstrates that fluid mechanical forces induce the expression of ITGA5. The reduced fluid flow in the space of Disse during aging might lead to the significant reduction of ITGA5 in the old rat liver. Since this study shows a correlation between the presence of ITGA5 and the release of HGF by HSC, affected mechanosensing might contribute to the impaired regenerative potential of the aged liver. In addition, ITGA5 seems to be important for the shear-stress induced expression of several ECM components suggesting that a decrease of ITGA5 in the aged rat liver could clarify age-related matrix alterations. This in turn, could result in fewer pro-HGF amounts bound to the aged hepatic ECM. Furthermore, ECM proteins that are essential for the maintenance of HSC characteristics such as LAMB2 and LAMC1 are diminished in the old liver matrix. This might lead to an impaired cell-matrix interaction and, thus, to weakened anchorage and increased migration accompanied by senescence. In addition, reduction of LAMB2 and LAMC1 in hepatic ECM during aging might contribute to the loss of HSC function since LN-521 promotes HGF synthesis by HSC. Consequently, less HGF is available for liver homeostasis or after liver injury.

## 5. Conclusion and Future Research

The insights gained in this research project demonstrate that several components in the microenvironment influence HSC function, for instance, proteins of the ECM, such as LN-521, and physical factors, such as shear stress. Alterations of the listed elements during aging seem to impair HSC characteristics which might contribute to the lowered regenerative capacity of the aged liver. Since the hepatic blood flow is decreased and the sinusoidal endothelium shows reduced fenestration during aging, the fluid flow reaching HSC in their niche might be lowered. Hence, HGF release by HSC might be also decreased in the aged liver. ITGA5 and ITGB1 are involved in the shear stress-induced release of HGF. Whether it is essential that HSC are activated and express ITGB1 protein to sense and transduce mechanical stimuli *in vivo* should be investigated in future studies. This work only included culture-activated HSC three days after isolation. No significant differences in HGF release using varying shear forces were observed indicating that upstream mechanisms are important for the response to mechanical forces in HSC such as the presence of ITGB1, which is only weakly present in their quiescent state. This question should be addressed by future research. Moreover, HGF release by HSC was apparently independent from the type of mechanical force applied, since the relative proportion of released HGF was the same when HSC were exposed to shear stress or stretched (Rohn *et al.*, under revision). Whether this is also true for other factors released by HSC or whether varying mechanical stimuli induce different cellular responses should be investigated in the future. Other possible age-related changes in the HSC niche such as the impact of an altered endothelium are also reasonable subjects of future research. Furthermore, it could also be investigated whether HSC innervation by the sympathetic nervous system is reduced during aging since HSC are in close contact to nerve endings. A first hint was obtained in this study by a significantly elevated expression of nerve growth factor (*Ngf*) in HSC (Table 11). Upregulation of *Ngf* might be a compensatory mechanism to guide nerve endings towards the space of Disse in the aged liver. Maryanovich *et al.* (2018) unveiled reduced innervation of bone marrow MSC by the sympathetic nervous system as a driving force for hematopoietic stem cell aging. Future research in this field will provide deeper insights into mechanisms that contribute to altered liver functions during aging and in chronic disease.

## 6. References

- Acosta JC, Banito A, Wuestefeld T, Georgilias A, Janich P, Morton JP, Athineos D, Kang TW, Lasitschka F, Andrulis M, Pascual G, Morris KJ, Khan S, Jin H, Dharmalingam G, Snijders AP, Carroll T, Capper D, Pritchard C, Inman GJ, Longerich T, Sansom OJ, Benitah SA, Zender L, Gil J. A complex secretory program orchestrated by the inflammasome controls paracrine senescence. *Nat Cell Biol* 2013;15:978-90.
- Ahsan T, Nerem RM. Fluid shear stress promotes an endothelial-like phenotype during the early differentiation of embryonic stem cells. *Tissue Eng Part A* 2010;16:3547-53.
- Alfaifi M, Eom YW, Newsome PN, Baik SK. Mesenchymal stromal cell therapy for liver diseases. *J Hepatol* 2018;68:1272-1285.
- Arias IM, Gatmaitan Z, Mikkelsen R, Penman S, Fay E. On the dynamic nature of hepatic endothelial-cell fenestrae. *Hepatology* 1986;6:1222-1222.
- Artavanis-Tsakonas S, Rand MD, Lake RJ. Notch signaling: cell fate control and signal integration in development. *Science* 1999;284:770-6.
- Aumailley M, Bruckner-Tuderman L, Carter WG, Deutzmann R, Edgar D, Ekblom P, Engel J, Engvall E, Hohenester E, Jones JC, Kleinman HK, Marinkovich MP, Martin GR, Mayer U, Meneguzzi G, Miner JH, Miyazaki K, Patarroyo M, Paulsson M, Quaranta V, Sanes JR, Sasaki T, Sekiguchi K, Sorokin LM, Talts JF, Tryggvason K, Uitto J, Virtanen I, von der Mark K, Wewer UM, Yamada Y, Yurchenco PD. A simplified laminin nomenclature. *Matrix Biology* 2005;24:326-332.
- Banas A, Teratani T, Yamamoto Y, Tokuhara M, Takeshita F, Quinn G, Okochi H, Ochiya T. Adipose tissue-derived mesenchymal stem cells as a source of human hepatocytes. *Hepatology* 2007;46:219-228.
- Bataller R, Brenner DA. Hepatic stellate cells as a target for the treatment of liver fibrosis. *Seminars in Liver Disease* 2001;21:437-451.
- Batra N, Burra S, Siller-Jackson AJ, Gu S, Xia X, Weber GF, DeSimone D, Bonewald LF, Lafer EM, Sprague E, Schwartz MA, Jiang JX. Mechanical stress-activated integrin  $\alpha 5\beta 1$  induces opening of connexin 43 hemichannels. *Proc Natl Acad Sci U S A* 2012a;109:3359-64.

- Batra N, Kar R, Jiang JX. Gap junctions and hemichannels in signal transmission, function and development of bone. *Biochim Biophys Acta* 2012b;1818:1909-18.
- Biondo-Simões Mde L, Matias JE, Montibeller GR, Siqueira LC, Nunes Eda S, Grassi CA. Effect of aging on liver regeneration in rats. *Acta Cir Bras* 2006;21:197-202.
- Blaner WS, O'Byrne SM, Wongsiriroj N, Kluwe J, D'Ambrosio DM, Jiang H, Schwabe RF, Hillman EM, Piantedosi R, Libien J. Hepatic stellate cell lipid droplets: a specialized lipid droplet for retinoid storage. *Biochim Biophys Acta* 2009;1791:467-473.
- Blümmel J, Perschmann N, Aydin D, Drinjakovic J, Surrey T, Lopez-Garcia M, Kessler H, Spatz JP. Protein repellent properties of covalently attached PEG coatings on nanostructured SiO<sub>2</sub>-based interfaces. *Biomaterials* 2007;28:4739-4747.
- Buckwalter JA, Woo SL, Goldberg VM, Hadley EC, Booth F, Oegema TR, Eyre DR. Soft-tissue aging and musculoskeletal function. *J Bone Joint Surg Am* 1993;75:1533-48.
- Cameron K, Tan R, Schmidt-Heck W, Campos G, Lyall MJ, Wang Y, Lucendo-Villarin B, Szkolnicka D, Bates N, Kimber SJ, Hengstler JG, Godoy P, Forbes SJ, Hay DC. Recombinant laminins drive the differentiation and self-organization of hESC-derived hepatocytes. *Stem Cell Reports* 2015;5:1250-1262.
- Caplan AI. Mesenchymal stem cells. *J Orthop Res* 1991;9:641-50.
- Carloni V, Romanelli RG, Pinzani M, Laffi G, Gentilini P. Expression and function of integrin receptors for collagen and laminin in cultured human hepatic stellate cells. *Gastroenterology* 1996;110:1127-36.
- Chamberlain J, Yamagami T, Colletti E, Theise ND, Desai J, Frias A, Pixley J, Zanjani ED, Porada CD, Almeida-Porada G. Efficient generation of human hepatocytes by the intrahepatic delivery of clonal human mesenchymal stem cells in fetal sheep. *Hepatology* 2007;46:1935-45.
- Chiu CC, Sheu JC, Chen CH, Lee CZ, Chiou LL, Chou SH, Huang GT, Lee HS. Global gene expression profiling reveals a key role of CD44 in hepatic oval-cell reaction after 2-AAF/CCI<sub>4</sub> injury in rodents. *Histochem Cell Biol* 2009;132:479-489.

- Christ B, Bruckner S, Winkler S. The therapeutic promise of mesenchymal stem cells for liver restoration. *Trends Mol Med* 2015;21:673-686.
- Cole MA, Quan T, Voorhees JJ, Fisher GJ. Extracellular matrix regulation of fibroblast function: redefining our perspective on skin aging. *J Cell Commun Signal* 2018.
- Coll M, El Taghdouini A, Perea L, Mannaerts I, Vila-Casadesús M, Blaya D, Rodrigo-Torres D, Affò S, Morales-Ibanez O, Graupera I, Lozano JJ, Najimi M, Sokal E, Lambrecht J, Ginès P, van Grunsven LA, Sancho-Bru P. Integrative miRNA and gene expression profiling analysis of human quiescent hepatic stellate cells. *Sci Rep* 2015;5:11549.
- Conover JC, Notti RQ. The neural stem cell niche. *Cell Tissue Res* 2008;331:211-24.
- Coppé JP, Desprez PY, Krtolica A, Campisi J. The senescence-associated secretory phenotype: the dark side of tumor suppression. *Annu Rev Pathol* 2010;5:99-118.
- Coppé JP, Patil CK, Rodier F, Sun Y, Munoz DP, Goldstein J, Nelson PS, Desprez PY, Campisi J. Senescence-associated secretory phenotypes reveal cell-nonautonomous functions of oncogenic RAS and the p53 tumor suppressor. *PLoS Biol* 2008;6:2853-68.
- Crisan M, Yap S, Casteilla L, Chen CW, Corselli M, Park TS, Andriolo G, Sun B, Zheng B, Zhang L, Norotte C, Teng PN, Traas J, Schugar R, Deasy BM, Badylak S, Buhring HJ, Giacobino JP, Lazzari L, Huard J, Peault B. A perivascular origin for mesenchymal stem cells in multiple human organs. *Cell Stem Cell* 2008;3:301-13.
- Davies PF. Flow-mediated endothelial mechanotransduction. *Physiol Rev* 1995;75:519-60.
- Doi M, Thyboll J, Kortessmaa J, Jansson K, Iivanainen A, Parvardeh M, Timpl R, Hedin U, Swedenborg J, Tryggvason K. Recombinant human laminin-10 ( $\alpha 5\beta 1\gamma 1$ ) Production, purification, and migration-promoting activity on vascular endothelial cells. *J Biol Chem* 2002;277:12741-12748.
- Durbeej M. Laminins. *Cell Tissue Res*. 2010;339:259.
- Eden E, Navon R, Steinfeld I, Lipson D, Yakhini Z. GOrilla: a tool for discovery and visualization of enriched GO terms in ranked gene lists. *BMC Bioinformatics* 2009;10:48.

- Ekblom P, Lonai P, Talts JF. Expression and biological role of laminin-1. *Matrix Biology* 2003;22:35-47.
- Enkhbold C, Morine Y, Utsunomiya T, Imura S, Ikemoto T, Arakawa Y, Saito Y, Yamada S, Ishikawa D, Shimada M. Dysfunction of liver regeneration in aged liver after partial hepatectomy. *J Gastroenterol Hepatol* 2015;30:1217-24.
- Espinosa MG, Taber LA, Wagenseil JE. Reduced embryonic blood flow impacts extracellular matrix deposition in the maturing aorta. *Dev Dyn* 2018;247:914-923.
- Fischer R, Reinehr R, Lu TP, Schonicke A, Warskulat U, Dienes HP, Häussinger D. Intercellular communication via gap junctions in activated rat hepatic stellate cells. *Gastroenterology* 2005;128:433-48.
- Fox JW, Mayer U, Nischt R, Aumailley M, Reinhardt D, Wiedemann H, Mann K, Timpl R, Krieg T, Engel J, et al. Recombinant nidogen consists of three globular domains and mediates binding of laminin to collagen type IV. *EMBO J* 1991;10:3137-46.
- Freije JM, Diez-Itza I, Balbin M, Sanchez LM, Blasco R, Tolivia J, Lopez-Otin C. Molecular cloning and expression of collagenase-3, a novel human matrix metalloproteinase produced by breast carcinomas. *J Biol Chem* 1994;269:16766-73.
- Freund A, Orjalo AV, Desprez PY, Campisi J. Inflammatory networks during cellular senescence: causes and consequences. *Trends Mol Med* 2010;16:238-46.
- Friedenstein AJ, Chailakhjan RK, Lalykina KS. The development of fibroblast colonies in monolayer cultures of guinea-pig bone marrow and spleen cells. *Cell Tissue Kinet* 1970;3:393-403.
- Frith JE, Thomson B, Genever PG. Dynamic three-dimensional culture methods enhance mesenchymal stem cell properties and increase therapeutic potential. *Tissue Eng Part C Methods* 2009;16:735-749.
- Fuchs E. Finding one's niche in the skin. *Cell Stem Cell* 2009;4:499-502.
- Fujita T, Uchida K, Maruyama N. Purification of senescence marker protein-30 (SMP30) and its androgen-independent decrease with age in the rat liver. *Biochim Biophys Acta* 1992;1116:122-8.
- Gersdorff N, Kohfeldt E, Sasaki T, Timpl R, Miosge N. Laminin  $\gamma$ 3 chain binds to nidogen and is located in murine basement membranes. *J Biol Chem* 2005;280:22146-22153.

- Gilgenkrantz H, Collin de l'Hortet A. Understanding liver regeneration: from mechanisms to regenerative medicine. *Am J Pathol* 2018;188:1316-1327.
- Glass R, Möller M, Spatz JP. Block copolymer micelle nanolithography. *Nanotechnology* 2003;14:1153-1160.
- Grube L, Dellen R, Kruse F, Schwender H, Stühler K, Poschmann G. Mining the secretome of C2C12 muscle cells: data dependent experimental approach to analyze protein secretion using label free quantification and peptide based analysis. *J Proteome Res* 2018;17:879-890.
- Guo G, von Meyenn F, Santos F, Chen Y, Reik W, Bertone P, Smith A, Nichols J. Naive pluripotent stem cells derived directly from isolated cells of the human inner cell mass. *Stem Cell Reports* 2016;6:437-446.
- Hahn E, Wick G, Pencev D, Timpl R. Distribution of basement membrane proteins in normal and fibrotic human liver: collagen type IV, laminin, and fibronectin. *Gut* 1980;21:63-71.
- Hanaoka F. DNA replication. SOS polymerases. *Nature* 2001;409:33-4.
- Häussinger D, Kordes C. Space of Disse: a stem cell niche in the liver. *Biol Chem* 2019: Ahead of print.
- Häussinger D, Kurz AK, Wettstein M, Graf D, Vom Dahl S, Schliess F. Involvement of integrins and Src in tauroursodeoxycholate-induced and swelling-induced cholestasis. *Gastroenterology* 2003;124:1476-1487.
- Häussinger D, Reinehr R, Schliess F. The hepatocyte integrin system and cell volume sensing. *Acta Physiologica* 2006;187:249-255.
- Haynes RH, Burton AC. Role of the non-Newtonian behavior of blood in hemodynamics. *Am J Physiol* 1959;197:943-50.
- Hendriks HFJ, Verhoofstad WAMM, Brouwer A, de Leeuw AM, Knook DL. Perisinusoidal fat-storing cells are the main vitamin A storage sites in rat liver. *Exp Cell Res* 1985;160:138-149.
- Higashi T, Friedman SL, Hoshida Y. Hepatic stellate cells as key target in liver fibrosis. *Advanced Drug Delivery Reviews* 2017;121:27-42.
- Higgins GM, Anderson RM. Experimental pathology of the liver – Restoration of the liver of the white rat following partial surgical removal. *Arch Pathol* 1931;12:186-202.

- Huang GS, Dai LG, Yen BL, Hsu SH. Spheroid formation of mesenchymal stem cells on chitosan and chitosan-hyaluronan membranes. *Biomaterials* 2011;32:6929-6945.
- Huang J, Grater SV, Corbellini F, Rinck S, Bock E, Kemkemer R, Kessler H, Ding J, Spatz JP. Impact of order and disorder in RGD nanopatterns on cell adhesion. *Nano Lett* 2009;9:1111-6.
- Huang Y, Jia X, Bai K, Gong X, Fan Y. Effect of fluid shear stress on cardiomyogenic differentiation of rat bone marrow mesenchymal stem cells. *Arch Med Res* 2010;41:497-505.
- Hui AY, Friedman SL. Extracellular matrix. Signaling pathways in liver diseases. Dufour J-F, Clavien P-A, Trautwein C and Graf R. Berlin, Heidelberg, Springer Berlin Heidelberg 2005:63-71.
- Hyun J, Oh SH, Premont RT, Guy CD, Berg CL, Diehl AM. Dysregulated activation of fetal liver programme in acute liver failure. *Gut* 2019;68:1076-1087.
- Ieronimakis N, Hays A, Prasad A, Janebodin K, Duffield JS, Reyes M. PDGFR $\alpha$  signalling promotes fibrogenic responses in collagen-producing cells in Duchenne muscular dystrophy. *J Pathol* 2016;240:410-424.
- Itskovitz-Eldor J, Schuldiner M, Karsenti D, Eden A, Yanuka O, Amit M, Soreq H, Benvenisty N. Differentiation of human embryonic stem cells into embryoid bodies comprising the three embryonic germ layers. *Mol Med* 2000;6:88-95.
- Janmey PA, McCulloch CA. Cell mechanics: integrating cell responses to mechanical stimuli. *Annu Rev Biomed Eng* 2007;9:1-34.
- Jones PH, Harper S, Watt FM. Stem cell patterning and fate in human epidermis. *Cell* 1995;80:83-93.
- Jones PH, Watt FM. Separation of human epidermal stem cells from transit amplifying cells on the basis of differences in integrin function and expression. *Cell* 1993;73:713-24.
- Kanninen LK, Harjumaki R, Peltoniemi P, Bogacheva MS, Salmi T, Porola P, Niklander J, Smutny T, Urtti A, Yliperttula ML, Lou YR. Laminin-511 and laminin-521-based matrices for efficient hepatic specification of human pluripotent stem cells. *Biomaterials* 2016;103:86-100.
- Katsumi A, Orr AW, Tzima E, Schwartz MA. Integrins in mechanotransduction. *J Biol Chem* 2004;279:12001-4.

- Kazanis I, Lathia JD, Vadakkan TJ, Raborn E, Wan R, Mughal MR, Eckley DM, Sasaki T, Patton B, Mattson MP, Hirschi KK, Dickinson ME, French-Constant C. Quiescence and activation of stem and precursor cell populations in the subependymal zone of the mammalian brain are associated with distinct cellular and extracellular matrix signals. *J Neurosci* 2010;30:9771-9781.
- Kikkawa Y, Sanzen N, Fujiwara H, Sonnenberg A, Sekiguchi K. Integrin binding specificity of laminin-10/11: laminin-10/11 are recognized by  $\alpha 3\beta 1$ ,  $\alpha 6\beta 1$  and  $\alpha 6\beta 4$  integrins. *J Cell Sci* 2000;113:869-876.
- Kim TH, Mars WM, Stolz DB, Michalopoulos GK. Expression and activation of pro-MMP-2 and pro-MMP-9 during rat liver regeneration. *Hepatology* 2000;31:75-82.
- Kim TH, Mars WM, Stolz DB, Petersen BE, Michalopoulos GK. Extracellular matrix remodeling at the early stages of liver regeneration in the rat. *Hepatology* 1997;26:896-904.
- Kisseleva T, Cong M, Paik Y, Scholten D, Jiang C, Benner C, Iwaisako K, Moore-Morris T, Scott B, Tsukamoto H, Evans SM, Dillmann W, Glass CK, Brenner DA. Myofibroblasts revert to an inactive phenotype during regression of liver fibrosis. *Proc Natl Acad Sci USA* 2012;109:9448-53.
- Kitani K. Aging of the liver: facts and theories. *Arch Gerontol Geriatr* 1991;12:133-54.
- Klaffky E, Williams R, Yao CC, Ziober B, Kramer R, Sutherland A. Trophoblast-specific expression and function of the integrin  $\alpha 7$  subunit in the peri-implantation mouse embryo. *Dev Biol* 2001;239:161-175.
- Kobold D, Grundmann A, Piscaglia F, Eisenbach C, Neubauer K, Steffgen J, Ramadori G, Knittel T. Expression of reelin in hepatic stellate cells and during hepatic tissue repair: a novel marker for the differentiation of HSC from other liver myofibroblasts. *J Hepatol* 2002;36:607-13.
- Kordes C, Häussinger D. Hepatic stem cell niches. *J Clin Invest* 2013;123:1874-1880.
- Kordes C, Häussinger D. Space of Disse: a stem cell niche in the liver. *Biological chemistry* 2019: Ahead of print.
- Kordes C, Sawitza I, Götze S, Häussinger D. Hepatic stellate cells support hematopoiesis and are liver-resident mesenchymal stem cells. *Cell Physiol Biochem* 2013;31:290-304.

- Kordes C, Sawitza I, Götze S, Herebian D, Häussinger D. Hepatic stellate cells contribute to progenitor cells and liver regeneration. *J Clin Invest* 2014;124:5503-5515.
- Kramann R, Schneider RK, DiRocco DP, Machado F, Fleig S, Bondzie PA, Henderson JM, Ebert BL, Humphreys BD. Perivascular Gli1+ progenitors are key contributors to injury-induced organ fibrosis. *Cell Stem Cell* 2015;16:51-66.
- Krizhanovsky V, Yon M, Dickins RA, Hearn S, Simon J, Miething C, Yee H, Zender L, Lowe SW. Senescence of activated stellate cells limits liver fibrosis. *Cell* 2008;134:657-67.
- Labun K, Montague TG, Gagnon JA, Thyme SB, Valen E. CHOPCHOP v2: a web tool for the next generation of CRISPR genome engineering. *Nucleic Acids Res* 2016;44:W272-6.
- Lane SW, Williams DA, Watt FM. Modulating the stem cell niche for tissue regeneration. *Nat Biotechnol* 2014;32:795-803.
- Laperle A, Hsiao C, Lampe M, Mortier J, Saha K, Palecek SP, Masters KS.  $\alpha$ -5 laminin synthesized by human pluripotent stem cells promotes self-renewal. *Stem Cell Reports* 2015;5:195-206.
- Lautt WW. *Hepatic circulation: physiology and pathophysiology*. San Rafael (CA) 2009.
- Lautt WW, Greenway CV. Hepatic venous compliance and role of liver as a blood reservoir. *Am J Physiol* 1976;231:292-295.
- Le Couteur DG, McLean AJ. The aging liver. Drug clearance and an oxygen diffusion barrier hypothesis. *Clin Pharmacokinet* 1998;34:359-73.
- LeCouter J, Moritz DR, Li B, Phillips GL, Liang XH, Gerber HP, Hillan KJ, Ferrara N. Angiogenesis-independent endothelial protection of liver: role of VEGFR-1. *Science* 2003;299:890-3.
- Li CJ, Cheng P, Liang MK, Chen YS, Lu Q, Wang JY, Xia ZY, Zhou HD, Cao X, Xie H, Liao EY, Luo XH. MicroRNA-188 regulates age-related switch between osteoblast and adipocyte differentiation. *J Clin Invest* 2015;125:1509-1522.
- Li Q, Uygun BE, Geerts S, Ozer S, Scalf M, Gilpin SE, Ott HC, Yarmush ML, Smith LM, Welham NV, Frey BL. Proteomic analysis of naturally-sourced biological scaffolds. *Biomaterials* 2016;75:37-46.

- Liétard J, Loréal O, Théret N, Champion JP, L'Helgoualc'h A, Turlin B, Ramée MP, Yamada Y, Clément B. Laminin isoforms in non-tumoral and tumoral human livers. Expression of  $\alpha 1$ ,  $\alpha 2$ ,  $\beta 1$ ,  $\beta 2$  and  $\gamma 1$  chain mRNA and an  $\alpha$  chain homologous to the  $\alpha 2$  chain. *J Hepatol* 1998;28:691-699.
- Lindroos PM, Zarnegar R, Michalopoulos GK. Hepatocyte growth-factor (hepatopoietin-a) rapidly increases in plasma before DNA-synthesis and liver-regeneration stimulated by partial-hepatectomy and carbon-tetrachloride administration. *Hepatology* 1991;13:743-750.
- Liu L, Yuan W, Wang J. Mechanisms for osteogenic differentiation of human mesenchymal stem cells induced by fluid shear stress. *Biomech Model Mechanobiol* 2010;9:659-70.
- Liu Y, Yang X, Jing Y, Zhang S, Zong C, Jiang J, Sun K, Li R, Gao L, Zhao X, Wu D, Shi Y, Han Z, Wei L. Contribution and mobilization of mesenchymal stem cells in a mouse model of carbon tetrachloride-induced liver fibrosis. *Sci Rep* 2015;5:17762.
- Livak KJ, Schmittgen TD. Analysis of relative gene expression data using real-time quantitative PCR and the  $2^{-\Delta\Delta CT}$  method. *Methods* 2001;25:402-408.
- Lohmüller T, Aydin D, Schwieder M, Morhard C, Louban I, Pacholski C, Spatz JP. Nanopatterning by block copolymer micelle nanolithography and bioinspired applications. *Biointerphases* 2011;6:MR1.
- Lorenz L, Axnick J, Buschmann T, Henning C, Urner S, Fang S, Nurmi H, Eichhorst N, Holtmeier R, Bodis K, Hwang JH, Mussig K, Eberhard D, Stypmann J, Kuss O, Roden M, Alitalo K, Häussinger D, Lammert E. Mechanosensing by  $\beta 1$  integrin induces angiocrine signals for liver growth and survival. *Nature* 2018;562:128-132.
- Lund T, Hermansen SE, Andreassen TV, Olsen JO, Osterud B, Myrmel T, Ytrehus K. Shear stress regulates inflammatory and thrombogenic gene transcripts in cultured human endothelial progenitor cells. *Thromb Haemost* 2010;104:582-91.
- Mabuchi A, Mullaney I, Sheard PW, Hessian PA, Mallard BL, Tawadrous MN, Zimmermann A, Senoo H, Wheatley AM. Role of hepatic stellate cell/hepatocyte interaction and activation of hepatic stellate cells in the early phase of liver regeneration in the rat. *J Hepatol* 2004;40:910-6.

- MacKenna DA, Dolfi F, Vuori K, Ruoslahti E. Extracellular signal-regulated kinase and c-Jun NH2-terminal kinase activation by mechanical stretch is integrin-dependent and matrix-specific in rat cardiac fibroblasts. *J Clin Invest* 1998;101:301-10.
- Mahrouf-Yorgov M, Collin de l'Hortet A, Cosson C, Slama A, Abdoun E, Guidotti JE, Fromenty B, Mitchell C, Gilgenkrantz H. Increased susceptibility to liver fibrosis with age is correlated with an altered inflammatory response. *Rejuvenation Res* 2011;14:353-363.
- Mankelov TJ, Burton N, Stefansdottir FO, Spring FA, Parsons SF, Pedersen JS, Oliveira CL, Lammie D, Wess T, Mohandas N, Chasis JA, Brady RL, Anstee DJ. The Laminin 511/521-binding site on the Lutheran blood group glycoprotein is located at the flexible junction of Ig domains 2 and 3. *Blood* 2007;110:3398-406.
- Marriott S, Baskir RS, Gaskill C, Menon S, Carrier EJ, Williams J, Talati M, Helm K, Alford CE, Kropski JA, Loyd J, Wheeler L, Johnson J, Austin E, Nozik-Grayck E, Meyrick B, West JD, Klemm DJ, Majka SM. ABCG2pos lung mesenchymal stem cells are a novel pericyte subpopulation that contributes to fibrotic remodeling. *Am J Physiol Cell Physiol* 2014;307:C684-98.
- Marubashi S, Sakon M, Nagano H, Gotoh K, Hashimoto K, Kubota M, Kobayashi S, Yamamoto S, Miyamoto A, Dono K, Nakamori S, Umeshita K, Monden M. Effect of portal hemodynamics on liver regeneration studied in a novel portohepatic shunt rat model. *Surgery* 2004;136:1028-37.
- Maryanovich M, Zahalka AH, Pierce H, Pinho S, Nakahara F, Asada N, Wei Q, Wang X, Ciero P, Xu J, Leftin A, Frenette PS. Adrenergic nerve degeneration in bone marrow drives aging of the hematopoietic stem cell niche. *Nat Med* 2018;24:782-791.
- Masumoto A, Yamamoto N. Sequestration of a hepatocyte growth factor in extracellular matrix in normal adult rat liver. *Biochem Biophys Res Commun* 1991;174:90-5.
- Maximow A. Über experimentelle Erzeugung von Knochenmarkgewebe. *Anat Anz* 1906;28:607-612.
- McLean AJ, Cogger VC, Chong GC, Warren A, Markus AM, Dahlstrom JE, Le Couteur DG. Age-related pseudocapillarization of the human liver. *J Pathol* 2003;200:112-7.

- Meschiari CA, Ero OK, Pan H, Finkel T, Lindsey ML. The impact of aging on cardiac extracellular matrix. *Geroscience* 2017;39:7-18.
- Michalopoulos GK. Liver regeneration. *J Cell Physiol* 2007;213:286-300.
- Michalopoulos GK. Liver regeneration after partial hepatectomy: critical analysis of mechanistic dilemmas. *Am J Pathol* 2010;176:2-13.
- Michalopoulos GK, DeFrances MC. Liver regeneration. *Science* 1997;276:60-6.
- Miner JH, Cunningham J, Sanes JR. Roles for laminin in embryogenesis: exencephaly, syndactyly, and placentopathy in mice lacking the laminin  $\alpha 5$  chain. *J Cell Biol* 1998;143:1713-1723.
- Miura Y, Matsui S, Miyata N, Harada K, Kikkawa Y, Ohmuraya M, Araki K, Tsurusaki S, Okochi H, Goda N, Miyajima A, Tanaka M. Differential expression of Lutheran/BCAM regulates biliary tissue remodeling in ductular reaction during liver regeneration. *Elife* 2018;7.
- Miyahara T, Schrum L, Rippe R, Xiong S, Yee HF, Jr., Motomura K, Anania FA, Willson TM, Tsukamoto H. Peroxisome proliferator-activated receptors and hepatic stellate cell activation. *J Biol Chem* 2000;275:35715-22.
- Mohammed FF, Khokha R. Thinking outside the cell: proteases regulate hepatocyte division. *Trends Cell Biol* 2005;15:555-63.
- Moro L, Venturino M, Bozzo C, Silengo L, Altruda F, Beguinot L, Tarone G, Defilippi P. Integrins induce activation of EGF receptor: role in MAP kinase induction and adhesion-dependent cell survival. *EMBO J* 1998;17:6622-32.
- Morsiani E, Aleotti A, Ricci D. Haemodynamic and ultrastructural observations on the rat liver after two-thirds partial hepatectomy. *J Anat* 1998;192 ( Pt 4):507-15.
- Morsiani E, Mazzoni M, Aleotti A, Gorini P, Ricci D. Increased sinusoidal wall permeability and liver fatty change after two-thirds hepatectomy: an ultrastructural study in the rat. *Hepatology* 1995;21:539-44.
- Nagae M, Re S, Mihara E, Nogi T, Sugita Y, Takagi J. Crystal structure of  $\alpha 5 \beta 1$  integrin ectodomain: atomic details of the fibronectin receptor. *J Cell Biol* 2012;197:131-40.
- Nakamura T, Nawa K, Ichihara A. Partial purification and characterization of hepatocyte growth factor from serum of hepatectomized rats. *Biochem Biophys Res Commun* 1984;122:1450-9.

- Naldini L, Vigna E, Narsimhan RP, Gaudino G, Zarnegar R, Michalopoulos GK, Comoglio PM. Hepatocyte growth factor (HGF) stimulates the tyrosine kinase activity of the receptor encoded by the proto-oncogene c-MET. *Oncogene* 1991;6:501-4.
- Nava MM, Raimondi MT, Pietrabissa R. Controlling self-renewal and differentiation of stem cells via mechanical cues. *J Biomed Biotechnol* 2012;2012:797410.
- Niki T, Pekny M, Hellemans K, De Bleser P, Van den Berg K, Vaeyens F, Quartier E, Schuit F, Geerts A. Class VI intermediate filament protein nestin is induced during activation of rat hepatic stellate cells. *Hepatology* 1999;29:520-527.
- Noh JK, Jung JG, Jang EM, Lee JH, Park HJ, Kim YA, Jung SM, Kwon CH, Lee DH, Lee SK. Live cell-imaging perfusion culture system of liver sinusoidal endothelial cells to mimic stem cell engraftment in liver. *Transplant Proc* 2012;44:1116-9.
- O'Hagan-Wong K, Nadeau S, Carrier-Leclerc A, Apablaza F, Hamdy R, Shum-Tim D, Rodier F, Colmegna I. Increased IL-6 secretion by aged human mesenchymal stromal cells disrupts hematopoietic stem and progenitor cells' homeostasis. *Oncotarget* 2016;7:13285-13296.
- Petersen BE, Bowen WC, Patrene KD, Mars WM, Sullivan AK, Murase N, Boggs SS, Greenberger JS, Goff JP. Bone marrow as a potential source of hepatic oval cells. *Science* 1999;284:1168-1170.
- Planas-Paz L, Strilic B, Goedecke A, Breier G, Fassler R, Lammert E. Mechanoinduction of lymph vessel expansion. *EMBO J* 2012;31:788-804.
- Poisson J, Lemoine S, Boulanger C, Durand F, Moreau R, Valla D, Rautou PE. Liver sinusoidal endothelial cells: physiology and role in liver diseases. *J Hepatol* 2017;66:212-227.
- Pöschl E, Fox JW, Block D, Mayer U, Timpl R. Two non-contiguous regions contribute to nidogen binding to a single EGF-like motif of the laminin  $\gamma$ 1 chain. *EMBO J* 1994;13:3741-7.
- Quesenberry PJ, Becker PS. Stem cell homing: rolling, crawling, and nesting. *Proc Natl Acad Sci USA* 1998;95:15155-7.
- Qvartskhava N, Jin CJ, Buschmann T, Albrecht U, Bode JG, Monhasery N, Oenarto J, Bidmon HJ, Gorg B, Häussinger D. Taurine transporter (TauT) deficiency impairs ammonia detoxification in mouse liver. *Proc Natl Acad Sci U S A* 2019;116:6313-6318.

- Rani HP, Sheu TW, Chang TM, Liang PC. Numerical investigation of non-Newtonian microcirculatory blood flow in hepatic lobule. *J Biomech* 2006;39:551-63.
- Rashidi H, Alhaque S, Szkolnicka D, Flint O, Hay DC. Fluid shear stress modulation of hepatocyte-like cell function. *Arch Toxicol* 2016;90:1757-61.
- Raven A, Lu WY, Man TY, Ferreira-Gonzalez S, O'Duibhir E, Dwyer BJ, Thomson JP, Meehan RR, Bogorad R, Koteliansky V, Kotelevset Y, Ffrench-Constant C, Boulter L, Forbes SJ. Cholangiocytes act as facultative liver stem cells during impaired hepatocyte regeneration. *Nature* 2017;547:350.
- Reeves HL, Friedman SL. Activation of hepatic stellate cells--a key issue in liver fibrosis. *Front Biosci* 2002;7:d808-26.
- Reinehr R, Häussinger D. CD95 activation in the liver: ion fluxes and oxidative signaling. *Arch Biochem Biophys* 2007;462:124-31.
- Reinehr R, Sommerfeld A, Häussinger D. Insulin induces swelling-dependent activation of the epidermal growth factor receptor in rat liver. *J Biol Chem* 2010;285:25904-12.
- Reister S, Kordes C, Sawitza I, Häussinger D. The epigenetic regulation of stem cell factors in hepatic stellate cells. *Stem Cells Dev.* 2011;20:1687-1699.
- Reuter S, Gupta SC, Chaturvedi MM, Aggarwal BB. Oxidative stress, inflammation, and cancer How are they linked? *Free Radic Biol Med* 2010;49:1603-1616.
- Rockey D, Boyles J, Gabbiani G, Friedman SL. Rat hepatic lipocytes express smooth muscle actin upon activation in vivo and in culture. *J Submicrosc Cytol Pathol* 1992;24:193-203.
- Rogers EH, Hunt JA, Pekovic-Vaughan V. Adult stem cell maintenance and tissue regeneration around the clock: do impaired stem cell clocks drive age-associated tissue degeneration? *Biogerontology* 2018;19:497-517.
- Rohn F, Kordes C, Castoldi M, Götze S, Poschmann G, Stühler K, Herebian D, Benk AS, Geiger F, Zhang T, Spatz JP, Häussinger D. Laminin-521 promotes quiescence in isolated stellate cells from rat liver. *Biomaterials* 2018;180:36-51.
- Ross TD, Coon BG, Yun S, Baeyens N, Tanaka K, Ouyang M, Schwartz MA. Integrins in mechanotransduction. *Curr Opin Cell Biol* 2013;25:613-8.
- Saito Y, Morine Y, Shimada M. Mechanism of impairment on liver regeneration in elderly patients: Role of hepatic stellate cell function. *Hepatol Res* 2017;47:505-513.

- Sawitza I, Kordes C, Reister S, Häussinger D. The niche of stellate cells within rat liver. *Hepatology* 2009;50:1617-1624.
- Scarabelli L, Cesarone CF, Giannoni P, Porotto A, Gallo G, Orunesu M. Effect of N-2-acetylaminofluorene on poly(ADP-ribose) polymerase activity and DNA synthesis in cultured rat hepatocytes exposed to epidermal growth factor. *Boll Soc Ital Biol Sper* 1992;68:55-62.
- Schirmacher P, Geerts A, Jung W, Pietrangelo A, Rogler CE, Dienes HP. The role of Ito cells in the biosynthesis of HGF-SF in the liver. *EXS* 1993;65:285-99.
- Schliess F, Reissmann R, Reinehr R, vom Dahl S, Häussinger D. Involvement of integrins and Src in insulin signaling toward autophagic proteolysis in rat liver. *J Biol Chem* 2004;279:21294-301.
- Schmucker DL. Hepatocyte fine structure in mature and senescent rats. *J Electron Microscop Tech* 1990;14:106-125.
- Schmucker DL, Sachs H. Quantifying dense bodies and lipofuscin during aging: a morphologist's perspective. *Arch Gerontol Geriatr* 2002;34:249-61.
- Schnabl B, Purbeck CA, Choi YH, Hagedorn CH, Brenner DA. Replicative senescence of activated human hepatic stellate cells is accompanied by a pronounced inflammatory but less fibrogenic phenotype. *Hepatology* 2003;37:653-664.
- Schofield R. The relationship between the spleen colony forming cell and the haemopoietic stem cell. *Blood Cells* 1978;4:7-25.
- Schumacher EC, Götze S, Kordes C, Benes V, Häussinger D. Combined methylome and transcriptome analysis during rat hepatic stellate cell activation. *Stem Cells Dev* 2017;26:1759-1770.
- Sera T, Sumii T, Fujita R, Kudo S. Effect of shear stress on the migration of hepatic stellate cells. *In Vitro Cell Dev Biol Anim* 2018;54:11-22.
- Shen Q, Wang Y, Kokovay E, Lin G, Chuang SM, Goderie SK, Roysam B, Temple S. Adult SVZ stem cells lie in a vascular niche: a quantitative analysis of niche cell-cell interactions. *Cell Stem Cell* 2008;3:289-300.
- Shu SN, Wei L, Wang JH, Zhan YT, Chen HS, Wang Y. Hepatic differentiation capability of rat bone marrow-derived mesenchymal stem cells and hematopoietic stem cells. *World J Gastroenterol* 2004;10:2818-22.
- Sies H. Strategies of antioxidant defense. *Eur J Biochem* 1993;215:213-9.

- Singh S, Kanungo MS. Changes in expression and CRE binding proteins of the fibronectin gene during aging of the rat. *Biochem Biophys Res Commun* 1993;193:440-5.
- Sokabe T, Yamamoto K, Ohura N, Nakatsuka H, Qin K, Obi S, Kamiya A, Ando J. Differential regulation of urokinase-type plasminogen activator expression by fluid shear stress in human coronary artery endothelial cells. *Am J Physiol Heart Circ Physiol* 2004;287:H2027-34.
- Spatz JP, Mossmer S, Hartmann C, Moller M, Herzog T, Krieger M, Boyen HG, Ziemann P, Kabius B. Ordered deposition of inorganic clusters from micellar block copolymer films. *Langmuir* 2000;16:407-415.
- Stolberg S, McCloskey KE. Can shear stress direct stem cell fate? *Biotechnol Prog* 2009;25:10-19.
- Stone LC, Thorne LS, Weston CJ, Graham M, Hodges NJ. Cytoglobin expression in the hepatic stellate cell line HSC-T6 is regulated by extracellular matrix proteins dependent on FAK-signalling. *Fibrogenesis Tissue Repair* 2015;8:15.
- Sui BD, Hu CH, Zheng CX, Jin Y. Microenvironmental views on mesenchymal stem cell differentiation in aging. *J Dent Res* 2016;95:1333-1340.
- Takagi J. Structural basis for ligand recognition by RGD (Arg-Gly-Asp)-dependent integrins. *Biochem Soc Trans* 2004;32:403-6.
- Takahashi K, Yamanaka S. Induction of pluripotent stem cells from mouse embryonic and adult fibroblast cultures by defined factors. *Cell* 2006;126:663-76.
- Tamkun JW, Desimone DW, Fonda D, Patel RS, Buck C, Horwitz AF, Hynes RO. Structure of integrin, a glycoprotein involved in the transmembrane linkage between fibronectin and actin. *Cell* 1986;46:271-282.
- Tan DWM, Barker N. Intestinal stem cells and their defining niche. *Curr Top Dev Biol* 2014;107:77-107.
- Tarbell JM, Pahakis MY. Mechanotransduction and the glycocalyx. *J Intern Med* 2006;259:339-50.
- Tatematsu M, Ho RH, Kaku T, Ekem JK, Farber E. Studies on the proliferation and fate of oval cells in the liver of rats treated with 2-acetylaminofluorene and partial hepatectomy. *Am J Pathol* 1984;114:418-430.

- Theise ND, Badve S, Saxena R, Henegariu O, Sell S, Crawford JM, Krause DS. Derivation of hepatocytes from bone marrow cells in mice after radiation-induced myeloablation. *Hepatology* 2000;31:235-40.
- Till JE, McCulloch EA. A direct measurement of the radiation sensitivity of normal mouse bone marrow cells. *Radiat Res* 1961;14:213-22.
- Timchenko NA. Aging and liver regeneration. *Trends Endocrinol Metab* 2009;20:171-6.
- Timpl R, Rohde H, Robey PG, Rennard SI, Foidart JM, Martin GR. Laminin--a glycoprotein from basement membranes. *J Biol Chem* 1979;254:9933-7.
- Trial J, Entman ML, Cieslik KA. Mesenchymal stem cell-derived inflammatory fibroblasts mediate interstitial fibrosis in the aging heart. *J Mol Cell Cardiol* 2016;91:28-34.
- Tschumperlin DJ, Ligresti G, Hilscher MB, Shah VH. Mechanosensing and fibrosis. *J Clin Invest* 2018;128:74-84.
- Urbich C, Walter DH, Zeiher AM, Dimmeler S. Laminar shear stress upregulates integrin expression: role in endothelial cell adhesion and apoptosis. *Circ Res* 2000;87:683-9.
- van Breemen RB, Nikolic D, Xu XY, Xiong YS, van Lieshout M, West CE, Schilling AB. Development of a method for quantitation of retinol and retinyl palmitate in human serum using high-performance liquid chromatography atmospheric pressure chemical ionization mass spectrometry. *J Chrom A* 1998;794:245-251.
- vom Dahl S, Schliess F, Reissmann R, Gorg B, Weiergraber O, Kocalkova M, Dombrowski F, Häussinger D. Involvement of integrins in osmosensing and signaling toward autophagic proteolysis in rat liver. *J Biol Chem* 2003;278:27088-95.
- Wallquist W, Plantman S, Thams S, Thyboll J, Kortesmaa J, Lannergren J, Domogatskaya A, Ogren SO, Risling M, Hammarberg H, Tryggvason K, Cullheim S. Impeded interaction between Schwann cells and axons in the absence of laminin  $\alpha 4$ . *J Neurosci* 2005;25:3692-3700.
- Wang H, Riha GM, Yan S, Li M, Chai H, Yang H, Yao Q, Chen C. Shear stress induces endothelial differentiation from a murine embryonic mesenchymal progenitor cell line. *Arterioscler Thromb Vasc Biol* 2005;25:1817-23.

- Warren A, Cogger VC, Fraser R, Deleve LD, McCuskey RS, Le Couteur DG. The effects of old age on hepatic stellate cells. *Curr Gerontol Geriatr Res* 2011;2011:439835.
- Watt FM, Hogan BLM. Out of Eden: stem cells and their niches. *Science* 2000;287:1427-1430.
- Webb AE, Sanderford J, Frank D, Talbot WS, Driever W, Kimelman D. Laminin  $\alpha 5$  is essential for the formation of the zebrafish fins. *Dev Biol* 2007;311:369-382.
- Wisse E, De Zanger RB, Charels K, Van Der Smissen P, McCuskey RS. The liver sieve: considerations concerning the structure and function of endothelial fenestrae, the sinusoidal wall and the space of Disse. *Hepatology* 1985;5:683-92.
- Yamamoto K, Sokabe T, Watabe T, Miyazono K, Yamashita JK, Obi S, Ohura N, Matsushita A, Kamiya A, Ando J. Fluid shear stress induces differentiation of Flk-1-positive embryonic stem cells into vascular endothelial cells in vitro. *Am J Physiol Heart Circ Physiol* 2005;288:H1915-24.
- Yamamoto K, Takahashi T, Asahara T, Ohura N, Sokabe T, Kamiya A, Ando J. Proliferation, differentiation, and tube formation by endothelial progenitor cells in response to shear stress. *J Appl Physiol* (1985) 2003;95:2081-8.
- Yang AT, Wang P, Tong XF, Cong M, Liu TH, Cong R, Wu P, Jia JD, Wang BE, You H. Connective tissue growth factor induces hepatic progenitor cells to differentiate into hepatocytes. *Int J Mol Med* 2013;32:35-42.
- Yang JT, Rayburn H, Hynes RO. Embryonic mesodermal defects in  $\alpha 5$  integrin-deficient mice. *Development* 1993;119:1093-105.
- Yourek G, McCormick SM, Mao JJ, Reilly GC. Shear stress induces osteogenic differentiation of human mesenchymal stem cells. *Regen Med* 2010;5:713-24.
- Yu J, Vodyanik MA, Smuga-Otto K, Antosiewicz-Bourget J, Frane JL, Tian S, Nie J, Jonsdottir GA, Ruotti V, Stewart R, Slukvin, II, Thomson JA. Induced pluripotent stem cell lines derived from human somatic cells. *Science* 2007;318:1917-20.
- Zhao G, Mizuta T, Ozaki I, Kajihara S, Yamamoto K, Sakai T. Laminin 2 (merosin), but not laminin 1 (EHS-laminin), may be a major laminin isoform present in normal and fibrotic rat liver. *Hepatol Res* 1999;13:183-192.

- Zhu AJ, Haase I, Watt FM. Signaling via  $\beta$ 1 integrins and mitogen-activated protein kinase determines human epidermal stem cell fate in vitro. *Proc Natl Acad Sci U S A* 1999;96:6728-33.
- Zhu C, Ikemoto T, Utsunomiya T, Yamada S, Morine Y, Imura S, Arakawa Y, Takasu C, Ishikawa D, Shimada M. Senescence-related genes possibly responsible for poor liver regeneration after hepatectomy in elderly patients. *J Gastroenterol Hepatol* 2014;29:1102-8.

## 7. List of Abbreviations

2AAF	2-acetylaminofluorene
8-OHG	8-hydroxyguanosine
$\alpha$ -SMA	$\alpha$ -smooth muscle actin
ANOVA	analysis of variance
BSA	bovine serum albumin
CK18	cytokeratin 18
CK19	cytokeratin 19
COL1A2	collagen type I $\alpha$ 2 chain
COL4A1	collagen type IV $\alpha$ 1 chain
CRISPR	clustered regularly interspaced short palindromic repeats
CSF	colony stimulating factor
CTGF	connective tissue growth factor
CXCL	chemokine (C-X-C motif) ligand
Cy3	cyanine dye 3
DAG1	dystroglycan-1
DAPI	4',6-diamidino-2-phenylindole
DMEM	Dulbecco's Modified Eagle Medium
ECM	extracellular matrix
EGF	endothelial growth factor
ELISA	enzyme-linked immunosorbent assay
ELN	elastin
ERK	extracellular-signal-related kinase
ESI	electrospray ionization
FABP4	fatty acid binding protein 4
FACS	fluorescence-activated cell sorting

FCS	fetal calf serum
FGF2	fibroblast growth factor 2
FITC	fluorescein isothiocyanate
FN	fibronectin
FS	functionalized surface
FS/LN-211	functionalized surface with laminin-211
FS/LN-521	functionalized surface with laminin-521
GFAP	glial fibrillary acidic protein
GO	gene ontology
gRNA	guide ribonucleic acid
HCC	hepatocellular carcinoma
HCD	higher energy collisional dissociation
HGF	hepatocyte growth factor
HRP	horseradish peroxidase
HSC	hepatic stellate cell
IL6	interleukin-6
IMDM	Iscove's Modified Dulbecco's Medium
ITGA3	integrin $\alpha_3$
ITGA5	integrin $\alpha_5$
ITGA6	integrin $\alpha_6$
ITGB1	integrin $\beta_1$
ITGB4	integrin $\beta_4$
ITS	insulin-selenite-transferrin
JNK1	c-Jun N-terminal kinase 1
LAMA1	laminin $\alpha_1$
LAMA2	laminin $\alpha_2$
LAMA4	laminin $\alpha_4$

LAMA5	laminin $\alpha$ 5
LAMB1	laminin $\beta$ 1
LAMB2	laminin $\beta$ 2
LAMC1	laminin $\gamma$ 1
LC-MS/MS	liquid chromatography-tandem mass spectrometry
LN-111	laminin-111
LN-211	laminin-211
LN-521	laminin-521
LRAT	lecithin retinol acyltransferase
LU/BCAM	Lutheran blood group/basal cell adhesion molecule
MAPK	mitogen-activated protein kinase
MMP	metalloproteinase
MRM	multiple reaction monitoring
MSC	mesenchymal stem cell
NAPDH	nicotinamide adenine dinucleotide phosphate
NGF	nerve growth factor
NID	nidogen
PBS	phosphate buffered saline
PCA	principal component analysis
PEG	poly(ethylene glycol)
PHx	partial hepatectomy
PPAR $\gamma$	peroxisome proliferator-activated receptor $\gamma$
PS	polystyrene
PS/LN-211	polystyrene coated with laminin-211
PS/LN-521	polystyrene coated with laminin-521
qPCR	quantitative polymerase chain reaction
SASP	senescence-associated secretory phenotype

SD	standard deviation
SDC1	syndecan-1
SDS	sodium dodecyl sulfate
SEC	sinusoidal endothelial cells
SEM	standard error of mean
SMP30/RGN	senescence marker protein 30/regucalcin
SPARCL1	secreted protein acidic and rich in cysteines-like 1
TIMP	tissue inhibitors of metalloprotease
TLN	talin
TGF $\beta$	transforming growth factor $\beta$
TNFR	tumor necrosis factor receptor
UHPLC	ultra-performance high pressure liquid chromatography
uPA	serine protease urokinase plasminogen activator
UV	ultra-violet light
VCL	vinculin
VEGF	vascular endothelial growth factor

## 8. List of Figures

Figure 1: The hepatic stellate cell niche in the space of Disse. ....	3
Figure 2: Schematic overview of the laminin protein structure. ....	4
Figure 3: Scheme of processes after PHx involved in liver regeneration. ....	6
Figure 4: Expression of different laminin $\alpha$ chains during liver regeneration. ....	8
Figure 5: Setup for HSC exposed to laminar pulsatile fluid flow with the ibidi perfusion system. ....	19
Figure 6: Verification of the specificity of anti-laminin $\alpha$ chain antibodies. ....	34
Figure 7: Laminin protein chains in normal rat liver. ....	35
Figure 8: Laminin $\alpha$ protein chains in regenerating rat liver. ....	36
Figure 9: Cell adhesion, morphology and retinoid storage of HSC cultured on uncoated or laminin-coated surfaces. ....	37
Figure 10: Identification of genes showing significant expression changes during culture-dependent activation of HSC. ....	39
Figure 11: PS/LN-521 promotes HSC quiescence. ....	40
Figure 12: Reduced activation in HSC cultured on PS/LN-521. ....	42
Figure 13: Support of quiescence in HSC cultured on PS/LN-521. ....	43
Figure 14: Analyses of receptors capable to bind laminins in isolated HSC and in rat liver. ....	45
Figure 15: Laminin-functionalized nanostructured surfaces. ....	47
Figure 16: Improved HSC quiescence on laminin-functionalized nanostructured surfaces. ....	48
Figure 17: Gene expression analyses of HSC on uncoated culture surfaces. ....	49
Figure 18: Re-establishment of a quiescent-like state in stellate cell-derived myofibroblasts on PS/LN-521. ....	51
Figure 19: Study design for the comparison of HSC, blood serum, whole liver tissue, and hepatic matrix of young and old rats. ....	53
Figure 20: Quality control of microarray raw data. ....	55
Figure 21: Altered ECM protein-associated gene expression in aged rat liver. ....	56
Figure 22: Altered ECM protein composition in aged rat liver. ....	58
Figure 23: FN and ECM receptors in aged rat liver. ....	59
Figure 24: Gene expression alterations in HSC from aged rat liver. ....	61
Figure 25: Expression of HSC-associated markers in aged rat liver. ....	64
Figure 26: Analysis of senescence-associated markers in whole liver tissue and blood serum from young and old rats. ....	68
Figure 27: Senescence- and inflammation-associated factors in conditioned culture medium of HSC. ....	70
Figure 28: Markers of oxidative stress in liver tissue from young and old rats. ....	71

---

Figure 29: HGF in liver tissue and blood serum from aged rats. ....	73
Figure 30: HGF in regenerating rat liver. ....	74
Figure 31: Fluid shear stress induces HGF release by HSC. ....	75
Figure 32: Fluid shear stress influences HSC function. ....	76
Figure 33: LN-521 supports HSC function. ....	77
Figure 34: Expression of ITGA5 in HSC. ....	78
Figure 35: Influence of shear stress on HSC with CRISPR/Cas9-mediated <i>Itga5</i> knockout. ....	79
Figure 36: Influence of shear stress on HSC with CRISPR/Cas9-mediated <i>Itgb1</i> knockout. ....	81
Figure 37: Laminin $\alpha 5$ is an element of the HSC niche. ....	86
Figure 38: The HSC niche is impaired by aging leading to senescence and loss of typical characteristics in HSC. ....	90

## 9. List of Tables

Table 1: Settings for low, medium, and high shear stress during culture of HSC under laminar pulsatile flow. ....	20
Table 2: Target sequences and primer pairs for <i>Itga5</i> and <i>Itgb1</i> gRNA. ....	20
Table 3: Primer pairs for qPCR analyses. ....	23
Table 4: Primary antibodies for immunofluorescence analyses.....	25
Table 5: Primary antibodies for Western blot analyses. ....	26
Table 6: Differential expression of genes encoding for ECM proteins and integrin subunits in liver tissue from aged rats.....	57
Table 7: Differential expression of genes encoding for ECM-associated proteins and integrins in HSC from aged rat liver. ....	62
Table 8: Differential expression of genes associated with quiescence or activation in HSC from old rats. ....	63
Table 9: Expression of differentiation-associated markers in HSC from old rat liver. ....	65
Table 10: Expression of senescence markers in HSC and liver tissue from young and old rats.....	67
Table 11: Differential expression of SASP factors in HSC from aged rat liver.....	69
Table 12: Expression of genes typically associated with oxidative stress response in liver tissue from young and old rats. ....	71

## List of Publications, Scientific Presentations, and Awards

### Publications:

Rohn F, Kordes C, Castoldi M, Götze S, Poschmann G, Stühler K, Herebian D, Benk AS, Geiger F, Zhang T, Spatz, JP, Häussinger D. Laminin-521 promotes quiescence in isolated stellate cells from rat liver. *Biomaterials*, 2018;180:36-51.

Rohn F, Kordes C, Buschmann T, Wammers M, Reichert D, Poschmann G, Stühler K, Benk AS, Geiger F, Zhang T, Spatz JP, Häussinger D. Impaired integrin  $\alpha_5/\beta_1$ -mediated hepatocyte growth factor release by stellate cells of the aged liver. *Aging Cell*, 2020;19:e13131.

Buschmann T, Rohn F, Moos MPW, Görg B, Kordes C, Häussinger D. Taurine transporter knockout mice show impaired liver vascularization and regeneration (in preparation).

### Oral presentations:

17/06/2017            “Laminin-521 promotes Quiescence in Hepatic Stellate Cells”, International Symposium on Cells of the Hepatic Sinusoid 2017 (14<sup>th</sup> – 17<sup>th</sup> June 2017 in Galway, Ireland)

28/09/2017            “Laminin-521 supports the quiescent state of isolated rat hepatic stellate cells”, PhD symposium “deLIVER 2017” (28<sup>th</sup> – 29<sup>th</sup> September 2017 in Düsseldorf, Germany)

04/10/2018            “Alterations of stellate cells and their niche in aging rat liver”, ECLCB-8 // European Club for Liver Cell Biology (4<sup>th</sup> – 6<sup>th</sup> October 2018 in Bonn, Germany)

### Poster presentations:

28/09/2017            “Laminin-521 supports the quiescent state of isolated rat hepatic stellate cells”, PhD symposium “deLIVER 2017” (28<sup>th</sup> – 29<sup>th</sup> September 2017 in Düsseldorf, Germany)

- 26/01/2018 “Laminin-521 supports the quiescent state of isolated rat hepatic stellate cells”, Annual meeting of the German Association of the Study of the Liver 2018 (26<sup>th</sup> – 27<sup>th</sup> January 2018 in Hamburg, Germany)
- 05/10/2018 “Laminin-521 promotes quiescence in isolated stellate cells from rat liver”, ECLCB-8 // European Club for Liver Cell Biology (4<sup>th</sup> – 6<sup>th</sup> October 2018 in Bonn, Germany)

**Online presentations:**

“Laminin-521 promotes quiescence in isolated stellate cells from rat liver”, BioLamina Webcast Series “Rising Stars” (11<sup>th</sup> January 2019; Weblink: <http://www.biolamina.com/rising-stars#/friederike-rohn>)

**Awards:**

“Young Investigator Award” for the best oral presentation at the International Symposium on Cells of the Hepatic Sinusoid 2017 (14<sup>th</sup> – 17<sup>th</sup> June 2017 in Galway, Ireland)

## Danksagung

Die Projekte der vorliegenden Doktorarbeit wurden von Mai 2016 bis November 2019 im Rahmen des Teilprojekts A02 des Sonderforschungsbereichs 974 „Kommunikation und Systemrelevanz bei Leberschädigung und Regeneration“ unter der Leitung von Professor Dr. Dieter Häussinger, Klinik für Gastroenterologie, Hepatologie und Infektiologie, angefertigt. Für die Unterstützung der an den aufgeführten Projekten beteiligten Personen möchte ich mich im Folgenden bedanken.

Zunächst bedanke ich mich herzlich bei Professor Dr. Dieter Häussinger für die Möglichkeit, all die spannenden Projekte bearbeiten zu können sowie für die anregenden Diskussionen der Ergebnisse, die hilfreichen Hinweise und die Unterstützung während der gesamten Promotionszeit.

Ein weiterer Dank gilt Professor Dr. Eckhard Lammert für die Übernahme des Zweitgutachtens meiner Dissertation.

Bedanken möchte ich mich besonders bei Dr. Claus Kordes für die professionelle Betreuung sowie für all die hilfreichen Anregungen und Erklärungen.

Für die hilfsbereite Unterstützung im Labor und die angenehme Arbeitsatmosphäre möchte ich mich herzlich bei Dr. Doreen Reichert und Claudia Rupprecht bedanken.

Weiterhin danke ich Dr. Marianne Wammers für die Sternzell-Aufreinigung mittels FACS, Dr. Tobias Buschmann für seine Unterstützung bei der Durchführung der Perfusionsexperimente sowie Dr. Silke Götze für die Expressionsanalysen der Laminin  $\alpha$ -Ketten in den Leberschädigungsmodellen.

Ich bedanke mich bei Professor Dr. Kai Stühler und Dr. Gereon Poschmann für die Proteomanalysen, bei Dr. Diran Herebian für die Retinoid-Analysen sowie bei der Gruppe von Professor Dr. Joachim Spatz für die Herstellung der Laminin-funktionalisierten Oberflächen.

Mein besonderer Dank geht an meine Familie, meinen Partner und meine Freunde für ihr Verständnis und ihre Unterstützung während der gesamten Zeit meiner Doktorarbeit.

## **Eidesstattliche Erklärung**

Ich versichere an Eides Statt, dass die Dissertation von mir selbständig und ohne unzulässige fremde Hilfe unter Beachtung der „Grundsätze zur Sicherung guter wissenschaftlicher Praxis an der Heinrich-Heine-Universität Düsseldorf“ erstellt worden ist.

Die Dissertation wurde weder in der vorgelegten noch in ähnlicher Form bei einer anderen Institution eingereicht. Ich habe bisher keine Promotionsversuche unternommen.

---

Düsseldorf, Juni 2020

Friederike Rohn